Quartz growth: understanding porosity-preserving microcrystalline quartz through EBSD, TEM, and NanoSIMS examination of low temperature silica

Thesis submitted in accordance with the requirements of the University of Liverpool for the degree of Doctor of Philosophy by

Marsha Whitlock French

June 2012

Contents

Contents

List of Tables

List of Figures

Figure 6.1 - A) Hand specimen of Citronelle Formation agate, B) petrographic microscope image in plane polarized light showing alternating chalcedony and quartz bands. Inset image C) is in plain polarized light at finer scale showing banding, arrow indicates growth direction of the agate, with the bands gradually widening, D) cross polarized light showing the banding and larger "host" quartz grains with the next generation of chalcedony, E) inset through crossed polars showing rhythmic banded fibres, F) cathodoluminescence image of the agate showing the alternating bands of quartz and chalcedony in the agate. Quartz (labelled zone 3) has euhedral terminations and displays sector and growth zoning in the CL and terminates with some bright luminescence. The chalcedony identified in light optics (Fig. 1B) has two sets of CL characteristics; some bands have dark luminescence (labelled zone 1) while other bands have brighter luminescence (labelled zone 2). The onset of the next quartz growth zone (zone 3) can be seen in the lower right corner of the image, G) EBSD band contrast image showing increase in brightness with increasing crystallinity. Euhedral quartz is labelled zone 3, in concord with the CL image. The chalcedony identified in light optics (Fig. 1B) has two sets of EBSD band contrast characteristics; some material is dark because it cannot be easily indexed (crystal structure identified using EBSD) and is therefore either not quartz or has crystal size below resolution by EBSD (labelled zone 1) while other material is composed of microcrystalline quartz (labelled zone 2), H) EBSD orientation image showing the crystallographic orientations of the quartz grains (zone 3), and chalcedony composed of alternating black zones (un-indexible) of non-quartz silica, and microcrystalline bands showing similar crystal orientations (by colour) along each fibre……124

Figure 6.2 - A) electron backscatter diffraction (EBSD) orientation map of the Citronelle Formation Agate showing microcrystalline quartz host grain orientation and chalcedony (multiple colours) indicating that the crystallographic orientations of the host microcrystalline quartz grains and the adjacent chalcedony crystals are different. B) Pole figure of the *c*-axis orientation of the microcrystalline quartz on the surface of the host grain. The orientation of the microcrystalline quartz in the chalcedony is spread in a girdle parallel to the host surface. The trace of a great circle of these microcrystalline quartz data, shown by the red line, matches the orientation of the face of the host grain (red line) indicating that the material on the surface of the host grain is controlling the growth of the microcrystalline quartz…….130

Abstract

Deeply buried sandstones in sedimentary basins typically have low porosity due to cementation and compaction. There are several known causes of anomalously high porosity in sandstones, one of which is microcrystalline quartz coatings on sand grains that inhibit the growth of quartz overgrowth cements. However, there has been no mechanistic understanding of why or how microcrystalline quartz grows, or why it maintains high porosity in sandstones.

The Cretaceous Heidelberg Formation, Germany, and the Oligocene Fontainebleau Formation, Paris Basin, France, provide a natural laboratory to study microcrystalline quartz and associated silica polymorphs to develop an understanding of their crystallography, paragenetic relationships, and growth mechanisms, leading to a new understanding of the growth mechanisms of porosity-preserving microcrystalline quartz.

Data from scanning electron microscopy (SEM), electron backscattered diffraction (EBSD), and transmission electron microscopy (TEM) illustrate that porosity-preserving microcrystalline quartz cement is misoriented with respect to the host grain upon which it grows. In contrast, ordinary quartz cement grows in the same orientation (syntaxially) as the host quartz sand grain, and typically fills pore spaces. EBSD and TEM observations reveal nanofilms of amorphous silica (~ 50-100 nm in thickness) between the microcrystalline quartz and the host grain. The amorphous silica has insulated the host quartz grain from any incipient syntaxial cement and helped to prevent further syntaxial growth. The microcrystalline quartz is interpreted to be misoriented relative to the host grain, because the amorphous silica nanofilm prevents growth of syntaxial quartz cement. Instead, the microcrystalline quartz is similar to chalcedony with [11-20] perpendicular to the growth surface and *c* axes parallel with, but rotated on, the host quartz grain surface. The subsequent growth of chalcedony-like microcrystalline quartz has also prevented further growth of quartz since the fast-growth *c* axes do not extend into the neighbouring pore but instead compete for space on the host grain surface. The combination of insulating

amorphous silica and the orientation of microcrystalline quartz has been effective in preventing any further syntaxial quartz cement and so has preserved porosity.

Spatially resolved isotopic and trace element analysis of silica polymorphs in the Cretaceous Heidelberg Formation, Germany, and determination of crystal growth patterns utilizing SEM-CL, TEM and EBSD imaging have also contributed to new evidence for growth mechanisms for microcrystalline quartz and associated silica polymorphs. High precision, *in situ* oxygen isotope analyses of Cretaceous Heidelberg Formation detrital grains and quartz cements show three varieties of authigenic silica grew on detrital quartz grains. Interpretation of these data shows that minor quartz overgrowths grew from meteoric water at about 80°C followed by concentric bands of silica cements that covered quartz grains and overgrowths alike. A thin layer of chalcedony was first deposited on both detrital quartz grains and quartz overgrowth cements followed by microcrystalline quartz; this cycle was then repeated. Trace element data support the petrological data and reveal two episodes of enrichment in aluminium and iron in the chalcedony. In contrast, aluminium concentrations in the microcrystalline quartz are below the detection limit for aluminium suggesting a low temperature of growth (< 70°C). If it is assumed that the closely-related chalcedony and microcrystalline quartz grew from the same water, then isotope data suggest that chalcedony grew at approximately 34°C while microcrystalline quartz grew at approximately 60°C from meteoric water.

To understand further the role of chalcedony in microcrystalline quartz growth, chalcedony in two agates from the Citronelle Formation in Louisiana and Lake Superior in Michigan were studied. This study combined the use of a variety of analytical techniques, including electron backscatter diffraction (EBSD), cathodoluminescence (CL) and Fourier Transform Infrared (FT-IR) spectroscopy, to characterize the silica minerals present and investigate their spatial and crystallographic relationships in the banding arrangement. Microstructural and spectroscopic observations reveal that chalcedony bands are composed of amorphous silica that also contains nanocrystalline and later formed microcrystalline quartz. Nano- and microcrystalline quartz grew with *a* axes perpendicular to the growth substrate, typical of length-fast chalcedony. This study concludes that the bands formed as a result of discrete influxes of siliceous fluid. Within these individual bands

there is a sequence of minerals; chalcedony A (with amorphous silica and nanocrystalline quartz) → chalcedony MQ (with microcrystalline quartz) → quartz. This sequence is reflected in the degree of crystallinity, crystal orientations and water content and is analogous to a diagenetic cycle; the initial chalcedony portion of the band commences with amorphous silica with nanocrystalline quartz followed by fibrous microcrystalline quartz crystals; chalcedony then grades into larger equiaxial mesoquartz crystals. This paragenetic sequence suggests a viable model for the growth of chalcedony in agates, which helps explain the growth of chalcedony and microcrystalline growth in sandstones. Now that it is known what controls microcrystalline quartz growth in sandstones and why it preserves porosity, it can be used to help identify, rank and appraise deeply buried petroleum accumulations.

Acknowledgments

There are many individuals whose guidance and support have made this research possible. First and foremost, I would like to express my most sincere gratitude to my primary academic and research advisor Richard Worden without whose guidance, encouragement, and expertise, I would have been lost. I owe Richard a tremendous debt for his inspiration, his unwavering patience, and especially his insightful discussions. Secondly, I owe Betty Mariani, my secondary academic and research advisor a tremendous debt for teaching me about EBSD and CHANNEL 5 and guiding me through the analytical thought process. I would also like to thank Dave Prior for many helpful scientific discussions and suggestions. I would like to thank Sasha Haddad for access to her Fontainebleau samples and her previous work on microquartz. I would like to thank Bill Heins for being my local advisor and for introducing me to the Heidelberg Formation and Cornelius Fischer from the University of Göttingen for the Heidelberg samples. I would also like to thank Ron Surdam for introducing me to siliciclastic diagenesis in graduate school.

I would like to thank my academic colleagues at the University of Liverpool for accepting me as a colleague and for their many helpful discussions especially Gemma Byrne, James Utley, and Paddy Dowey. I would like to thank my colleagues at the ExxonMobil Upstream Research Company for their encouragement and support especially Joann Welton, Sabrina Innocenti, Mauro Lo Cascio, and Jen Shosa and my colleagues at the ExxonMobil Corporate Strategic Research Company especially Hubert King, Russ Mueller, Chris Kliewer, Bill Lamberti and Bill Horn. I would especially like to thank Joyce Cox for her friendship, drive, wisdom, and Dick Larese for his outstanding experimental work.

I could not have completed this research without the support of the ExxonMobil Upstream Research Company who funded this work and especially to my supervisor, Richard Barke and Manager, Jean-Christophe Sempere for allowing me the time and resources to complete it.

Finally, but most importantly, I would like to thank my family for all of their support and encouragement: my husband, Art for his infinite patience and for letting me pursue this dream so late in my career when most people are considering retirement, my daughters, Katie and Julia for helping me become computer literate and for actually being proud that their mom is a science nerd, my mother for giving me my quest for knowledge, teaching me that hard work does pay off and for driving me to countless rock shops in my youth, my father for always believing in me and never questioning that I could become a geologist even though I was a girl, and my sister, Pam for blazing the PhD trail for the Whitlock Family and for making me take riding lessons with her when I was six so I could discover my first sample of quartz.

1 Introduction

1.1 Porosity preserving microcrystalline quartz

Finding new petroleum reservoirs with high porosity is increasingly important as demand for energy increases. In sandstones, the main cause of porosity-loss is authigenic quartz cement (Sorby, 1880; McBride, 1989; Worden and Morad, 2000), which forms at temperatures near or above 80°C, and eventually occludes the pores between host grains. Thus, sedimentary researchers have assumed that when sandstones are buried to temperatures > 80°C, they rapidly lose porosity and potentially have limited reservoir potential. A subset of sandstones contain microcrystalline quartz cement (defined as 0.5 to 10.0 μm; Vagle et al., 1994) and exhibit anomalously high porosity deep in sedimentary basins (typically > 3500 m). Microcrystalline quartz occurs as fine coatings of crystallites on quartz grains that prevent the growth of ordinary quartz cement (Aase et al., 1996; Aase and Walderhaug, 2005; Bloch et al., 2002; Jahren and Ramm, 2000; Lima and De Ros, 2002; McBride, 1989; Ramm, 1992; Vagle et al., 1994). Sedimentary microcrystalline quartz has been found in Devonian to Miocene sandstones (Haimson and Lee, 2004; Lima and De Ros, 2002) from regions as diverse as Brazil (Lima and De Ros, 2002), Colombia (Warren and Pulham, 2001), the United States (Haimson and Lee, 2004), the North Sea Basins (Aase et al., 1996; Hendry and Trewin, 1995; Ramm et al., 1997; Vagle et al., 1994; Weibel et al., 2010), Continental Europe (Worden et al., 2012), North Africa (Goldstein and Rossi, 2002), modern eolian deposits in the Uluru Formation in Australia (W. Heins, Personal communication), Saudi Arabia (Cagatay et al., 1996) and Japan (Hattori et al., 1996).

Formation	Age	Location/Field	State/Country	Meters	Silica Source	EOD	Reference
Fontainebleau	Oligocene	Paris Basin	France	Outcrop	Silica-rich meteoric fluids	Marine	Haddad et al, 2006
Heidelberg	Upper Cretaceous	Tuefelsmauer Outcrop	Germany	Outcrop	Silica-rich meteoric fluids	Fluvial	Weidmar et.al
Brora	Upper Jurassic	North Sea	UK, North Sea	Outcrop	Sponge spicules	Marine	Vagle et al., 1994
Fulmar	Upper Jurassic	Shearwater, Martha Flds.	UK, North Sea	4000.0	Sponge spicules	Marine	Stewart, 1986
Ula	Upper Jurassic	Ula Field	Norway, North Sea	3400-3800	Sponge spicules	Marine	Aase et al., 1996; Jahren and Ramm, 2000
Gyda	Upper Jurassic	Gyde Field	Norway, North Sea	3650-4165	Sponge spicules	Marine	Aase et al., 1996
Brae	Upper Jurassic	Miller Field, Kingfisher	UK, North Sea	4000 - 4870	Sponge spicules, pressure solu	Marine	Asse & Walderhaug; 2005, Haddad, 2006
Valhall	L. Cretaceous	Scapa Field	UK, North Sea	1000-2000	Sponge Spicules	Marine	Hendry and Trewin, 1995
St. Peter	Ordovician	C. Michigan Basin	Michigan	1600-3600	Illite Smectite	Marine	Barnes, D. A. et al. 1992
Belly River	Upper Cretaceous	W. Alberta	Canada	2175.2	Pressure solution	Fluvial	Putnam, P.E. 1993
Tallahatta	Middle Eocene	Clarke. Co.	Alabama	Outcrop	Diatoms	Marine	Laws, R.A. et al 1992
Kunimi	Miocene	Niu Mountains	Japan	Outcrop	Volcanic tuffs	Shallow Marine	Hattori, I., et al. 1996
Monterey	Miocene	Santa Barbara Basin	California	Outcrop	Diatoms	Marine	Issacs, 1980
Uluru	Cambrian	Roxby Downs	Australia	Outcrop	Silica-rich meteoric fluids	Eolian	Bill Heins, personal communication
Tallahatta	M. Eocene	Clarke. Co.	Alabama	Outcrop	Diatoms	Marine	Laws, R.A. et al 1992
Citronelle	Pliocene	St. Francisville	Louisiana	Outcrop	Hydrothermal fluids	Igneous volcanic	Fisk, 1939; Woodward et al., 1941
Barnett	L. Mississippian	Fort Worth Basin	Texas	Outcrop	Sponge spicules	Marine	Milliken et al., 2007
Scollard	Cretaceous	Red Deer Valley	Alberta, Canada	Outcrop	Feldspar dissolution	Fluvial	Khidir and Catuneanu, 2003
Arab-D	Upper Jurassic	Ghawar Field	Saudi Arabia	Zone - 2B	Sponge spicules	Marine	Siddiqui, 2006
Abu-Durba & Abu-Thora	Carboniferous	Arabian Shield, SW Sinai	Egypt	Outcrop	Silica-rich meteoric fluids	Shallow Marine	Salem et al., 1998
Wabumun	Upper Devonian	Parkland Field	B.C., Canada	3262-3278	Silica-rich hydrothermal fluids	Marine	Packard et al., 2001
Mirador	Tertiary	Cusiana Field	Colombia	5000-5100	Silica-rich hydrothermal fluids	Marine	Warren and Pulham, 2001
Jaten	Miocene	Pacitan	Java	Outcrop	Volcanic tuffs	Marine	Smyth et al., 2003

Table 1.1 Summary of previously reported microcrystalline quartz examples and characteristics.

1.2 Low temperature silica polymorphs

Quartz overgrowth cement is typically syntaxial with the host grain, growing in optical and crystallographic continuity with the detrital host quartz grain (McBride, 1989). Quartz overgrowth cements are typically assumed to begin growing at temperatures greater than approximately 80^{o} C and range in size from 10 to 100+ μm (McBride, 1989, Ramm et al., 1997; Lander and Walderhaug, 1999; Walderhaug, 2000; and Worden and Morad, 2000).

In contrast, microcrystalline quartz does not grow in optical continuity with the host quartz grain (Worden et al., 2012; Haddad et al., 2006; Hendry and Trewin, 1995), but instead grows as apparently "randomly" oriented crystals 0.5 to 10 μm in length (Vagle et al., 1994). Borrowing from tectonite fabrics, the Heidelberg microcrystalline quartz predominantly displays an "S" fabric or planar fabric (strong c-axis orientation, but somewhat randomly oriented in the a-axes) and could be termed an S-diagenite, while the Fontainebleau microcrystalline quartz displays a linear or "L" fabric (some control on the linear a-axes), as well as, the "S" fabric and could be termed an LS-diagenite. Various sizes of microcrystalline quartz have been reported in the literature: Jahren and Ramm (2000) reported microcrystalline quartz from the Upper Jurassic sandstones in the Norwegian continental shelf ranging between 0.5 and 5 μm in diameter (prism length) with an average diameter between 1 and 1.5 μm. Vagle et al., (1994) reported 5-10 μm diameter crystals commonly growing on chalcedonic quartz substrates in the North Sea Brora Arenaceous Formation (Oxfordian), while Aase et al., (1996) reported 0.1-2 μm thick coats of microcrystalline quartz with an average size of 1 μm in Upper Jurassic sandstones in the Central Graben of the North Sea. Microcrystalline quartz is routinely associated with sandstone beds rich in biogenic silica, such as sponge spicules (Aase and Walderhaug, 2005; Hendry and Trewin, 1995) and seems to develop at the expense of silica bioclasts at temperatures of about 50°C (Vagle et al., 1994). Once detrital quartz grains have a continuous coating of microcrystalline quartz, the overgrowth of optically- and crystallographically-continuous quartz cement is prevented. Therefore, early microcrystalline quartz inhibits ordinary quartz cement growth, preserves porosity and leads to anomalously high porosity in deeply buried sandstones. It has

been suggested that elevated silica saturation, resulting from the very presence of microcrystalline quartz, inhibits quartz dissolution during burial and prevents quartz cementation (Hendry and Trewin, 1995). In the repeated bands present in agates, chalcedony is often succeeded by fine-quartz or quartz. Fine-quartz is a microcrystalline variety of quartz with a granular texture and individual grains typically < 20 μm (Flörke et al., 1982).

Chalcedony is defined as microcrystalline (< 100 μm length) fibrous silica, following the classification system of Flörke et al. (1991) and Heaney (1993). Wall-lining chalcedony is characterized by its parallel fibrous microstructure and forms by nucleation onto the wall of the host cavity (Graetsch, 1994). The fibres in chalcedony are elongate along the *a*-axes (specifically the [11-20] directions) toward the center of agates, perpendicular to the banding pattern. As a consequence, chalcedony exhibits a length-fast optical character; resulting in lower refractive index in the direction of the fibre (Flörke et al., 1982). Chalcedony is normally length-fast with its *c*-axis oriented perpendicular to the fibres (Knauth, 1973). In some cases the fibres can be length-slow indicating that the *c*-axis intersects the fibres at angles of 90^{o}. Length-slow chalcedony forms in evaporite environments (Pittman and Folk, 1971; Knauth, 1973).

Amorphous silica or Opal-A is the most common form of highly disordered opaline silica, typically derived from biogenic sources (Lee, 2006b, Knauth, 1994). Langer and Flörke (1974) categorized opal-A into opal-AN (high temperature networked opal such as hyalites) and opal-AG (gel-like). Opal-AG is precipitated biogenically from aqueous solutions at low temperatures (< 100^{o} C) (Stamatakis et al, 1991). Potch opals and precious opals are considered opal-AG (Flörke et al, 1991). Precious opal is composed of close packed homometric spheres of amorphous silica, typically 1 – 8 μm in diameter with additional silica cement partly filling the interstices (Darragh et al., 1966; Herdianita et al., 2000). These are visible using scanning electron microscopy. Graetsch (1994) stated that the structure of the spheres is usually highly disordered with abundant stacking faults. Potch opals are composed of irregularly packed heterometric spheres with the interstices commonly filled with silica cement (Graetsch, 1994).

Crystal Structure	Variety	Sub-variety	Morpology	'Crystal' size	Total water (H_2O_{tot})	H_2O_{SiOH}/H_2O_{mol}	Additional References
crystalline quartz	megaquartz	macroquartz	crystalline	>50 µm	0.5 - 2.5 wt.%	~0	Hesse, 1989; Hendry & Trewin, 1995
		mesoquartz		20 - 50 µm			
microcrystalline quartz	fine-quartz		granular	20 - 5 µm			Hesse, 1989; Graetsch, 1994; Knauth, 1994
	chalcedony	wall-lining	parabolic fiber bundles (length-fast)	>1 µm (typically 50 - 350 nm)			Langer & Flörke, 1974; Heaney, 1993; Graetsch, 1994; Knauth, 1994; Cady et al., 1996, 1998; Moxon et al., 2006
		horizontally banded	radiating spherulites (length-fast)	~100 - 200 nm			
		quartzine	parabolic fiber bundles (length-slow)	~100 - 200 nm			
microcrystalline opal	opal-C	lussatine	platy (length-fast)	10 - 100 nm	1 - 3 wt.%	0.02	Jones and Segnit, 1971, Langer & Flörke, 1974; Murata and Larsen, 1975, Williams et al., 1985; Graetsch, 1994; Knauth, 1994; Cady et al., 1996, 1998; Alexandre et al., 2004, Lynne et al., 2005
	opal-CT	lussatite	fibrous (length-slow)	10 - 100 nm	3 - 10 wt.%		
		massy opal	bumpy microspheres, clustered nanospheres, aligned nanospheres, beaded blades, sharply bladed lepispheres	1 - 10 µm spheroids			
non-crystalline opal	opal-A	Precious opal	Botryoidal, amalgamated microspheres	1 - 8 µm spheres	10 - 12 wt.%	0.1 - 0.7	Darragh et al., 1966; Langer & Flörke, 1974; Graetsch, 1994; Herdianita et al., 2000, Lynne et al., 2005
		Potch opal	Nano- and microspheres				

Table 1.2 Summary of silica polymorphs and their characteristics.

1.3 Growth mechanisms of microcrystalline quartz and previous methods

The growth mechanisms of microcrystalline quartz, and how it inhibits ordinary quartz cement, have only recently been investigated. While microcrystalline quartz has been previously studied with light microscopes and SEMs (Aase et al., 1996; Hendry and Trewin, 1995; Ramm et al., 1997; Vagle et al., 1994; Weibel et al., 2010), microcrystalline quartz cement growth on detrital quartz sand grains was only recently studied and documented using electron backscatter diffraction (EBSD) (Haddad et al., 2006). Several authors have reported data on the microanalysis of detrital quartz and quartz overgrowths (Hervig et al., 1995; Williams et al., 1997; Lehmann et al., 2011) and cherts (Abruzzese et al., 2005), but little microanalysis data have been reported on the paragenetic sequence of silica polymorphs in sedimentary rocks from detrital quartz grains, quartz overgrowths, amorphous silica, chalcedony or microcrystalline quartz. Trace element data have been reported from various authors

for hydrothermal quartz (Rusk et al., 2008; Lehmann et al., 2009; Götte et al., 2011; and Lehmann et al., 2011) and agates (Götze et al., 2001).

1.4 Aim of this study

The aim of this study was to develop a mechanistic understanding of why and how microcrystalline quartz grows and why it maintains high porosity in sandstones. The steps taken to achieve this aim were: 1) develop an understanding of microcrystalline quartz and associated silica polymorphs, and 2) develop an understanding the mechanism of microcrystalline quartz growth, and crystallographic analysis of detrital quartz, and the quartz cements including quartz overgrowths, amorphous silica, chalcedony, and microcrystalline quartz.

1.5 Samples

In order to understand the mechanism responsible for the growth of microcrystalline quartz, this work utilized sandstone samples from the Upper Cretaceous Heidelberg Formation in the Subhercynian Basin, Germany (Voigt et al., 2006) and the Oligocene Fontainebleau Formation in the Paris Basin, France (Thiry, 2001; Haddad et al., 2006). In addition, two agate samples were studied in this research, one from the Pliocene Citronelle Formation in Louisiana, which is a fluvial sand and gravel deposit thought to be weathered out of volcanic vugs from the Upper Mississippi River Valley. The second agate studied was from Lake Superior in Michigan (Moxen, 2002) and has a similar origin and was described in an unpublished Master's thesis from the University of Liverpool by Lee (2006a). Samples were made into 30 mm thin sections after impregnation with blue-stained epoxy resin for porosity identification.

1.6 Methods

This study utilized high resolution electron microscope techniques to study the silica polymorphs and to evaluate the crystallographic and compositional controls on the formation of microcrystalline quartz. The quartz cements were studied using

SEM/Cathodoluminescence (CL), Electron Backscatter Diffraction (EBSD), Energy Dispersive Spectroscopy (EDS), Wavelength Dispersive Spectrometry (WDS), Transmission Electron Microscopy (TEM), Fourier Transfer Infrared (FT-IR), and Secondary Ion Mass Spectrometry (SIMS) techniques. SEM/CL was used to understand the crystal chemistry differences between microcrystalline quartz and quartz overgrowths. EBSD was used to determine the crystallographic orientation of the microcrystalline quartz and the quartz overgrowths and identify the statistically significant differences. WDS, EDS, and SIMS were used to measure the trace element content of the silica polymorphs to try to understand what, if any trace element controls there were on quartz growth. NanoSIMS was used to measure oxygen isotope signatures of the silica polymorphs to determine the temperature of formation.

Technique	Equipment _ location	Identifies	Area of observation	Maximum resolution	Used to examine diagenetic quartz	Used to examine microquartz
Transmitted-light optics	Zeiss Axiophot binocular microscope_ XOM Upstream Research Co.	Quartz overgrowths euhedral form and dust rims	Approx. 100 μm	Approx. 50 μm	Sorby, 1880, McBride, 1989, Vagle et al., 1994; Aase et al., 1996; Ramm et al., 1997; Jahren and Ramm, 2000; Lima and De Ros, 2002; Aase and Walderhaug, 2005, Haddad et al., 2006	McBride, 1989; Vagle et al., 1994; Hendry and Trewin, 1995Aase et al., 1996; Ramm et al., 1997; Jahren and Ramm, 2000; Lima and De Ros, 2002; Aase and Walderhaug, 2005, Haddad et al., 2006
Secondary Electron Imaging (SEI)	JEOL JSM 6100, JEOL JSM 6490LV, _ XOM Upstream Research Co., LEO 1530_XOM Corporate Strategic Research Co., Philips XL-30_ Univ. of Liverpool, Scanning Electron Microscopes (SEM)	Quartz overgrowths euhedral form	Approx. 100 μm	Approx. 50 μm	McBride, 1989; Vagle et al., 1994; Aase et al., 1996; Ramm et al., 1997; Jahren and Ramm, 2000; Lima and De Ros, 2002; Aase and Walderhaug, 2005	McBride, 1989; Vagle et al., 1994; Hendry and Trewin, 1995Aase et al., 1996; Ramm et al., 1997; Jahren and Ramm, 2000; Lima and De Ros, 2002; Aase and Walderhaug, 2005, Haddad et al., 2006
Backscatter Electron Imaging (BSE)	JEOL JSM 6100, JEOL JSM 6490LV_ XOM Upstream Research Co., LEO 1530_XOM Corporate Strategic Research Co., Philips XL-30_Univ. of Liverpool, Scanning Electron Microscopes (SEM)	Quartz overgrowths euhedral form and dust rims	Approx. 100 μm	Approx. 50 μm	McBride, 1989; Vagle et al., 1994; Aase et al., 1996; Ramm et al., 1997; Jahren and Ramm, 2000; Lima and De Ros, 2002; Aase and Walderhaug, 2005	McBride, 1989; Vagle et al., 1994; Hendry and Trewin, 1995; Aase et al., 1996; Ramm et al., 1997; Jahren and Ramm, 2000; Lima and De Ros, 2002; Aase and Walderhaug, 2005, Haddad et al., 2006
Energy Dispersive Spectrometry (EDS)	JEOL JSM 6490_ XOM Upstream Research Co., Scanning Electron Microscope (SEM)	Elemental analysis	Approx. 100 μm	ppm		
Wavelength Dispersive Spectroscopy (WDS)	JEOL 6400_XOM Upstream Research Co. SEM with WDS	Elemental analysis and potential to discriminate chemical states	Approx. 100 μm	ppm		
Transmission Electron Microscope (TEM)	Philips CM200F_XOM Corporate Strategic Research Co., TEM/STEM	Amorphous silica phase with with no crystalline structure from crystalline microquartz	Tens of microns	atomic scale, ~ 0.14 nm image	Wahl et al. 2002, Graetsch et al. 1987, Florke et al., 1991; Cady et al., 1998, Miehe et al. 1984, Heaney et al. 1994, Haddad et al., 2006	Haddad et al., 2006, Worden et al., 2012
Fourrier Transform Infra-Red Spectroscopy (FT-IR)	Nicolet Centaurus FT-IR _Univ. of Liverpool, microscope (Thermo electron Corporation) with OMNIC software	Amorphous silica by detecting total water, molecular water, and silanol contents	4 cm^{-1}		Langer and Florke 1974, Graetsch et al, 1985,Kronenberg 1994, Haddad et al., 2006	Langer and Florke 1974, Graetsch et al, 1985,Kronenberg 1994, Haddad et al., 2006
Secondary Ion Mass Spectroscopy (SIMS)	Cameca SIMS IMS 3F_XOM Corporate Strategic Research Co.	Dynamic Imaging Secondary Ion Mass Spectrometry identifies trace elements	wide field of view	~ 1 micron resolution, extensive quantitative imaging capabilities	et al., 1996; Williams et al., 1997, Lyon et al., 2000, Macaulay et al,., 2000, Marchand et al., 2002, Kelly et al., 2007; Kita et al., 2009; Valley and Kita, 2009, Pollington et al., 2012.	
Cathodoluminescence (CL)	JEOL 6490LV SEM fitted with a Gatan cathodoluminescence detector (ChromaCL-006)_XOM Upstream Research Co., Philips XL-30 SEM fitted with a K.E. Developments Ltd_Univ. of Liverpool cathodoluminescence detector (D308122).	Distinguishes detrital sand grain from quartz overgrowth. May depict zones of growth in overgrowth.	Up to 1.5 mm (when montaged)	Up to 1 μm	Walderhaug and Rykkje, 2000).	Vagle et al, 1994, Hendry and Trewin, 1995, Haddad et al., 2006
Electron Backscatter Diffraction (EBSD)	Leo 1530 SEM_XOM Corporate Strategic Research Co., CamScan X500 Crystal Probe SEM_Univ. of Liverpool, fitted with an Osford-HKL EBSD system	Hundreds of thousands of individual diffraction patterns to create a map of crystallographic orientation of grains	Map of up to 800 μm^2 containing ~ 105,000 data points	1 pattern of area 1 μm	Haddad et al., 2006, Mørk and Moen, 2007	Haddad et al., 2006, Worden et al., 2012
Focused Ion Beam Scanning Electron Microscope (FIB-SEM)	FEI NOVA 200_Purdue University Birck Nanotechnology Center	Used to prepare sample for TEM		High resolution imaging	Worden et al., 2012	Worden et al., 2012
NanoSIMS	Cameca NanoSIMS N50_XOM Corporate Strategic Research Co.	Ultra-trace element detection (ppb range) using scanned ion beam, industry-leading capability for ion imaging	smaller field of view than SIMS	~ 0.025 micron (25 nm) resolution, up to 5 simultaneous ion images		

Table 1.3 Methods used in this study, their characteristics, and previous work.

Chalcedony was studied in the agates using transmitted-light optics, SEM/Cathodoluminescence (CL), Electron Backscatter Diffraction (EBSD), and Fourier Transform Infrared (FT-IR) spectroscopy.

1.6.1 Transmitted-light optics

Transmitted-light optical analysis using a Zeiss Axiophot binocular microscope was used to characterize the samples and identify the silica polymorphs based on crystal size and their distribution throughout the samples. Transmitted-light optical analysis identified and located quartz overgrowths and microcrystalline quartz on detrital host quartz grains. The location of the quartz overgrowths was based on the identification of euhedral grains, with sharp, clean edges and, to some extent, on the presence of dust rims. Microcrystalline quartz lining the pore spaces was identified with a petrographic microscope, but due to the small size, the scanning electron microscope has better resolution for studying 0.5 to 10 μm microcrystalline quartz.

1.6.2 Scanning Electron Microscopy (SEM)

Scanning electron microscopy resolved microcrystalline quartz by its high resolution capabilities. High-resolution secondary electron images (SEI) and backscattered electron images (BEI) were acquired using a JEOL 6330F FEG-SEM and a JEOL 6490LV SEM.

1.6.3 Cathodoluminescence (CL)

CL is a rapid, high-resolution SEM technique for crystal orientation and chemistry determination. SEM/CL studies on igneous and metamorphic quartz have shown that quartz CL colours and intensities are dependent on crystallographic orientation (Walderhaug and Rykkje, 2000). Cathodoluminescence results from the emission transitions of electrons from an excited electronic state to a ground state with lesser energy after being bombarded by incoming cathode rays (Marfunin, 1979). Cathodoluminescence microscopy identified and distinguished detrital quartz grains from syntaxial quartz overgrowths and microcrystalline quartz (Evans et al. 1994) and

crystalline quartz grains from fine bands of chalcedony. A JEOL 6490LV SEM, fitted with a Gatan cathodoluminescence detector (ChromaCL-006) was used for cathodoluminescence analysis. CL images were taken with an accelerating voltage of 10 kV (in contrast to 20 kV for BSE), 8 nA beam current, and 16.5 mm working distance. CL images were collected by accumulating a signal of 500 frames using a slow-scanning raster and red, green, and blue wavelengths.

1.6.4 Electron Backscattered Diffraction (EBSD)

The principles and techniques of EBSD have been explained previously (Venables and Harland, 1973; Dingley, 1984; Lloyd, 1987; Schmidt and Olesen, 1989; Lloyd and Freeman, 1991; Adams et al., 1993; Wilkinson and Hirsch, 1997; Prior, 1999; Prior et al., 2009). This work is the third investigation (following Haddad et al. 2006, and Mörk and Moen, 2007) to utilize EBSD to address sandstone diagenetic questions. EBSD is a rapid, high-resolution SEM technique for measuring crystallographic orientation. EBSD creates electron backscattered patterns (EBSPs) based on Bragg's equation. When a sample is bombarded with an electron beam, electrons are diffracted at specific angles when they encounter an ordered crystal lattice. The diffracted electrons are focused by the planes of the crystal lattice. Each set of lattice planes generates a unique pattern, termed a Kukuchi band (EBSPs are made up of multiple Kukuchi bands) which can then be compared to known quartz patterns and indexed. Orientation angles would be rejected in the data whenever MAD (mean angular deviation) was greater than 1 to assure the reliability of the EBSD measurement. Sample preparation (polished sections) and operating conditions are critical to data quality.

EBSD has the capability to resolve the crystallographic orientations at a resolution as small as 200 nanometres to reveal microstructural information about the crystal structure and mineralogy of the material being analysed. This technique has guided interpretations regarding the mechanisms of quartz, chalcedony and microcrystalline crystal growth. EBSD analysis was performed on the samples on polished thin sections using a LEO 1530 SEM fitted with an Oxford-HKL EBSD system and a CamScan X500 crystal probe field emission gun SEM. Working conditions were 20

kV accelerating voltage, 30 nA beam current and ~ 25 mm working distance. EBSD patterns were auto-indexed using the CHANNEL 5 software from Oxford Instruments HKL A/S. The software was used to display maps and pole figure data.

1.6.5 Wavelength Dispersive Spectroscopy (WDS) and Energy Dispersive Spectroscopy (EDS)

WDS is a quantitative spectral tool for measuring trace element content. The electron beam generates characteristic X-rays which are selected using analytical crystals with specific lattice spacing. The X-rays of specific wavelengths are passed on to the detector where they are converted to photoelectrons which generate an electrical signal whose magnitude is proportional to the abundance of the element being detected. EDS is a similar technique except that WDS spectrometers have significantly higher spectral resolution and enhanced quantitative potential compared to EDS.

Wavelength dispersive spectroscopy analysis was performed using a JEOL 6400 SEM with wavelength dispersive spectrometers. The trace elements measured in the quartz overgrowth and concentric bands were: Al, Na, Mg, K, Ca, Ti, Fe, Cr, and Mn. Analysis times were 300 seconds on peak, 50 seconds on each background. Accelerating voltage was 15 kV, beam current 115 nA, probe size ~ 3 μm and spot size of 5-10 microns. The standards employed were SRM-1212 for Al, Na, K, and Ca, MgO for Mg, TiO_2 for Ti, Cr_2O_3 for Cr, and manganese metal for Mn. Data were quantified using Probe for EPMA software. Limits of detection (3 sigma) are: 12 ppm for Al, 24 ppm for Na, 19 ppm for Mg, 22 ppm for K, 26 ppm for Ca, 38 ppm for Ti, 216 ppm for Fe, 112 ppm for Cr, and 129 ppm for Mn. All analysis points were below detection for Cr and Mn and these elements are not discussed further.

1.6.6 Secondary Ion Mass Spectrometry (SIMS)

SIMS is an analytical tool for measuring trace detection of all isotopes and all species. SIMS generates maps of trace element distribution at concentrations in the ppm to ppb range. SIMS is performed on the fragments of secondary electrons which are ejected when an energetic beam of ions strikes a solid surface. SIMS can produce

mass spectra, depth profiles and ion images. A Cameca N50 NanoSIMS in ExxonMobil's Corporate Strategic Research Company was used in this study for oxygen isotope analyses with a spot size of 5-10 μm. Analysis conditions were 16keV, 250pA Cs+ primary beam; 8 keV negative secondary ions; sample charge neutralization; 10μm x 10μm rastered analysis area; FC-EM detection (180~6E4 cps); and instrumental mass resolution ~5000 yielding a precision of ±0.15‰ (1SD). Ion microprobe spots were selected based on CL, SEI, and BEI images taken before the samples were put in the NanoSIMS. After analysis, each spot was investigated by SEM and CL to define the analysis point as being located in one of the following: detrital grain, quartz overgrowth, microcrystalline quartz, or microcrystalline quartz with chalcedony. Isotope data are reported relative to the V-SMOW standard.

1.6.7 Fourier Transfer-Infrared (FT-IR) Spectroscopy

The utilization of infrared spectra to determine silica mineral phases by water content and speciation has been outlined previously by Langer and Flörke, 1974; Graetsch et. al., 1985; and Kronenberg, 1994. Infrared spectra of the sample were obtained using a liquid-nitrogen-cooled Nicolet Centaurus FT-IR microscope (Thermo Electron Corporation). Binocular lens (x 10) gave an optical image of the sample and rectangular apertures 300 x 300 μm were used for taking the measurement. Spectra were collected at 4 cm^{-1} resolution with 100 scans collected and averaged. Reflectance spectra were generated and converted to absorption spectra using OMNIC software (Thermo Electron Corporation). Peak positions were determined by taking positions of local maxima following linear baseline correction. The position of these peaks was within ± 3 cm^{-1} since a wavenumber resolution of 4 cm^{-1} was applied for the IR measurement.

1.6.8 Transmission Electron Microscopy (TEM)

TEM can resolve crystallographic orientations with nanometre scale resolution to reveal microstructural information (crystal structure and mineralogy) which can lead to interpretations regarding mechanisms of crystal growth and has been used to characterize crystal structure and microstructures in various silica polymorphs (Wahl

et al., 2002; Graetsch et al., 1987; Miehe et al., 1984; Florke et al, 1991; Heaney et al., 1994, Cady et al., 1998, and Haddad et al., 2006). TEM was used in this study to distinguish the different silica polymorphs. A Focused Ion Beam Scanning Electron Microscope (FIB-SEM) was used to prepare samples for TEM analysis. The FIB-SEM uses a finely focused beam of ions (generally gallium) that can be operated at a high beam current for milling the sample. Beginning with the thin section, the sample is first examined with a petrographic microscope to identify the area of interest, then with EBSD to identify the non-diffracting zone, and finally with CL to focus on the area to sample. The sample is then ion milled, extracted from the thin section and mounted on a TEM grid. The TEM samples were prepared using a FEI NOVA 200 focused ion beam (FIB) SEM at Purdue University in the Birck Nanotechnology Center. Samples prepared using FIB-SEM were then analysed in a Philips CM200F TEM/STEM at ExxonMobil's Corporate Strategic Research Company operated in the bright field imaging TEM mode at an accelerating voltage of 200kV.

1.7 Research Questions

Nine questions regarding microcrystalline quartz growth were investigated during this research and evidence to answer each question was collected using the above mentioned analytical tools. These questions can be categorized into two overarching questions to answer the fundamental research aim of this thesis: 1) What is microcrystalline quartz, and 2) How does microcrystalline quartz grow?

What is microcrystalline quartz and what are the associated silica polymorphs?

1. What are the silica polymorphs in quartz cements?
2. What is the paragenesis of the silica polymorphs?
3. What is the crystallographic orientation of porosity-preserving microcrystalline quartz?
4. What are the similarities and differences between the microcrystalline quartz in the Heidelberg Formation and the microcrystalline quartz in the Fontainebleau Formation?
5. What are the similarities and differences between the silica polymorphs in agates and in the Heidelberg and Fontainebleau sandstones?

How does microcrystalline quartz grow and how do the associated silica polymorphs grow?

6. How do trace elements effect the growth of silica polymorphs?
7. Is there a link between stable oxygen isotope values and silica polymorph variations in microcrystalline quartz cemented sandstones?
8. How does the temperature of formation vary related to original water source and what are the controls on the $\delta^{18}O$ in the silica cements?
9. How does porosity-preserving microcrystalline quartz grow?

1.7.1 What are the silica polymorphs in quartz cements?

To understand microcrystalline quartz better this research describes microcrystalline quartz and associated silica polymorphs. This research has focused on studying the silica polymorphs as analogues for low temperature quartz growth including amorphous silica, chalcedony in agate, porosity-preserving microcrystalline quartz and porosity occluding quartz overgrowths in order to develop an understanding of diagenetic quartz growth in sandstone reservoirs.

1.7.2 What is the paragenesis of the silica polymorphs?

This question relates to how each of the silica polymorphs form and in what order they grow to determine the conditions required for microcrystalline quartz growth. Different case studies need to be compared to ascertain any universal patterns.

1.7.3 What is the crystallographic orientation of porosity-preserving microcrystalline quartz?

Syntaxial quartz overgrowths have been observed to nucleate and grow only on a clean quartz sandstone surface. In contrast, microcrystalline quartz has been observed to grow on quartz sandstone surfaces, quartz overgrowths, feldspar grains, apatite and other non-quartz surfaces. Quartz overgrowths inherit the crystallographic orientation

of the host detrital quartz grain. However, porosity-preserving microcrystalline quartz is crystallographically misoriented with respect to the host grain (Haddad et al., 2006). Understanding the cause of the crystallographic orientation of the porosity-preserving microcrystalline quartz is the key to understanding the conditions for its growth versus syntaxial quartz overgrowths.

1.7.4 What are the similarities and differences between the microcrystalline quartz in the Heidelberg Formation and the microcrystalline quartz in the Fontainebleau Formation?

The results of this study will test if the Heidelberg microcrystalline quartz growth mechanism is an exception or a rule. This will provide additional insights into the growth mechanism for microcrystalline quartz by providing a second test example to elucidate the growth mechanism of microcrystalline quartz and porosity preservation in sandstone reservoirs.

1.7.5 What are the similarities and differences between the silica polymorphs in agates and in the Heidelberg and Fontainebleau sandstone?

The comparison of the silica polymorphs and especially chalcedony in agates and the silica polymorphs in the Heidelberg and Fontainebleau sandstones would lead to understanding the conditions for microcrystalline quartz growth and the controls on growth.

1.7.6 How do trace elements effect the growth of silica polymorphs?

Understanding the role of trace elements might help determine the conditions for the growth of the silica polymorphs and if their growth is controlled by the presence of any particular trace elements.

1.7.7 Is there a link between stable oxygen isotope values and silica polymorph variations in microcrystalline quartz cemented sandstones?

Understanding the stable oxygen isotope values for each of the silica polymorphs could facilitate understanding the growth conditions and controls on the silica polymorphs in silica cements.

1.7.8 How does the temperature of formation vary related to original water type and what are their controls on the δ18O in the silica cements?

Identifying the temperatures of formation and the original water source related to the silica cements would help in understanding the conditions for formation and controls on the silica polymorphs in silica cements.

1.7.9 How does porosity-preserving microcrystalline quartz grow?

This question is the focus of the research because understanding the growth mechanism could lead to identifying the conditions for porosity-preserving microcrystalline quartz in sandstone reservoirs, which in turn could lead to improved prediction of porosity in deeply buried sandstone reservoirs, a target for hydrocarbon exploration.

1.8 Introduction to Chapters

Chapter 2: Amorphous silica nanofilms result in growth of misoriented microcrystalline quartz cement maintaining porosity in deeply buried sandstones

Published in: *Geology*, online 6 January 2012, in print, February, 2012.
Authors: Richard H. Worden, Marsha W. French, and Elisabetta Mariani.
Idea: High level summary paper that used high resolution scanning electron microscopy, electron backscattered diffraction and transmission electron microscopy to study the microcrystalline quartz cemented Upper Cretaceous Heidelberg

Formation, Germany. The analyses revealed that a nanofilm of amorphous silica (50-100 nm) and a layer of chalcedony sit between the detrital grain and microcrystalline quartz cement. The amorphous silica insulates the detrital quartz grains and prevents syntaxial growth while microcrystalline quartz adopts the orientation of the underlying chalcedony with its fast-growth *c*-axis parallel to the grain surface thus preventing growth into the pore.

Work contributed: Richard Worden provided extensive editing and preparation for Geology and significant advice. Betty Mariani provided editing and advice especially in recognizing the [11-20] orientation of the microcrystalline quartz and the surface control on the microcrystalline quartz growth as well as, the model graphic (Figure 2.4). Cornelius Fischer supplied the sample from the Heidelberg Formation, Russ Mueller operated the LEO SEM for EBSD work (Figure 2.2), Chris Kliewer operated the TEM (Figure 3), Dmitri Sakarov prepared the focused ion beam samples for TEM analysis, Joyce Cox operated the SEM for high resolution photographs of rock chips (Figure 2.1), and Jane Rees provided valuable advice on writing.

Chapter 3: Microcrystalline Quartz Generation and the Preservation of Porosity in Sandstones: evidence from the upper Cretaceous of the Subhercynian Basin, Germany

Published in: Journal of Sedimentary Research, online, June 2012.

Authors: Marsha W. French, Richard H. Worden, Elisabetta Mariani, Richard E. Larese, Russell R. Mueller, and Chris E. Kliewer.

Idea: Detailed paper on the Heidelberg Formation microcrystalline quartz and how it forms including SEM, EBSD, and TEM analysis and evidence of amorphous silica nanofilms forming an initial surface coat followed by [11-20] chalcedony growth. The chalcedony growth is perpendicular to the host grain surface which acts as a precursor for the microcrystalline quartz growth thus inhibiting the development of pore-filling quartz overgrowths and subsequently preserving porosity.

Work contributed: Richard Worden provided editing and advice, Betty Mariani provided editing, advice, and the microcrystalline quartz model graphic, as with Chapter 3, Cornelius Fischer supplied the sample from the Heidelberg Formation, Russ Mueller operated the LEO SEM for EBSD work (Figs. 3.2B, 3.4, 3.5), Chris Kliewer operated the TEM (Figs. 3.2H, I, and 3.7), Dmitri Sakarov prepared the focused ion beam samples for TEM analysis (Figs. 3.2D, E, F, G), Dick Larese

conducted the experimental work (Fig. 3.8), Joyce Cox operated the SEM for high resolution photographs of rock chips (Figure 3.6), Hubert King, Joann Welton, and Mauro Lo Cascio provided many helpful discussions, Editor Gene Rankey, associate editor Fernando De Ros, corresponding editor John Southard, Medard Thiry and Steve Franks, provided constructive, supportive, and helpful comments.

Chapter 4: The origin of quartz cements revealed by spatially resolved oxygen isotope microanalysis, WDS, SEM-CL, TEM and EBSD imaging; Heidelberg Formation, Germany.

Submitted to: Geochemica et Cosmochimica Acta, December, 2011

Authors: Marsha W. French, Richard H. Worden, Elisabetta Mariani, Hubert E. King, William A. Lamberti, and William C. Horn

Idea: Spatially resolved isotopic and trace element analysis of silica polymorphs and determination of crystal growth patterns using SEM-CL, TEM, and EBSD show three varieties of authigenic silica growing on detrital quartz grains with an average $\delta^{18}O$ of +9.4‰ for detrital quartz, $\delta^{18}O$ of +20.3‰ for quartz overgrowths, $\delta^{18}O$ of +22.7‰ for microcrystalline quartz and $\delta^{18}O$ of +27.4‰ for chalcedony. Trace element data reveals two episodes of enrichment in aluminium and iron in the chalcedony. Assuming chalcedony and microcrystalline quartz grew from the same water, isotope data suggests chalcedony grew at approximately 34^{o}C and microcrystalline quartz grew at 60^{o}C from meteoric water.

Work contributed: Richard Worden provided editing and advice, Betty Mariani provided advice, Cornelius Fisher supplied the sample from the Heidelberg Formation, Hubert King coordinated the NanoSIMS work and provided many helpful discussions, Bill Lamberti led the NanoSIMS and WDS work, Bill Horn provided the technical analysis using the NanoSIMS and WDS, and as this work was based on the initial work in Chapters 1 and 2, the EBSD work from Russ Mueller, TEM work from Chris Kliewer, and FIB samples from Dmitri Sakarov, also contributed to this chapter.

Chapter 5: Orientation of microcrystalline quartz in the Fontainebleau Formation, Paris Basin and why it preserves porosity

Submitted to: Sedimentary Geology, submitted March, 2012

Authors: Marsha W. French and Richard H. Worden

Idea: Detailed paper on the Oligocene Fontainebleau Formation microcrystalline quartz and how it forms including SEM, EBSD, and TEM analysis and evidence of amorphous silica nanofilms forming an initial surface coat followed by [11-20] chalcedony growth perpendicular to the host grain surface which acts as a precursor for the microcrystalline quartz growth thus inhibiting the development of pore-filling quartz overgrowths and subsequently preserving porosity. The microcrystalline quartz in the Fontainebleau Formation is similar to the microcrystalline quartz in the Heidelberg Formation in that both form from a chalcedony precursor on top of amorphous silica and the two are compared and contrasted in the chapter.

Work contributed: Richard Worden provided editing, advice and the FT-IR analysis, Sasha Haddad provided the samples and this work is based on her Ph.D. thesis and published paper (Haddad et al., 2006), Russ Mueller provided the EBSD assistance, Chris Kliewer provided TEM assistance, Dimitri Sakarov prepared the FIB samples for the TEM, and Joyce Cox provided SEM assistance.

Chapter 6: Electron Backscatter Diffraction investigation of length-fast chalcedony in agate: implications for agate genesis and growth mechanisms

Submitted to: Geofluids, June, 2012

Authors: Marsha W. French, Richard H. Worden and David R. Lee

Idea: This study combines the use of a variety of analytical techniques, including electron backscatter diffraction (EBSD), cathodoluminescence (CL) and Fourier Transform Infrared (FT-IR) spectroscopy, to characterize the silica minerals present in agate and investigate the relationships between them in the banding arrangement. Crystallographic orientation data reveals a strong *a*-axis lineation which is present throughout the sample, suggesting the crystallographic orientation of bands of length-fast chalcedony is related initially to a surface control followed by inheritance of the crystallographic orientation of the preceding band of chalcedony.

Work contributed: Richard Worden provided editing, advice, and FT-IR analysis, David Lee contributed to the manuscript, provided the Lake Superior Agate sample and some of the analysis, Dave Prior and Angela Halfpenny provided helpful discussions and suggestions, Terry Moxon provided the Lake Superior agate sample,

Nick Seaton and Jo Jun provided EBSD expertise, Carol Pinnington and Joyce Cox provided SEM assistance.

2 Amorphous silica nanofilms result in growth of misoriented microcrystalline quartz cement maintaining porosity in deeply buried sandstones

2.1 Abstract

Deeply buried sandstones in sedimentary basins typically have low porosity due to cementation and compaction. There are several known causes of anomalously high porosity in sandstones, one of which is the presence of microcrystalline quartz coatings on sand grains that seems to inhibit growth of quartz cement. However, there has been no mechanistic understanding of why or how microcrystalline quartz grows, or why its presence maintains high porosity in sandstones. High resolution scanning electron microscopy, electron backscattered diffraction and transmission electron microscopy were used to study the microcrystalline quartz cemented Upper Cretaceous Heidelberg Formation, Germany. It was revealed that a nanofilm of amorphous silica (50-100 nm) and a layer of chalcedony sit between the detrital grain and microcrystalline quartz cement. The amorphous silica insulates the detrital quartz grains and prevents syntaxial growth while microcrystalline quartz adopts the orientation of the underlying chalcedony with its fast-growth *c*-axis parallel to the grain surface thus preventing growth into the pore. Now that that the controls on microcrystalline quartz growth and why it preserves porosity have been identified, it can be used to help identify, rank and appraise deeply buried petroleum accumulations.

2.2 Introduction

Finding new petroleum reservoirs in sandstones with high porosity is increasingly important in these times of dwindling resources. In sandstones, the main cause of porosity-loss is quartz cement (McBride, 1989; Worden and Morad, 2000), which forms at temperatures > 80°C, grows syntaxially as simple crystal extensions from

detrital quartz grains and which eventually occludes the pores between host grains. Thus, sedimentary researchers have assumed that when sandstones are buried to temperatures > 100°C, they rapidly loose porosity and have limited reservoir potential. A subset of sandstones, although rich in quartz, contain microcrystalline quartz cement (microcrystalline quartz; defined as 0.5 to 10.0 μm; Vagle et al., 1994) and exhibit anomalously high porosity in deep sedimentary basins (typically > 3500 m). Microcrystalline quartz in sandstones is typically derived from biologically-derived silica (Hendry and Trewin, 1995; Lima and De Ros, 2002; Vagle et al., 1994) and occurs as fine coatings of crystallites on quartz grains that prevent the growth of ordinary quartz cement (Aase et al., 1996; Bloch et al., 2002; Jahren and Ramm, 2000; Lima and De Ros, 2002; McBride, 1989; Vagle et al., 1994). Sedimentary microquartz has been found in Devonian to Miocene sandstones (Haimson and Lee, 2004; Lima and De Ros, 2002) from regions as diverse as Brazil (Lima and De Ros, 2002), Colombia (Warren and Pulham, 2001), the United States (Haimson and Lee, 2004), the North Sea Basins (Aase et al., 1996; Hendry and Trewin, 1995; Ramm et al., 1997; Vagle et al., 1994; Weibel et al., 2010), North Africa (Goldstein and Rossi, 2002) and Saudi Arabia (Cagatay et al., 1996).

Quartz cement grows in optical and crystallographic continuity with the host detrital quartz grain (McBride, 1989). In contrast microcrystalline quartz does not grow in optical continuity with the host quartz grain (Haddad et al., 2006; Hendry and Trewin, 1995). Instead it grows as apparently randomly oriented crystals < 5 μm in length (Vagle et al., 1994). Borrowing from tectonite fabrics, the Heidelberg microcrystalline quartz predominantly displays an “S” fabric or planar fabric (strong c-axis orientation, but somewhat randomly oriented in the a-axes) and could be termed an S-diagenite, while the Fontainebleau microcrystalline quartz displays a linear or “L” fabric (some control on the linear a-axes), as well as, the “S” fabric and could be termed an LS-diagenite. It is routinely associated with sandstone beds rich in biogenic silica, such as sponge spicules (Aase et al., 1996; Hendry and Trewin, 1995) and seems to develop at the expense of bioclasts at temperatures of about 50°C (Vagle et al., 1994). Once detrital grains have a continuous coating of microcrystalline quartz, the overgrowth of optically- and crystallographically-continuous quartz cement is prevented. Therefore, early microcrystalline quartz inhibits ordinary quartz cement growth, preserves

porosity and leads to anomalously high porosity in deeply buried petroleum sandstone reservoirs. It has been suggested that elevated silica saturation, resulting from the very presence of microcrystalline quartz, inhibits quartz dissolution during burial and prevents quartz cementation (Hendry and Trewin, 1995), but until now there has been no mechanistic data that explains why or how microcrystalline quartz grows.

In order to understand the mechanism responsible for the growth of misoriented microcrystalline quartz, sandstone samples from the Upper Cretaceous Heidelberg Formation in the Subhercynian Basin, Germany (Voigt et al., 2006) were studied. While microcrystalline quartz has been previously studied with light microscopes and SEMs (Aase et al., 1996; Hendry and Trewin, 1995; Ramm et al., 1997; Vagle et al., 1994; Weibel et al., 2010), this study utilized high resolution electron microscope techniques to study the microcrystalline quartz and its relationship with the host grain. The aim of this study was to assess the crystallographic orientation of microquartz crystals relative to their host quartz grains, to understand the mechanism of microcrystalline quartz growth and to determine the controls on the misorientation of microcrystalline quartz.

2.3 Methods

High resolution secondary electron images (SEI) and backscattered electron images (BSEM) were acquired using a JEOL 6330F field emission gun-SEM. Electron backscatter diffraction (EBSD) analysis was performed on polished thin sections using a LEO 1530 SEM fitted with an Oxford-HKL EBSD system. Samples were prepared for TEM analysis using a FEI NOVA 200 focused ion beam (FIB) SEM at Purdue University in the Birck Nanotechnology Center. Samples were analysed in a Philips CM200F TEM/STEM transmission electron microscope operated in the bright field TEM imaging mode at an accelerating voltage of 200kV.

2.4 Results

High resolution secondary electron images (SEI) revealed the morphology of the microcrystalline quartz and its relationship to the host quartz grain surface.

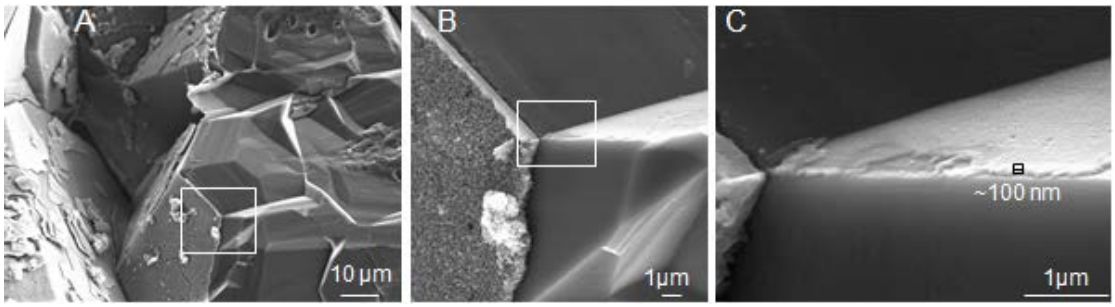

Figure 2.1 - High resolution secondary electron images (SEI) of surface coating at increasing magnifications (A) x1,000, (B) x5,000 (C) x25,000. These show that the initial surface coating (C), before microcrystalline quartz growth, is approximately 50-100 nanometres in thickness. Megaquartz facets represent pre-existing overgrowths which is syntaxial quartz overgrowth cement beneath the silica surface coating.

In these rocks, a microcrystalline quartz coating, with a thickness of approximately 1 µm, has grown over pre-existing syntaxial quartz cement (Figs. 2.1A and B). At the highest resolution, a ~ 50-100 nm film is also observed lying between the host quartz sand grain and the microcrystalline quartz crystals (Figs. 2.1B and C).

To gain insight into the orientation of the microcrystalline quartz and its crystallographic relationship with the detrital host grain, electron backscattered diffraction (EBSD) analysis was performed on polished thin sections from the Heidelberg sandstone. The EBSD analyses confirmed that the microcrystalline quartz is misoriented with respect to the host grain. This is represented by the multiple colour variations of the microcrystalline quartz crystals relative to the host detrital grain in EBSD images. Figure 2.2 is an EBSD orientation map (Band Contrast + All Euler + Grain Boundary 10). Texture component maps for each grain in Fig. 2.2 show that none of the microcrystalline quartz inherit the crystallographic orientation of the adjacent host grain (See Appendix Vol. 2, Samples Teufelsmauer EBSD).

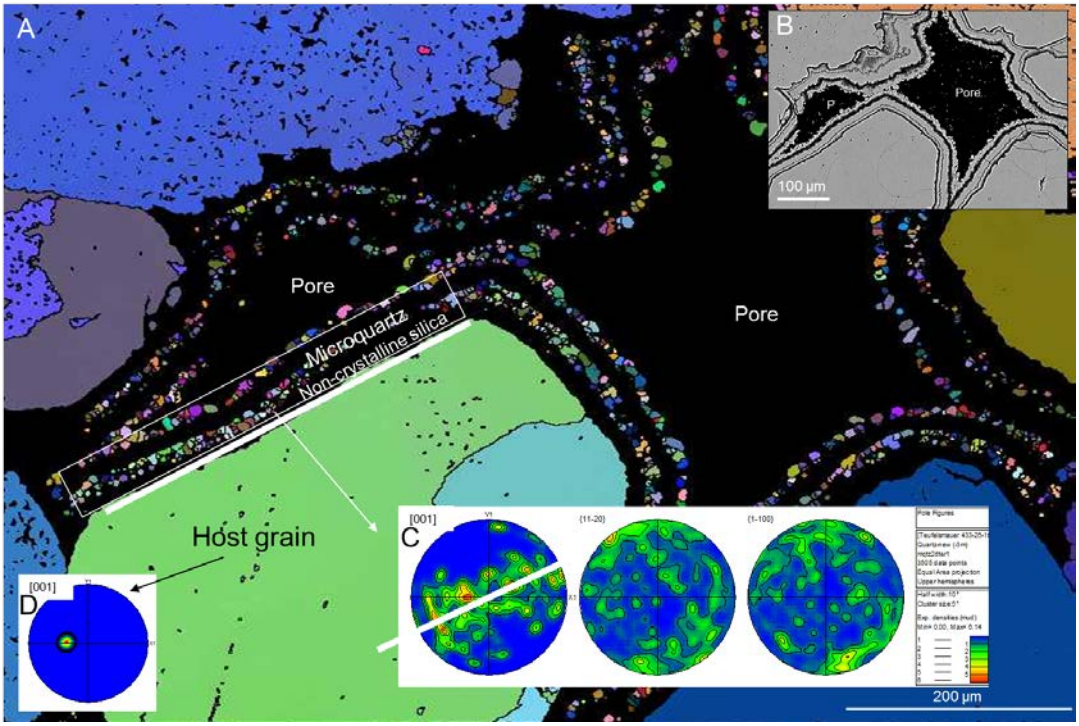

Figure 2.2 (A)Electron backscatter diffraction (EBSD) orientation map showing host grain orientation and microcrystalline quartz (multiple colours) indicating that the crystallographic orientations of the host grain and the adjacent microcrystalline quartz crystals are different. (B) Electron back-scatter image of the area revealing the pore space and that even the un-indexed layers of cement are composed of silica. (C) Pole figure of the c-axis orientation of the microcrystalline quartz on the surface of the host grain. The orientation of the microcrystalline quartz is spread in a girdle parallel to the host surface. The trace of a "great circle" of these microcrystalline quartz data, shown by the white line, matches the orientation of the face of the host grain (white line) indicating that the material on the surface of the host grain is controlling the growth of the microcrystalline quartz. (D) Pole figure of the *c*-axis orientation of the host grain showing that the microcrystalline quartz is not syntaxial.

Although one previous study quantified the degree of misorientation of microcrystalline quartz (Haddad et al., 2006), there has been no evidence, prior to this study, that misorientation was controlled in any way. In the Heidelberg microcrystalline quartz there is a distinct control on the misorientation. Quartz has trigonal symmetry and thus the angle between the [11-20] direction and *c*-axis is 90º. Quartz typically grows faster in the prismatic *c*-axis direction (Lander et al., 2008). Directions of *c* axes of a subset of the Heidelberg microcrystalline quartz crystals adjacent to the host grain (white rectangle) were plotted on a stereogram (Fig 2.2C). The orientations of the *c*-axes from the microcrystalline quartz crystals are arranged in a great circle (whose trace is indicated by white line on the figure) rotating within the

plane of the quartz grain facet, with a ±15° extent of scatter. This pattern indicates that crystals of microcrystalline quartz have grown with their *c* axes parallel to, but rotated) on the host quartz grain surface. In the Heidelberg microcrystalline quartz, in every pore examined, the microcrystalline quartz has its fast-growth *c*-axis parallel to the host grain surface. Given that the *c* axes are parallel to the grain surface, the [11-20] directions are perpendicular to the grain surface. This is consistent with the silica polymorph chalcedony (Flörke et al., 1983; Miehe et al., 1984) which has [11-20] (perpendicular to the *c*-axis) as the fast growth direction. However, chalcedony crystals are < 200 nm in size (Graetsch, 1994; i.e. below detection with this EBSD); what is actually observed is microcrystalline quartz that has adopted the orientation of chalcedony. The implication is that microcrystalline quartz inherited its *c*-axis orientation from pre-existing chalcedony adjacent to the largely amorphous silica nanofilm, the black area between the host grain and the microcrystalline quartz in Fig. 2.2.

This leads to a question of the nature of the ~ 50-100 nm film. EBSD analysis revealed layers within the cement that could not be "indexed" *(i.e.* crystallographically-resolved) despite being silica (SiO_2) as defined by backscatter electron microscopy (Fig. 2.2A) and energy dispersive X-ray analysis. Two options to explain the lack of indexing are that the crystal size was below the detection limit of this technique (i.e. < 0.2 μm), or that the un-indexed layer is amorphous silica. To investigate further the surface material between the host detrital grain and the microcrystalline quartz, samples were prepared with a focused ion beam (FIB) SEM and examined with a transmission electron microscope (TEM). The FIB-SEM samples were all cleaned with a low energy milling strategy to remove any amorphous silica from beam damage during preparation.

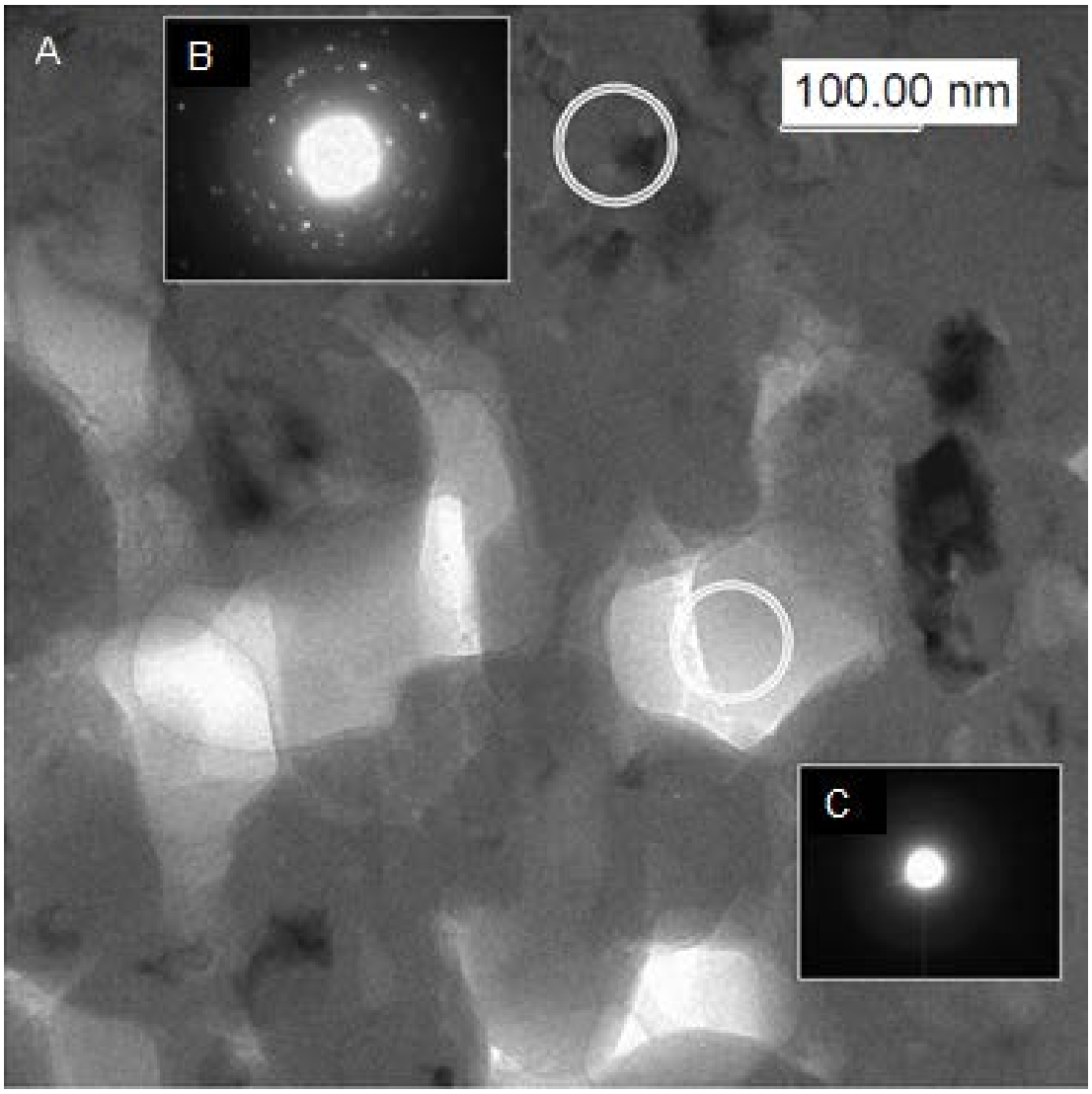

Figure 2.3 (A) Bright field TEM image at a magnification of approximately 200,000 showing crystalline material, amorphous material and their respective microdiffractions. (B) Microdiffraction of material in adjacent circle showing crystalline diffraction patterns with some degree of rotation suggested in the diffraction spots. (C) Microdiffraction of material in adjacent circle showing only the transmitted beam (no diffracted intensities); evidence for amorphous silica.

Figure 2.3 is a TEM image of the surface nanofilm lying beneath the microcrystalline quartz. Selected area electron diffraction patterns demonstrate that part of the surface material is composed of nanometre-sized crystals of crystalline silica (Fig. 2.3B). The hint of rotation of the diffraction spots (Wahl et al., 2002) and the very small size of the crystals (Graetsch, 1994) suggests that this material may have been chalcedony. However, there is also material which did not diffract the electron beam (Fig. 2.3C)

proving that the nanofilm contains amorphous silica. This amorphous nanofilm is ubiquitous on the sand grain surfaces.

2.5 Discussion

Opaline (amorphous) silica transforms to quartz via a series of metastable intermediates (Williams and Crerar, 1985; Williams et al., 1985) (Opal A → Opal CT → cryptocrystalline quartz or chalcedony → microcrystalline quartz). It is unlikely that quartz would co-precipitate with amorphous silica since quartz grows much more slowly than amorphous silica (Rimstidt and Barnes, 1980). The occurrence of a cryptocrystalline phase within amorphous silica thus suggests that the amorphous phase has undergone partial transformation to quartz during the long history of this Cretaceous rock. The presence of the amorphous silica between the host grain and the microcrystalline quartz therefore suggests that it was a precursor to the microcrystalline quartz.

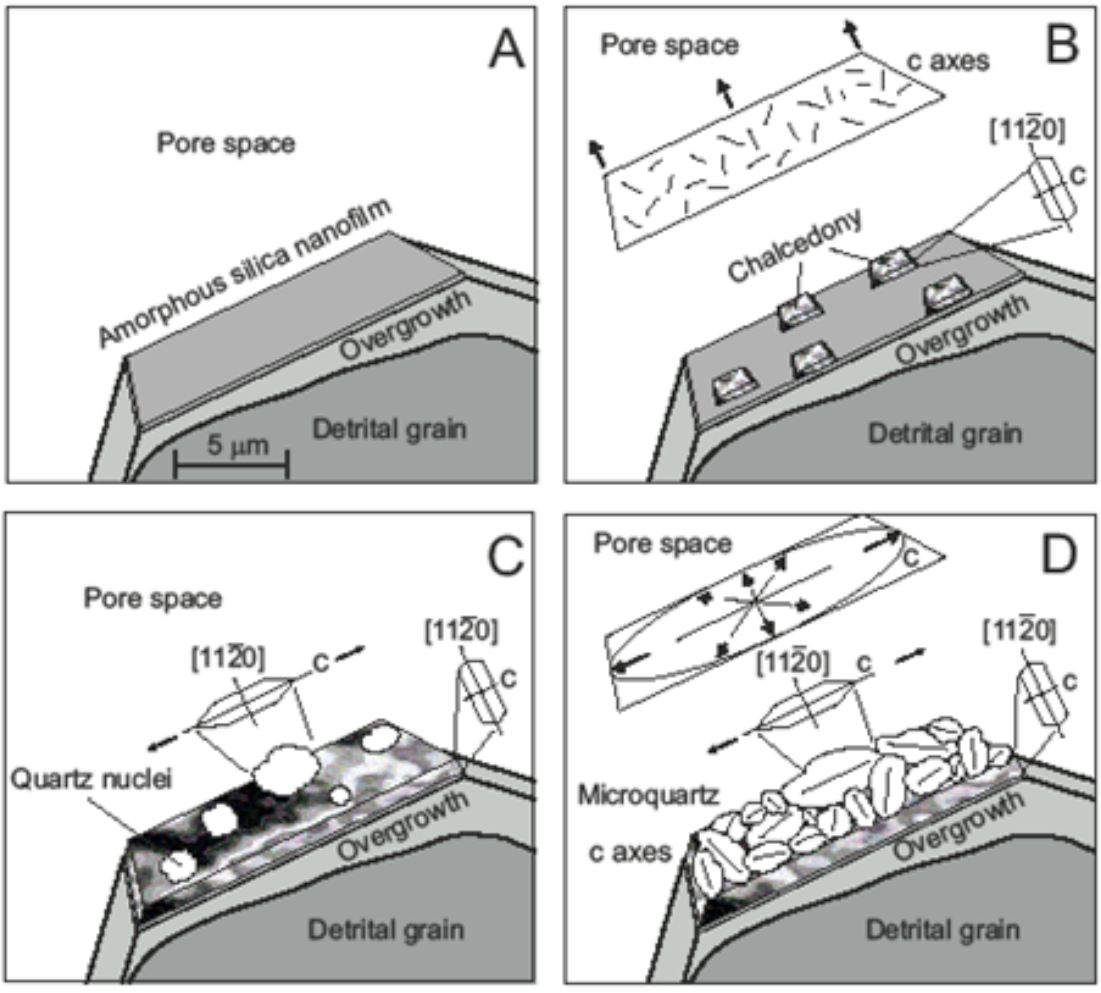

Figure 2.4 - Model showing microcrystalline quartz growth on amorphous silica nanofilms, with chalcedony. (A) During early diagenesis, quartz overgrowths form around detrital quartz sand grains. These have the same crystallographic orientation as the detrital grain and tend to fill and close pore spaces. An amorphous silica nanofilm is deposited on the overgrowth. (B) Fibrous crystals of chalcedony crystallise in the amorphous silica and grow into the pore space along their [11-20] directions. In quartz, the *c*-axis is always perpendicular to [11-20]; therefore, due to the growth direction of chalcedony, *c* axes are somewhat rotated within the nanofilm plane. (C) Microcrystalline quartz nucleates on the chalcedony-coated substrate and uses the chalcedony crystal structure and orientation (*c*-axis parallel to grain surface) as a template. (D) Microcrystalline quartz then grows along the *c*-axis and sub-parallel (within a few degrees) to the nanofilm plane. Further growth is inhibited when microcrystalline quartz crystals impinge on each other. No significant quartz growth into the pore occurs. Scale is reported in (A). All thicknesses are exaggerated for clarity. Black arrows indicate the direction of growth.

Figure 2.4 illustrates the possible sequence of diagenetic events starting with the initial deposition of the amorphous silica nanofilm (Fig. 2.4A). The next step is the proposed development of chalcedony within the amorphous silica with the [11-20] direction (its fast growth axis; Flörke et al., 1982; Heaney et al., 1994) perpendicular to the host grain surface (Fig. 2.4A). Microcrystalline quartz nucleates on the chalcedony layer, inheriting its *c*-axis surface-parallel orientation (Fig. 2.4C). Microcrystalline quartz continues to grow with its *c* axes parallel to the surface of the grain (Fig. 2.4D). This has important implications for how porosity is preserved in deeply buried sandstone reservoirs.

Traditionally, sandstone reservoirs below ~ 4,000 metres have not been explored due to the assumption that above ~ 80°C syntaxial quartz overgrowths would have progressively occluded porosity. During ordinary quartz cement growth in sandstones, quartz crystals (50-100 μm) grow into pore spaces after burial, inheriting the exact crystallographic orientation of the host detrital quartz grain upon which they have grown. In contrast, misoriented microcrystalline quartz crystals (0.1-5 μm), preserve porosity by coating the surface of the host detrital sandstone grain during early diagenesis. Biogenic amorphous silica, co-deposited with the sand when there is a supply of sand-grade siliceous bioclastic debris to the sediment, undergoes dissolution during relatively early burial. This leads to very high silica saturations, which ultimately results in a 50-100 nm film of amorphous silica on all grain surfaces once the critical saturation is exceeded (Williams and Crerar, 1985).

The initial amorphous silica subsequently underwent partial crystallisation and is now an intergrowth of chalcedony and remnant amorphous silica. As silica concentration decreased, chalcedony may have been precipitated with its [11-20] direction perpendicular to the grain surfaces (*c* axes oriented parallel to the grain surface). Initial microcrystalline quartz growth followed as silica concentration progressively declined. This combination of amorphous silica nanofilm, [11-20] growth for chalcedony and planar oriented (S-diagenites) *c* axes of microcrystalline quartz (parallel to the host surface) inhibits the growth of large single crystals of quartz. The inhibition is due to two factors: first the clean surface of detrital quartz is coated by the combination of amorphous silica and chalcedony masking any nucleation sites for quartz overgrowths; second, the fast growth direction of microcrystalline quartz is parallel to the grain surface preventing any significant growth into the pore. Together these inhibit syntaxial quartz growth and preserve anomalously high porosity in deep sandstone reservoirs.

Understanding that an amorphous silica precursor, and microcrystalline quartz fast growth direction being parallel to the grain surface, are necessary for porosity preserving microcrystalline quartz growth is the first step in developing a novel predictive model for the preservation of anomalously high porosity in deep, high-temperature sandstone reservoirs. Now that why and how microcrystalline quartz preserves porosity in deeply buried sandstones is known it can be confidently used as a way to help rank potential exploration targets. Sandstones expected to contain microcrystalline quartz will have a lower risk of poor reservoir quality than those without microcrystalline quartz. Prediction of the co-deposition of the essential bioclastic amorphous silica precursor in sandstone requires further research but there are likely to be clear stratigraphic, palaeoenvironment and palaeolatitude controls. Now that it is known that high silica saturations are required to create the amorphous silica layer that results in misoriented microcrystalline quartz there may be other, non-biogenic mechanisms by which high silica saturations can form in sandstones. These may include: detrital chert-bearing sandstones, zeolite- or smectite-cemented sandstones and hydrothermally-altered sandstones, although all of these have other reservoir quality issues due to either ductile deformation or clay mineral problems for reservoir quality (Worden et al., 2000) that potentially render them poor exploration targets.

3 Generation of microcrystalline quartz and the preservation of porosity in sandstones: evidence from the Upper Cretaceous of the Subhercynian Basin, Germany

3.1 Abstract

Formation of microcrystalline quartz has proven to be effective at preserving porosity in deeply buried sandstone petroleum reservoirs, typically cemented by syntaxial quartz cement. There remains much uncertainty about what controls the growth of microcrystalline quartz and how it prevents syntaxial quartz overgrowths. Here, the Cretaceous Heidelberg Formation, Germany, provides a natural laboratory to study silica polymorphs and develop an understanding of their crystallography, paragenetic relationships, and growth mechanisms, leading to a new understanding of the growth mechanisms of porosity-preserving microcrystalline quartz. Data from scanning electron microscopy (SEM), electron backscatter diffraction (EBSD), and transmission electron microscopy (TEM) illustrate that porosity-preserving microcrystalline quartz cement is misoriented with respect to the host grain upon which it grows. In contrast, ordinary quartz cement grows in the same orientation (syntaxially) as the host quartz sand grain, and typically fills pore spaces. EBSD and TEM observations reveal nanofilms of amorphous silica (~ 50-100 nm in thickness) between the microcrystalline quartz and the host grain. The microcrystalline quartz is interpreted to be misoriented relative to the host grain, because the amorphous silica nanofilm prevents growth of syntaxial quartz cement. Instead, the microcrystalline quartz is similar to chalcedony with [11-20] perpendicular to the growth surface and *c* axes parallel with, but distributed (rotated) on, the host quartz grain surface. Development of pore-filling quartz growing into the pore (in the fast-growing *c*-axis direction) is thus inhibited due to the amorphous silica nanofilm initially and, subsequently, to the misoriented microcrystalline quartz that grew on the amorphous silica.

3.2 Introduction

Authigenic quartz cement is the most important pore-occluding mineral in deeply buried (> 2500 m) sandstone (Sorby, 1880; Worden and Morad, 2000). However, some deeply buried reservoirs contain more porosity than predicted by existing conceptual models of quartz cementation (e.g., Lander et al., 2008). These conceptual cementation models commonly fail to predict the occurrence of anomalous porosity in reservoirs hotter than 80ºC, confirming that our understanding of quartz diagenesis is still limited. Several oil fields have been identified with anomalous porosity which occurs in association with microcrystalline quartz, and appears to preserve porosity by inhibiting quartz overgrowths. Microcrystalline quartz cement coating the surfaces of grains in sandstone has been previously identified in numerous studies (McBride, 1989; Ramm, 1992; Vagle et al., 1994; Aase et al., 1996; Jahren and Ramm, 2000; Lima and De Ros, 2002; and Aase and Walderhaug, 2005). In the North Sea Basin, microcrystalline quartz occurs in sandstone reservoirs that contained biologically derived amorphous silica (sponge spicules) (Vagle et al., 1994; Lima and De Ros, 2002). Although microcrystalline quartz has been observed in numerous previous studies noted above, the growth mechanisms of microcrystalline quartz, and how it inhibits ordinary quartz cement, have only recently been investigated. For example, microcrystalline quartz cement growth on detrital quartz sand grains was recently studied and documented using electron backscatter diffraction (EBSD) (Haddad et al., 2006), and is the only previous study to quantify the misorientation of microcrystalline quartz.

These results distinguish between microcrystalline quartz and chalcedony. Chalcedony, with a [11-20] fast growth direction, has been defined as being less than 0.5 μm in size (Heaney, 1993; Florke et al., 1991). In contrast, microcrystalline quartz, with a *c*-axis fast growth direction, is here defined as being between 0.5 and 10 μm in size. Microcrystalline quartz was previously defined as between 5 and 10 μm (Vagle et al., 1994) or between 0.5 and 5 μm in size (Aase and Walderhaug, 2005). The range of 0.5 and 10 μm was selected to take microcrystalline quartz down to the maximum size of chalcedony crystals of Vagle et al., 1994.

Questions remain about microcrystalline quartz, including aspects of crystallography, paragenetic relationships, and growth mechanisms of the silica polymorphs. In this context, this paper describes a study of the growth of microcrystalline quartz using advanced electron optic studies of the Heidelberg Formation in Germany, addressing the following questions:

1) What silica polymorphs occur in the Heidelberg Formation?

2) What is the paragenesis of the silica polymorphs?

3) What is the growth mechanism for porosity-preserving microcrystalline quartz?

The results of this study provide insights into the growth mechanism for microcrystalline quartz and porosity preservation in sandstone reservoirs.

3.3 Geological setting

The Subhercynian Cretaceous Basin is located at the northern border of the Paleozoic-cored Harz Mountains and forms a narrow syncline approximately 90 km in length

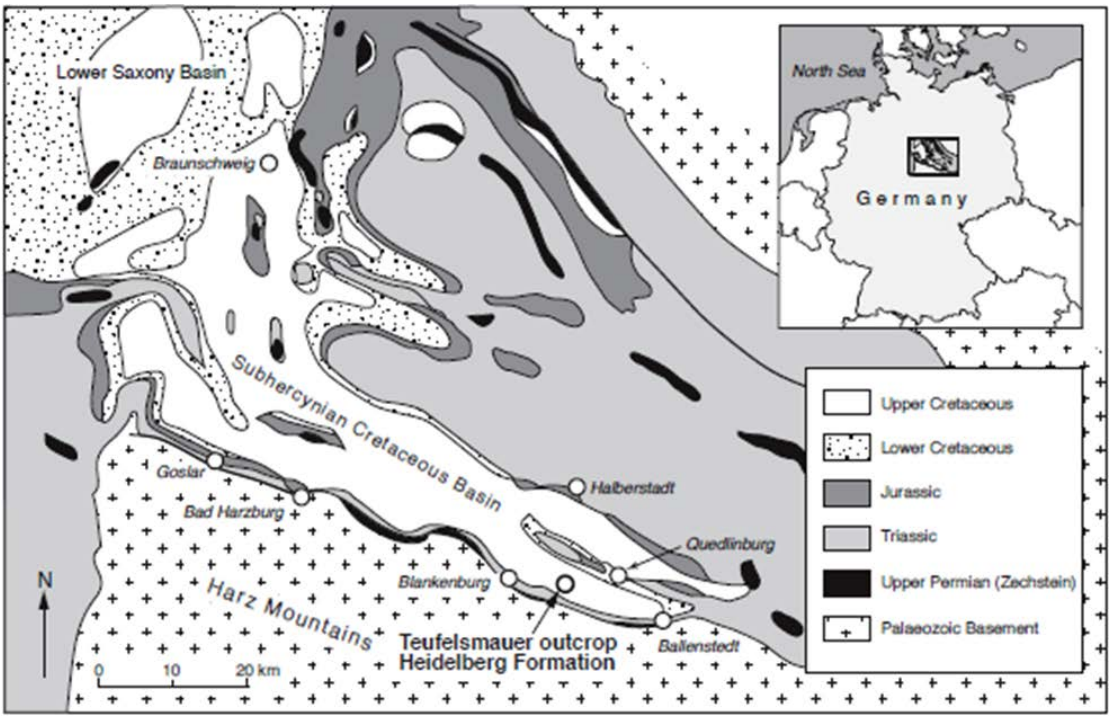

Figure 3.1 Outcrop map of the Harz Mountains, the Subhercynian basin, and surrounding outcrop geology (after von Eynatten et al. 2008). The Teufelsmauer outcrop and the Heidelberg Formation are marked.

The basin contains an Upper Cretaceous succession greater than 2000 m thick from Lower Cenomanian transgressive limestones to Lower Campanian siliciclastics (Troger, 1995; Voigt et al., 2006). It has a strong asymmetric shape similar to many foreland basins, with the strongest subsidence near the northern Harz Thrust. Thrusting of the Harz Mountains onto its foreland led to flexuring of Permian to Upper Cretaceous strata that now form a steeply dipping sequence in front of the Harz Mountains (Franzke, 1990; Voigt et al., 2004). Exhumation and thrusting of the Harz Mountains occurred largely in the Coniacian to Early Campanian (Voigt et al., 2006; von Eynatten et al., 2008). The Harz Mountains mining district has been operating since the Thirteenth century and is a known source of hydrothermal copper-lead-zinc ore deposits (Liebmann, 1992).

The Heidelberg Formation consists mainly of marine, fine-grained, variably quartz-cemented sandstones (Voigt et al., 2006). The formation is approximately 400-500 m thick and covers the eastern Subhercynian Cretaceous Basin between Quedlinburg and Blankenburg, Germany. The highly cemented Teufelsmauer (Devil's Tower) outcrop is formed by the Königsteine and Mittelsteine cliffs and consists of almost vertically dipping Upper Santonian quartz arenites of the Heidelberg Formation. In contrast to the cliff-forming steeply inclined sandstones in the Teufelsmauer outcrops, flat-bedded sandstones of the Heidelberg Formation occur as virtually unconsolidated sediments approximately 400 metres away. The quartz cements in the Heidelberg Formation have some unusual characteristics (Waldmann, 2006) reminiscent of the microcrystalline-quartz and amorphous-silica-bearing Oligocene Fontainebleau Formation in France (Haddad et al., 2006). Therefore a range of high-resolution electron optic techniques were selected to study the cements in the Heidelberg Formation.

3.4 Samples and methods

3.4.1 Samples

Outcrop samples from the Heidelberg Formation were collected by C. Fischer and S. Waldmann (University of Göttingen, Germany) and described in the Ph.D. thesis of

Waldmann (2006). Three of these samples were analysed for porosity-preserving microcrystalline quartz. The samples were made into 30 µm thin sections after impregnation with blue-stained epoxy resin for porosity identification. After standard polishing, thin sections were chemically polished to high quality using colloidal silica (Flynn and Powell, 1979; Lloyd, 1987; Prior et al., 1996) for several hours, to remove any mechanical damage to the surface and to enable the best possible electron backscatter diffraction (EBSD) analysis. Samples were carbon-coated using a Cressington 208 Carbon Coater (< 10 nm thickness). A variety of analytical techniques including transmitted-light optics, scanning electron microscopy, electron backscatter diffraction, and transmission electron microscopy were used in this study.

3.4.2 Transmitted-Light Optics

Transmitted-light optical analysis identified and located quartz overgrowths and microcrystalline quartz on detrital host quartz grains. The location of the quartz overgrowths was based on the identification of euhedral grains, with sharp, clean edges and, to some extent, on the presence of dust rims. Microcrystalline quartz lining the pore spaces was identified with a petrographic microscope, but due to the small size, microcrystalline quartz is best characterized with the scanning electron microscope.

3.4.3 Scanning Electron Microscopy (SEM)

Scanning electron microscopy resolved microcrystalline quartz by its high resolution capabilities. High-resolution secondary electron images (SEI) and backscattered electron images (BEI) were acquired using a JEOL 6330F FEG-SEM and a JEOL 6490LV SEM.

3.4.4 Cathodoluminescence (CL)

Cathodoluminescence study identified and distinguished detrital quartz grains from syntaxial quartz overgrowths and microcrystalline quartz (Evans et al. 1994). CL

images were taken with an accelerating voltage of 10 kV (in contrast to 20 kV for BSE), 8 nA beam current, and 16.5 mm working distance. CL images were collected by accumulating a signal of 500 frames using a slow-scanning raster, and red, green, and blue wavelength CL were collected and added using processing to produce a ChromaCL image. A JEOL 6490LV SEM, fitted with a Gatan cathodoluminescence detector (ChromaCL-006), was used for cathodoluminescence analysis.

3.4.5 Electron Backscatter Diffraction (EBSD)

The principles and techniques of EBSD have been explained in previous papers (e.g., Venables and Harland, 1973; Dingley, 1984; Schmidt and Olesen, 1989; Adams et al., 1993; Wilkinson and Hirsch, 1997; Prior, 1999; Prior et al., 2009). This paper is the third investigation (following Haddad et al., 2006, and Mörk and Moen, 2007) to utilize EBSD to address sandstone diagenetic questions. EBSD has the capability to resolve the crystallographic orientations at a resolution as small as 200 nanometres to reveal microstructural information about the crystal structure and mineralogy of the material being analysed. This technique has guided interpretations regarding the growth mechanisms of microcrystalline crystals. EBSD analysis was performed on polished thin sections using a LEO 1530 SEM fitted with an Oxford-HKL EBSD system. EBSD patterns were auto-indexed using the CHANNEL 5 software from Oxford Instruments HKL A/S. The software was used to display maps and pole figure data.

3.4.6 Transmission Electron Microscopy (TEM)

TEM is capable of imaging at markedly higher resolution than light microscopes and, with selected area electron diffraction (SAED), has been used to characterize crystal structure and microstructures in various silica polymorphs (Wahl et al., 2002; Graetsch et al., 1987; Miehe et al., 1984; and Heaney et al., 1994). This technique was used in this study to distinguish the different silica polymorphs. A focused-ion-beam scanning electron microscope (FIB-SEM) was used to prepare samples for TEM analysis. The FIB-SEM uses a finely focused beam of ions (generally gallium) that can be operated at a high beam current for milling the sample. Beginning with the

thin section (Figure 3.2A), the sample is first examined with a petrographic

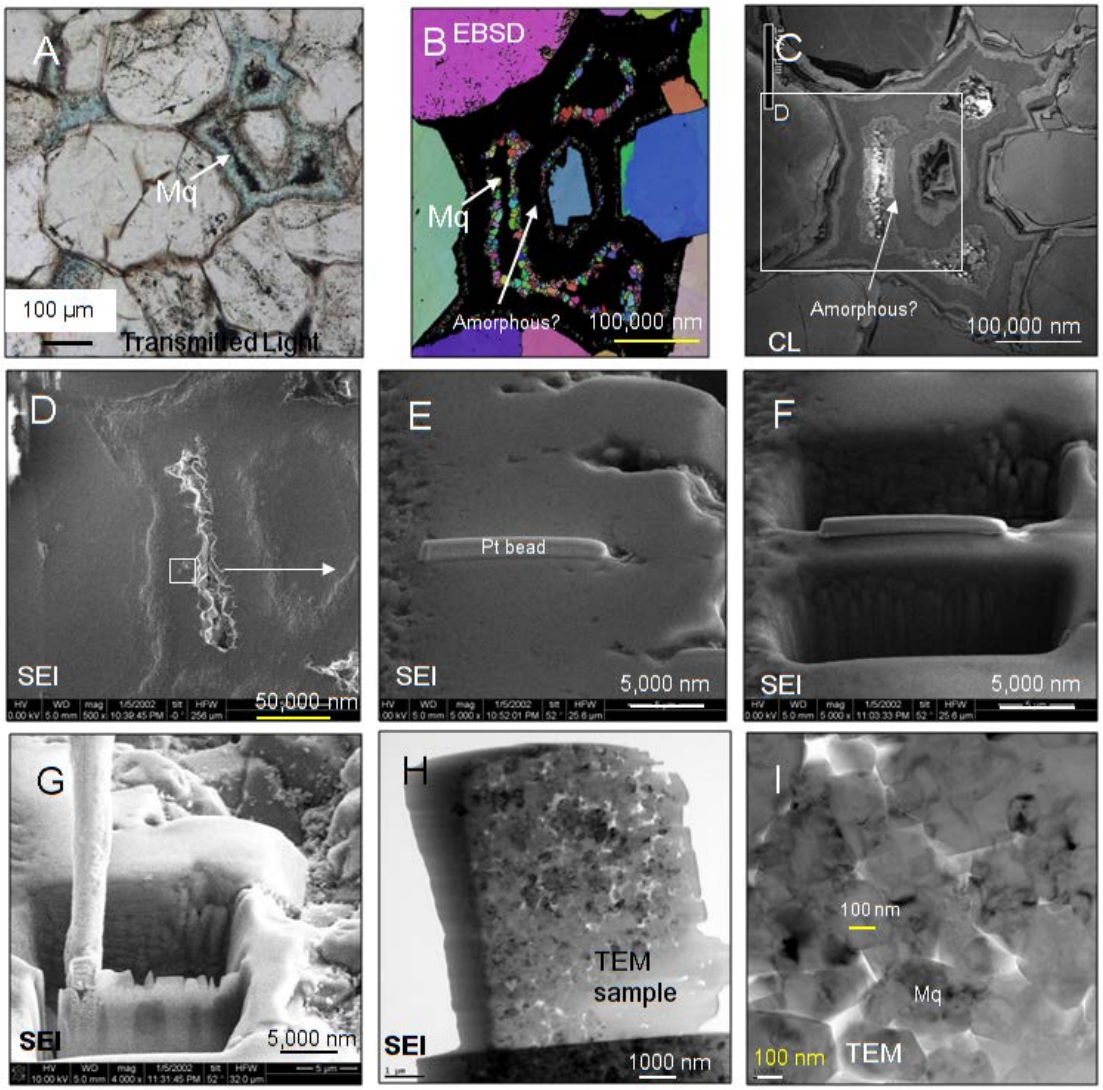

Figure 3.2 Images showing FIB-SEM steps for preparing a sample for TEM. A) petrographic microscope image showing area of interest, B) electron backscatter diffraction image showing microquartz and non-indexed zone postulated to contain amorphous silica, C) red spectrum cathodoluminescence image showing area of interest, D) area of interest at 500x, E) image from Part D with platinum bead (Pt bead) on the surface of the sample, F) previous image showing that the FIB-SEM gallium beam has milled out the area in front of, and behind, the platinum-bead-protected sample, G) probe attached to the sample, H) the prepared TEM sample and I), TEM photograph of small crystals. Mq refers to microcrystalline quartz.

microscope to identify the area of interest, then with EBSD to identify the non-diffracting zone (Fig. 3.2B), and finally with CL to focus on the area to sample (Fig. 3.2C). The additional figures show each step of the sample preparation in the FIB-SEM, which involves depositing a platinum bead on the surface to be ion milled (3.2E), milling in front of and then behind the sample with the gallium beam (3.2F),

attaching a probe using a platinum bead (3.2G), and finally extracting the sample from the thin section (3.2H). The final photograph (3.2I) is the sample in the TEM showing the size of the crystallites. The TEM samples were prepared using a FEI NOVA 200 focused-ion-beam (FIB) SEM at Purdue University in the Birck Nanotechnology Center. Ten TEM samples from samples 1 and 3 were prepared using the above procedure so that each band from the detrital grain into the porosity was sampled. Samples prepared using FIB-SEM were then analysed in a Philips CM200F TEM/STEM operated in the bright-field imaging TEM mode at an accelerating voltage of 200 kV.

3.4.7 Laboratory Studies

Experimental quartz diagenesis was conducted in the laboratory to test the hypothesis that microcrystalline quartz inhibits the development of quartz overgrowths thereby preserving porosity. The experiments were conducted using the techniques developed by Heald and Renton (1966). Heidelberg Formation sample 2, which has microcrystalline quartz coatings similar to samples 1 and 3, was placed in a Hastelloy hydrothermal reactor at 305^{o} C with a 0.03M Na_2CO_3 solution at 69 Mpa (10,000 psi) pressure for 7 days, using a natural quartz sandstone (Jordan Sandstone from Wisconsin) as a silica source (after being photographed in SEM). Sample 2 was placed in the reactor, and a temperature differential between the source Jordan Sandstone (high temperature) and the Heidelberg Formation sample (low temperature) was imposed to induce fluid convection. The reactor was divided into two isothermal zones by a perforated copper baffle that served to control circulation. Sample 2 was placed in the upper zone of the reactor, and natural (sacrificial) quartz grains were placed in the lower zone of the reactor to serve as the source material for microcrystalline quartz and overgrowths. The experimental materials were removed from the reactor after seven days and analysed using the SEM to document the changes in the growth of quartz overgrowths and microcrystalline quartz.

3.5 Results

3.5.1 Transmitted-Light and SEM Analysis

Optical images of sample 1 (Fig. 3.3A) show cemented quartz grains which are subangular with some strong angular facets caused by quartz cementation. Optical images of sample 1 (Fig. 3.3A) also highlight the presence of concentric layers which are parallel to the surface of the detrital host grain, but with large areas of porosity between the grains and pore-lining microcrystalline quartz. The secondary electron image (SEI) (Fig. 3.3B) shows that SEI cannot distinguish between the quartz overgrowths and the detrital host grains. It also highlights that concentric layers with microcrystalline quartz are the final layer of the diagenetic quartz-generated cement. The BSE image (Fig. 3.3C) shows several dark bands alternating with lighter bands within the overgrowth and cement parallel to the edges of earlier overgrowth rims. Each lighter band follows the same pattern and direction as the previously described darker band. These lighter bands correspond to the concentric layers (Fig. 3.3A). The rest of the BSE image has a uniform signal, suggesting that the overgrowth is pure silica (confirmed by secondary X-ray analysis using energy-dispersive spectroscopy (EDS) in the SEM).

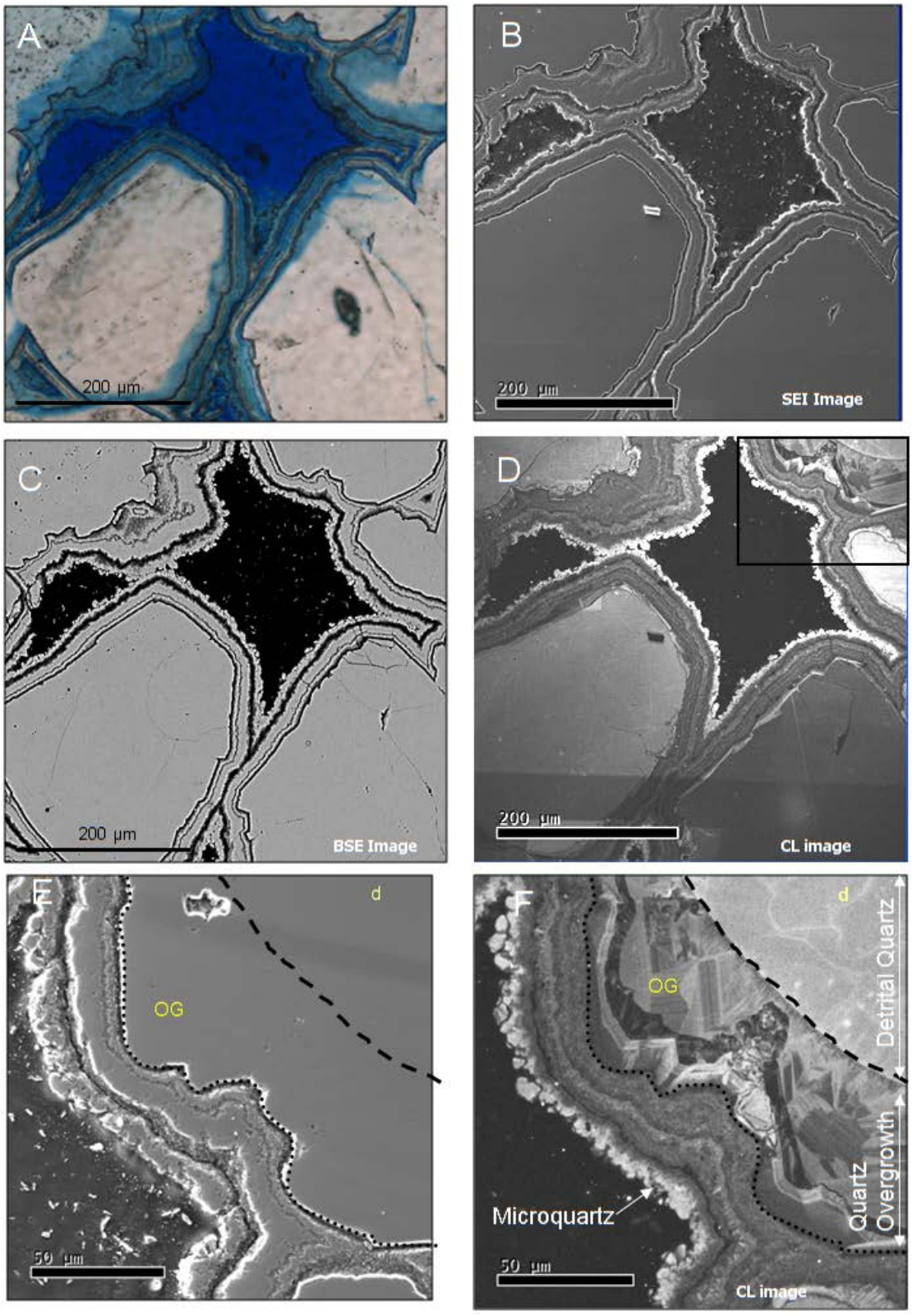

Figure 3.3 A) Petrographic microscope image of the angular cemented quartz grains and the concentric, isopachous layers parallel to the detrital grain or overgrowth edges with porosity in blue. B) Secondary electron image of the pore shown in Part A, C) backscatter electron image of the pore in Part A, D) red

spectrum cathodoluminescence image of the pore and index box for E) SEI image and F) red spectrum cathodoluminescence image which differentiates the quartz overgrowth ("OG") from the detrital grain "d". The electron backscatter image of the pore reveals that the grains and cements are composed of silica.

3.5.2 Cathodoluminescence (CL) Analysis

The CL images (Figs. 3.3D and 3.3F) discriminate the detrital grains that luminesce brightly, zoned overgrowths with highly variable luminescence, the brightly luminescent microcrystalline quartz which coats the edge of the pore, and the nonluminescent porosity. The edge of the overgrowth can be mapped using the SEI image and BSE image and is differentiated by the smoothness of the polished surface, which matches the boundary of the complex growth history in CL versus the first concentric layer parallel to the overgrowth edge (Figs. 3.3D, E, F). Whereas the BSE and CL images can differentiate several bands and the complexity of the quartz overgrowth (Fig. 3.3F), integrating BSE and CL with EBSD is an optimal approach for differentiating the concentric layers.

3.5.3 SEM-BSE, SEM-CL, and EBSD Analysis

The significance of the range of BSE and CL characteristics was examined through EBSD analysis (Fig. 3.4). The concentric layers can be divided into four bands, which repeat once, totalling eight distinct bands (Figs. 3.4A, B, C, D). Band 1 resides on the surface of the detrital host grain and is a very thin dark band in BSE and CL that is less than 1 µm in thickness. Band 2 is brighter in CL, BSE, and EBSD, and is 5-8 µm in thickness. Band 3 is a second dark band in CL and is 8 to10 µm thick. The last phase of cement growth (band 4) occurs as a microcrystalline quartz band (as defined by Vagle et al., 1994 and Lima and De Ros, 2002), which has many small (0.5 to 10 µm) individual quartz crystals in a band between 2 and 4 µm thick. The layer then repeats the four bands with similar thicknesses and alternating light and dark bands in CL and BSE, culminating in a second final bright band of microcrystalline quartz. The microcrystalline quartz luminesces quite brightly and propagates along the edge of the pores (Fig. 3.4D).

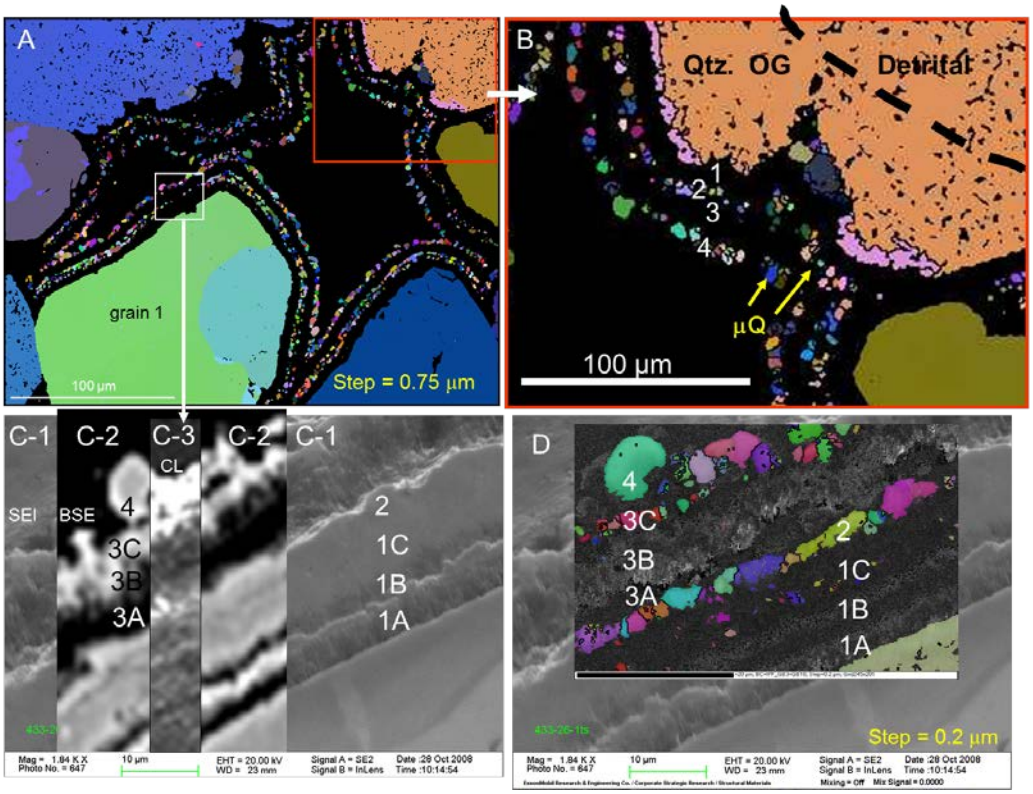

Figure 3.4 A) Electron backscatter diffraction (EBSD) orientation map (step size 0.75 µm) showing host grain (labelled grain 1) orientation (green) and microcrystalline quartz (multiple colours) indicating that the crystallographic orientation of the microcrystalline quartz crystals adjacent to the host grain (i.e., the microcrystalline quartz) is crystallographically misoriented with respect to the host grain. B) EBSD orientation map of a subsection of the image in Part A showing that the quartz overgrowth and detrital grain do not show any colour variation indicating there is no difference in the crystallographic orientation of the detrital host grain and quartz overgrowth. C) Composite SEI (C1), BSE (C2), and CL (C3) image of another subsection of Part A. D) Same as Part C with highest resolution EBSD image (step size 0.2 µm) superimposed. Part C and D reveal the coincidence of the CL and EBSD images. The numbers identify each of the bands of the concentric layers.

3.5.4 EBSD - Orientation Analysis

The EBSD crystal-orientation map (Fig. 3.4A) reveals that each detrital host grain has a different crystallographic orientation (different colour), as would be expected in shallowly buried sandstones that have not undergone any extensive compaction or deformation. The crystal-orientation images show colour variations within some individual grains; for example in grain 1 there are two different colours and hence two different crystal orientations (Fig. 3.4A); in this grain this situation is Dauphine

twinning, in other grains this could be due to polycrystalline grains. The EBSD orientation images (Fig. 3.4A, 3.4B), displaying the orientation of each grain in the field of view with a different colour, do not depict any colour difference between detrital host grains and their quartz overgrowths, indicating that there is no difference in their crystallographic orientation (Fig. 3.4B). The EBSD orientation data (Fig 3.4A) also show that the microcrystalline quartz has a variety of crystallographic orientations and that none of the microcrystalline quartz adjacent, for example, to grain 1 (labelled) has inherited the same crystallographic orientation as grain 1.

3.5.5 EBSD - Identification of the Non-Diffracting Band

The EBSD orientation maps (Figs. 3.4A and 3.4B) show four bands numbered 1-4 in (B). The bands between the microcrystalline quartz (bands 2 and 4) and the detrital grains and between the first and second bands of microcrystalline quartz (bands 1 and 3) have yielded no crystallographic orientation data, i.e., they are non-diffracting bands. Following the approach explained by Haddad et al., (2006), these bands are non-diffracting because the initial EBSD analysis from this area yielded no Kikuchi patterns (electron backscatter patterns). CL and qualitative secondary X-ray analysis (EDAX) revealed that this band is silica (SiO_2). There are two possible explanations for the non-diffracting SiO_2 bands: (1) the crystal size is below the detection resolution of the EBSD, or (2) this material is amorphous or poorly crystalline silica and does not have enough long-range crystal structure to diffract electrons.

To understand the non-diffracting bands further, EBSD was conducted over a smaller area across the band using a reduced step size of 0.2 μm in an attempt to resolve any crystal orientations at the highest spatial resolution of this EBSD for quartz (Fig. 3.4D) Moving from the detrital grain out into the pore space, the eight bands previously described by BSE (Fig. 3.4C-2) and CL (Fig. 3.4C-3) can be identified: Bands 1A and 1B are very thin and show no crystal diffractions, band 1C shows some small crystals 0.2-0.5 μm in size, and band 2 shows the first layer of microcrystalline quartz (identified previously in B and C). The four bands then repeat with the first two bands, (bands 3A and 3B) again showing no EBSD solution, band 3C showing small crystals and band 4 again, a second microcrystalline quartz band at the edge of

the pore space. This higher EBSD resolution, using a step size of 0.2 μm (Fig. 3.4D), enables the detection of a layer of the silica polymorph chalcedony, based on composition and size (Heaney et al., 1994) in bands 1C and 3C, beneath the microcrystalline quartz. A small step size (0.2 μm) enabled the identification of the chalcedony layer and other regions (bands 1A and 1B, and bands 3A and 3B) could not be crystallographically resolved with EBSD. To resolve these regions, further investigation utilized a transmission electron microscope.

3.5.6 EBSD – Pole-Figure Analysis

Pole figures of selected EBSD data are stereographic projections that represent the orientation of crystallographic planes and directions in sample coordinates (Fig. 3.5). The microcrystalline quartz adjacent to the northwest face of grain 1 (Fig. 3.5A), when plotted on a stereographic projection, has its *c*-axis orientation [0001] spread in a girdle parallel to the grain surface on which it grew. The trace of the girdle is sub parallel to the trace of the growth surface, indicating that the orientation of the underlying chalcedony has controlled the growth of the microcrystalline quartz (the microcrystalline quartz is growing on the chalcedony). The microcrystalline quartz growing on the east surface of grain 1 (Fig. 3.5B) plotted on a stereographic projection reveals that its *c*-axis orientation is spread in a girdle sub parallel to the surface of grain 1. Similar cases for microcrystalline quartz grown on the surface of another grain (Figs. 3.5C, 3.5D) show that the *c*-axis orientation of the microcrystalline quartz is spread in a girdle parallel to the local surface of the grain on which it grows, indicating that the material on the grain surface has controlled the growth of the microcrystalline quartz. This analysis was repeated in multiple grains in multiple pores in multiple samples, and in each case the results were consistent. See Appendix Vol. 2, Teufelsmauer sample for additional data.

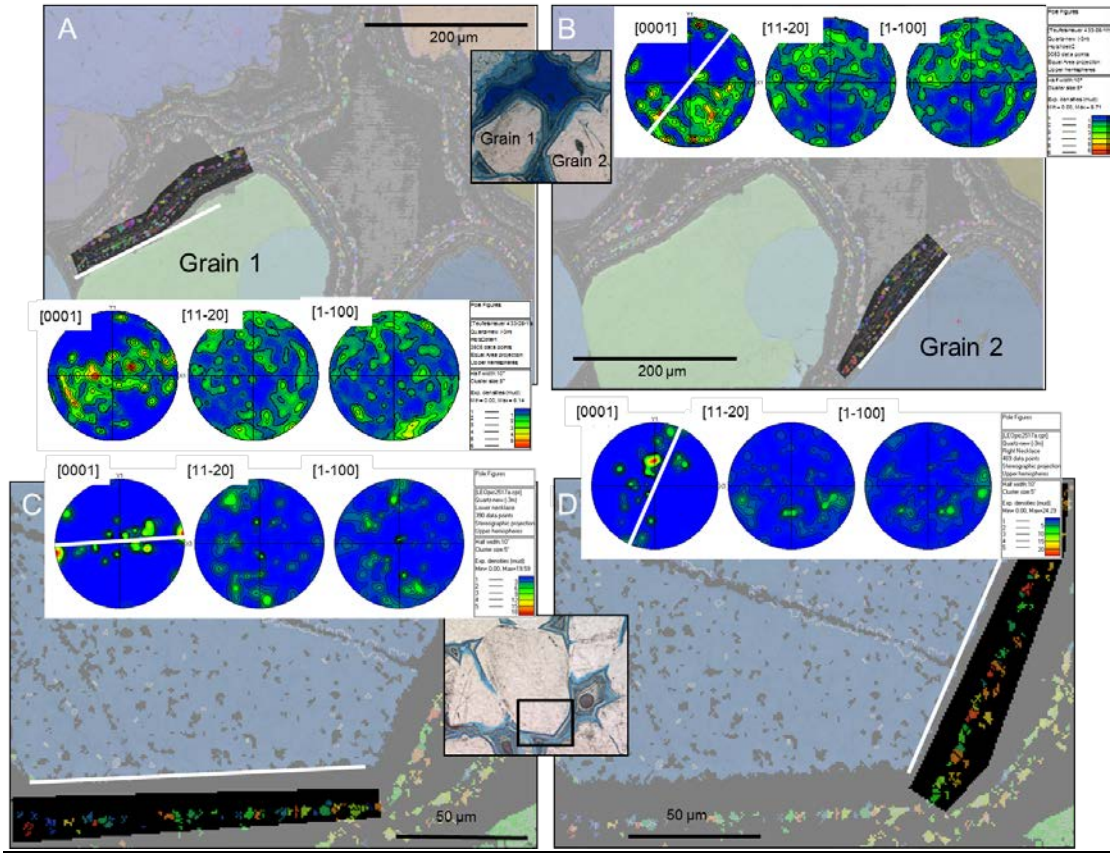

Figure 3.5 Electron backscatter diffraction (EBSD) orientation maps highlighting the microcrystalline quartz growing on different grains (A, B, C, and D) with pole figures showing the *c*-axis [0001] orientation of the microcrystalline quartz on the surface of the host grain. Parts A and B are from grain 1 and grain 2 in the upper inset light optical image, and Parts C and D are from two sides of another grain (see lower inset light optical image). The traces of the "great circle" of each of these sets of microcrystalline quartz [0001] data are shown by the white line through the pole figures. These match the orientations of the face of the host grain on which the microcrystalline quartz grew (shown by the white line on the EBSD images). The great circle through the *c* axes of the microcrystalline reveals that the *c* axes are parallel to the substrate surface but rotated on that surface. The amorphous material on the surface of the host grain has controlled the orientation of growth of the microcrystalline quartz.

3.5.7 SEM Analysis of Non-Diffracting Bands

To examine the non-diffracting bands in more detail, rock chip samples were imaged with SEI in an SEM (Fig. 3.6A), revealing the material that coats the surface of the detrital grains (Fig. 3.4) and that presumably controls the growth of the microcrystalline quartz. Closer examination (at 5,000x) reveals a surface layer (Fig.

3.6C), approximately 50-100 nm in thickness, coating the surface of the quartz overgrowth. The surface material of a second grain (Fig. 3.6D), approximately 1 μm in thickness, appears morphologically similar to the experimentally derived opal-CT lepispheres (Fig. 3.6F).

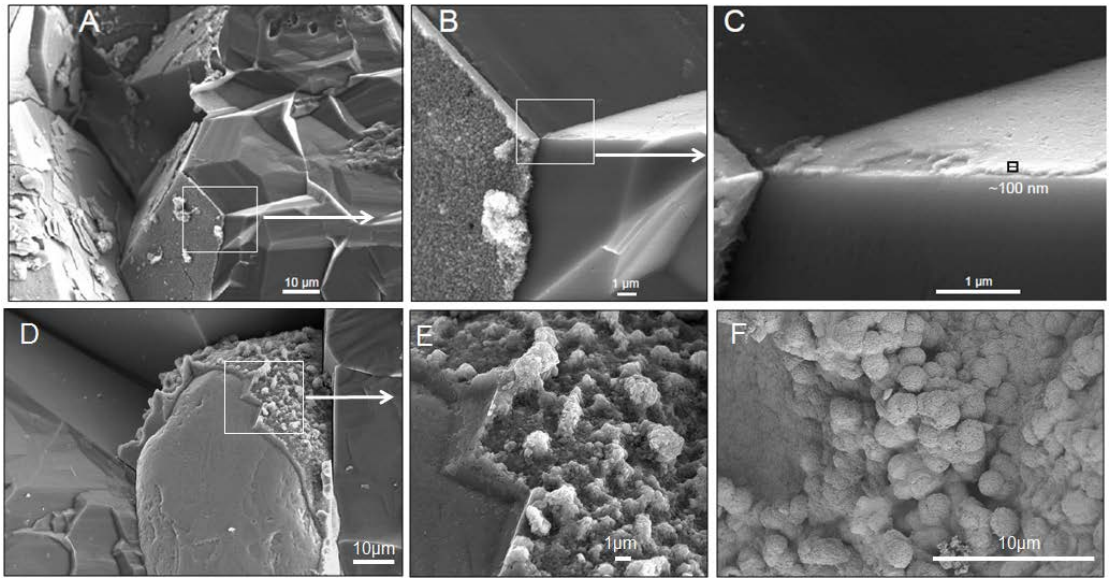

Figure 3.6 High-resolution secondary electron images (SEI) of surface coating at various magnifications: A)1,000x, B) 5,000x, and C) 25,000x. These show that the initial surface coating, before microcrystalline quartz growth, is approximately 50-100 nanometres in thickness. Second grain showing surface coating at D) 1,000x, E) 4,000x compared to F) experimentally grown Opal-CT lepispheres at 1,000x.

3.5.8 TEM Analysis of Non-Diffracting Bands

As with the EBSD analysis, small crystals were identified using micro-diffractions from the crystal lattice in the microcrystalline quartz zone. In the sample taken adjacent to the detrital host grain surface in the EBSD "zero-solution zone," the bright-field TEM image (Fig. 3.7A), collected at a magnification of 200,000x, showed crystalline material with a distinct diffraction pattern (Fig. 3.7C); given the crystal size, hint of rotation of the diffraction spots (Heaney, 1993) and composition, it is likely that this material is chalcedony. The bright-field TEM image (Fig. 3.7A) also contained a material that did not diffract the electron beam (Fig. 3.7B), strong evidence for some of the material in this band being noncrystalline, or amorphous silica, forming on the surface of the detrital host grain.

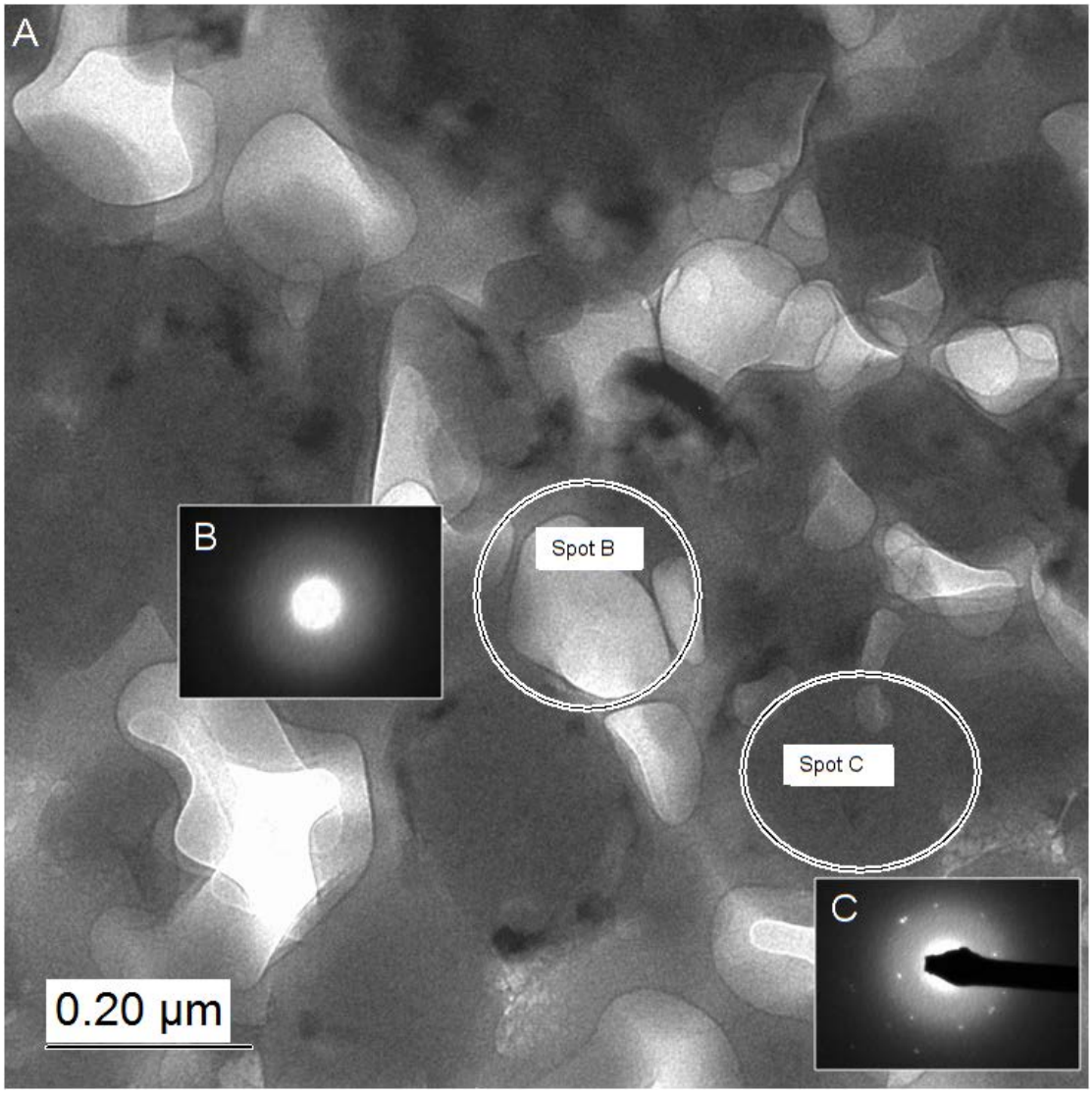

Figure 3.7 A) Bright-field TEM image at a magnification of approximately 200,000 showing crystalline material, amorphous material, and their respective microdiffractions. B) Microdiffraction of material in adjacent circle Spot B, showing only the transmitted beam (no diffracted intensities); evidence for amorphous silica. C) Microdiffraction of material in adjacent circle (Spot C) showing crystalline diffraction patterns with some degree of rotation, suggested by the smeared diffraction spots.

3.5.9 Analysis of Porosity-Preserving Experimental Quartz

SEM photographs of sample 3 before the experimental study (Fig. 3.8, left column), and exactly the same location imaged after the experiment (Fig. 3.8, right column) are shown at different magnifications. The detrital host grain surfaces coated with

microcrystalline quartz (Figs. 3.8A, C, E) are similar to those shown previously (Fig. 3.6) at three increasing magnifications before being placed in the Hastelloy reactor.

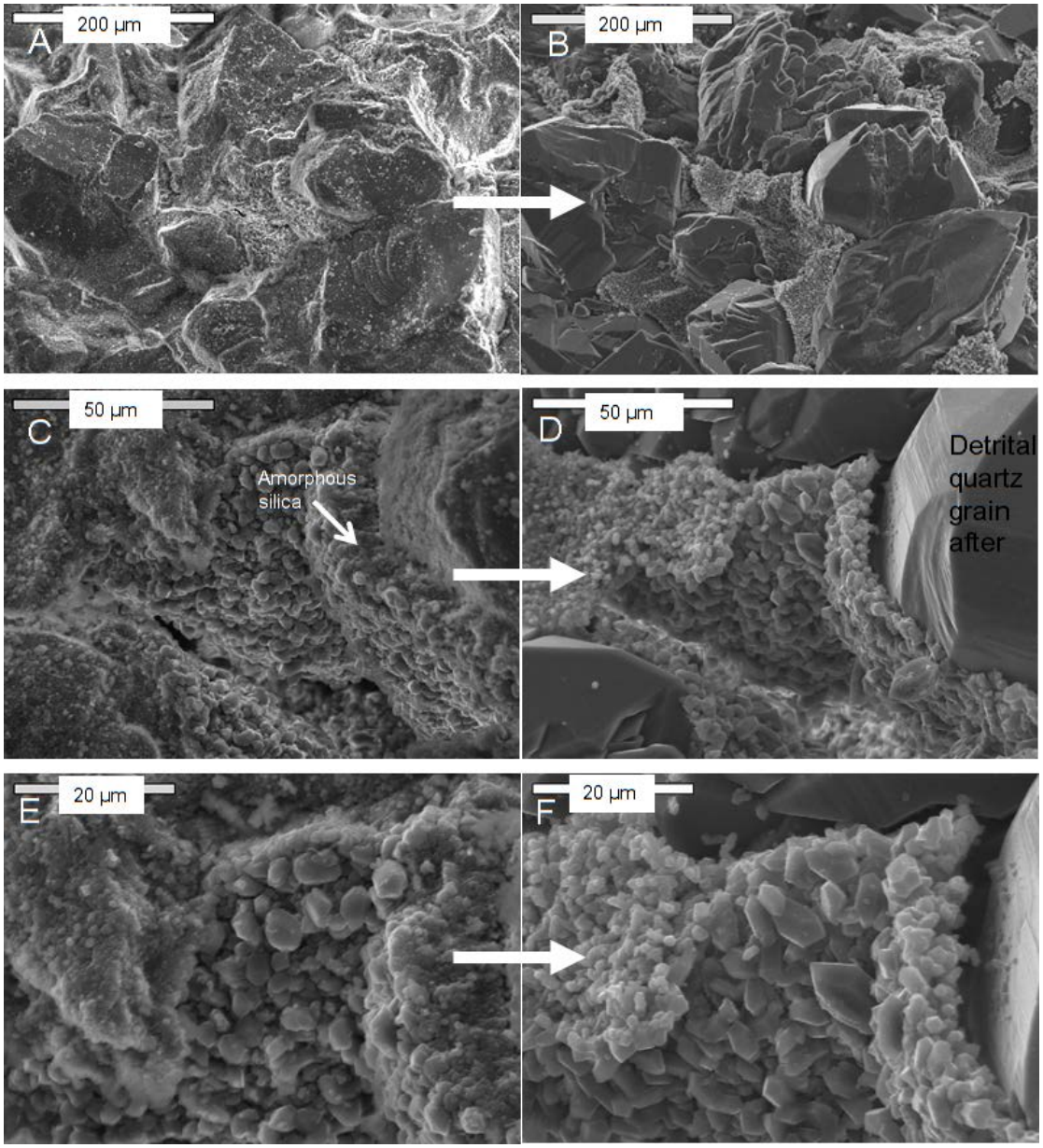

Figure 3.8 Scanning-electron-microscope photographs of before (left column: A, C, E) and after (right column: B, D, F) being placed in a Hastelloy reactor at 305°C for 7 days, showing the detrital host grain or overgrowth surfaces coated with microcrystalline quartz. F) Microcrystalline quartz that has preserved porosity continues to grow and inhibit quartz overgrowths from growing on the surface. Where microcrystalline quartz was absent from grain surfaces in the experiment, quartz overgrowths have started to develop. Parts E and F show that the amorphous silica and chalcedony dissolve within 7 days when exposed to the high-temperature (305°C) fluid supersaturated with respect to quartz.

The detrital host grain surfaces (Figs. 3.8 B, D, F), at the same magnifications are shown *after* the seven day experiment in the reactor. After the experiment, the microcrystalline quartz shows further growth, but in the majority of the crystals the *c* axes of the microcrystalline quartz appear to be parallel to the surface of the detrital host grains. On the uncoated quartz grain surfaces, there has been extensive development of quartz overgrowths. Additionally, the amorphous silica and chalcedony layers (labelled amorphous silica in Fig. 3.8C) are absent after the experiment (Fig. 3.8D), indicating that the amorphous silica layer and the chalcedony layer dissolved during the experiment. This observation suggests that the fluid in contact with the sample (Fig. 3.8F) was undersaturated with respect to amorphous silica and chalcedony. During the experiment, grain surfaces coated with microcrystalline quartz grew further microcrystalline quartz which inhibited the formation of quartz overgrowths and therefore effectively preserved porosity.

3.6 Discussion

3.6.1 Silica Polymorphs in the Heidelberg Formation

3.6.1.1 Quartz Overgrowths

EBSD and SEM-CL observations (Fig. 3.3) reveal that syntaxial quartz overgrowth cements grow on detrital quartz grains. The CL image (Fig. 3.3D) shows that the majority of the quartz overgrowths in the Heidelberg Formation are poorly developed and therefore represent incipient cements. These nascent quartz overgrowths did not occlude much of the porosity before being coated with an amorphous silica phase. The quartz overgrowths inherited the crystallographic orientation of the detrital host grains they grew upon, unlike the microcrystalline quartz in the Heidelberg Formation (Fig. 3.4).

3.6.1.2 Amorphous Silica

At the highest resolution in a SEM, an ~ 50-100 nm thin film is revealed between the detrital host grain and a multitude of microcrystalline quartz crystals (Figs. 3.6A-C).

Chemical analysis, carried out using EDS, indicates that the surface-coating nanofilm is silica (SiO_2). However, static probing of the surface-coating film during EBSD analysis revealed no diffraction patterns, indicating either that the crystal size was below the detection limit of this particular technique, i.e., smaller than 0.2 μm, or that the surface-coating film layer was nanocrystalline (i.e., amorphous). To investigate further the surface-coating film between the host detrital grain and the microcrystalline quartz, samples were prepared using a FIB-SEM and examined with a TEM. A selected-area electron diffraction (SAED) pattern in the TEM demonstrates that part of the surface material consists of nanometre-size crystals of quartz (Fig. 3.7C). However, there is also a surface-coating material that did not diffract the electron beam (Fig. 3.7B), suggesting that the thin surface-coating film contains amorphous silica. TEM examination of numerous grains suggests that this amorphous material is ubiquitous on the sandstone grain surfaces.

3.6.1.3 Chalcedony and Microcrystalline Quartz

Chalcedony, less than 0.5 μm in size and with the [11-20] perpendicular to the grain surface, was identified as one of the silica polymorphs in the Heidelberg Formation by examining the band between the amorphous silica and the microcrystalline quartz. The *c* axes of the Heidelberg microcrystalline quartz, measured on a specific face of a host quartz grain facing into a pore, were plotted on stereograms (Figs. 3.5A-D). The *c* axes are spread on a great circle (the white line on the figure representing a plane through that great circle) parallel to the plane of the quartz grain face, within a ± 15° scatter. This evidence indicates that crystals of microcrystalline quartz have grown with their *c* axes parallel to, but rotated on, the host surface, which is coated with an ~ 50-100 nm film. This observation is consistent with the presence of the silica polymorph chalcedony in the film. When nucleating within amorphous silica, competitive crystal growth of chalcedony ensures that favourably oriented grains grow along [11-20], and into the pore space, resulting in the alignment of [11-20] orthogonal to the surface upon which the amorphous silica had deposited. As explained above, EBSD data of microcrystalline quartz strongly suggests that the microcrystalline quartz grew on the chalcedony, inheriting its *c*-axis orientation first and then growing fast along the *c* axis and parallel to the detrital host grain surface.

This interpretation is supported further by high-resolution EBSD data revealing small crystals of chalcedony 0.2-0.5 μm in size (Fig. 3.4D) on which the microcrystalline quartz grows (Heaney et al. 1994). Additionally, the indications of rotation of the selected area electron diffraction spots (Fig. 3.7C) is also strong evidence for chalcedony.

3.6.2 Microcrystalline Quartz – Crystallographic Orientation

In the Heidelberg Formation, a layer of microcrystalline quartz with a thickness of approximately 1 μm has grown over syntaxial quartz overgrowth cement (Figs. 3.3A, B). To gain insight into the orientation of the microcrystalline quartz crystals and their crystallographic relationship with the host grain, EBSD analysis was performed on polished thin sections. The analyses confirm that the microcrystalline quartz, unlike syntaxial quartz overgrowths, is misoriented with respect to the host grain. This attribute is represented by the multiple colour variations of the microcrystalline quartz crystals, relative to the detrital host grain in the EBSD images (Figs. 3.4A, B).

The concept of the misorientation of microcrystalline quartz relative to the host grain has been reported in one previous paper (Haddad et al., 2006), but the control on the misorientation has not been previously explained. It has been shown here for the microcrystalline quartz from the Heidelberg Formation that there is a distinct control on the misorientation of the grains. Quartz, including microcrystalline quartz, typically grows faster in the *c*-axis direction. Length-fast chalcedony is microcrystalline fibrous quartz which grows faster in the [11-20] direction (Miehe et al., 1984; Frondel, 1982). The microcrystalline quartz in the Heidelberg Formation inherited the crystallographic orientation of the chalcedony precursor it grew upon.

3.6.3 Microcrystalline Quartz – Preservation of Porosity

The particular geometry of microcrystalline quartz crystals, grown on top of the ~ 50-100 nm film and misoriented relative to the host grain, has ensured that the pore space within the adjacent pore is preserved. This factor is due to: (1) the *c*-axis (fastest-growth axis) of the microcrystalline quartz grows parallel to the surface and not into

the pore, i.e., most of the microcrystalline quartz growth is not expanding into the pore space, thereby occluding porosity; (2) the microcrystalline quartz growing parallel to the grain surface and along the fast *c*-axis results in crystals that impinge on each other as they grow, limiting their growth length and size, preserving pore space; (3) the microcrystalline quartz grows on a cryptocrystalline substrate of chalcedony, and this cryptocrystalline substrate generates small quartz crystals. In general, small crystals grow faster than large crystals (Ostwald ripening; Chang and Yortsos, 1994), but small crystals more quickly adopt the energetically favourable euhedral form than large crystals and thereafter grow more slowly (Lander et al., 2008). The experimental evidence here demonstrates that the presence of the amorphous silica, chalcedony, and microcrystalline quartz layer coating the surface of detrital grains, and covering any potential nucleation sites for quartz overgrowths, is effective in preserving porosity.

3.6.4 Paragenesis of the Silica Polymorphs

Amorphous silica has been reported to transform to quartz via a series of metastable intermediates: Opal A → Opal CT → chalcedony → microcrystalline quartz (Williams and Crerar, 1985; Williams et al., 1985). In the Heidelberg Formation, amorphous silica coats the surfaces of many detrital grains. It is unlikely that quartz would co-precipitate with amorphous silica since quartz grows significantly slower than amorphous silica (Rimstidt and Barnes, 1980). The occurrence of chalcedony within amorphous silica bands suggests that the amorphous phase has undergone partial recrystallization to chalcedony during the geological history of this Cretaceous rock, and therefore that the amorphous material is a precursor to the microcrystalline quartz and chalcedony. Similarly, the occurrence of chalcedony growing within and above the amorphous silica and beneath the microcrystalline quartz explains the *c*-axis orientation of the microcrystalline quartz growing sub parallel to the surface of the host grain. The experimental work in this study corroborates this conclusion. The paragenesis of the silica polymorphs in the Heidelberg Formation, from amorphous silica → chalcedony → microcrystalline quartz, is similar to the amorphous silica transformation noted by Williams and Crerar (1985) and Williams et al., (1985).

3.6.5 Growth Mechanism for Porosity-Preserving Microcrystalline Quartz

The observations revealed in this study led to a conceptual model for a sequence of diagenetic transformations, from the initial deposition of the amorphous silica surface-coating nanofilm (Fig. 3.9A) on the host grain, to the growth of chalcedony with its [11-20] direction (fast growth axis, e.g., Florke et al., 1982) perpendicular to the surface of the host grain (Fig. 3.9B) to the nucleation or recrystallization and growth of microcrystalline quartz (Fig. 3.9C). The microcrystalline quartz inherits the *c*-axis orientation of the chalcedony on which it grows, which is parallel to the surface of the host grain (Fig. 3.9D) because chalcedony grows into the pore space along its fast growth direction, orthogonal to the *c*-axis (Heaney et al., 1994).

During the formation of quartz overgrowths in sandstones, relatively large quartz crystals (50-100 μm) grow into pore spaces after burial, inheriting the exact crystallographic orientation of the detrital host grain upon which they have grown (Waugh, 1970). Syntaxial quartz overgrowths extend into the pore space and effectively occlude most of the porosity in sandstones buried to depths where temperatures have exceeded ~ 80°C (Worden and Morad, 2000). In contrast, misoriented microcrystalline quartz crystals (0.1-10 μm) preserve porosity by coating the surface of the detrital sandstone grain during early diagenesis (Aase et al., 1996; Aase and Walderhaug, 2005). A film of amorphous silica initially coats the grain surfaces, growing from fluids which are saturated with respect to amorphous silica. Once precipitation of amorphous silica starts, the silica concentration of the fluid must decrease. As silica saturation decreases, chalcedony begins to crystallize (Williams et al., 1985), growing with its [11-20] direction perpendicular to the amorphous layer. This requires the *c*-axis to be parallel to the amorphous layer, but the *c* axes of the collection of chalcedony crystals are assumed to be rotated on that layer. Initial growth of microcrystalline quartz occurs on the chalcedony. The amorphous silica may subsequently undergo further crystallization to become an intergrowth of nano-sized quartz crystals or chalcedony and remnant amorphous silica. This combination of amorphous nano-film, length-fast chalcedony, and somewhat randomly spread *c* axes of microcrystalline quartz (parallel to the host surface) inhibits the growth of large crystals of quartz into available space, thus preserving porosity for the storage

and migration of petroleum in the subsurface. Understanding that an amorphous-silica precursor is necessary for porosity-preserving growth of microcrystalline quartz is the first step in developing a predictive model for preserving porosity in deep, high-temperature sandstone reservoirs. The development of an intermediate chalcedony phase is likely to be important, because it favours the systematic misorientation of microquartz.

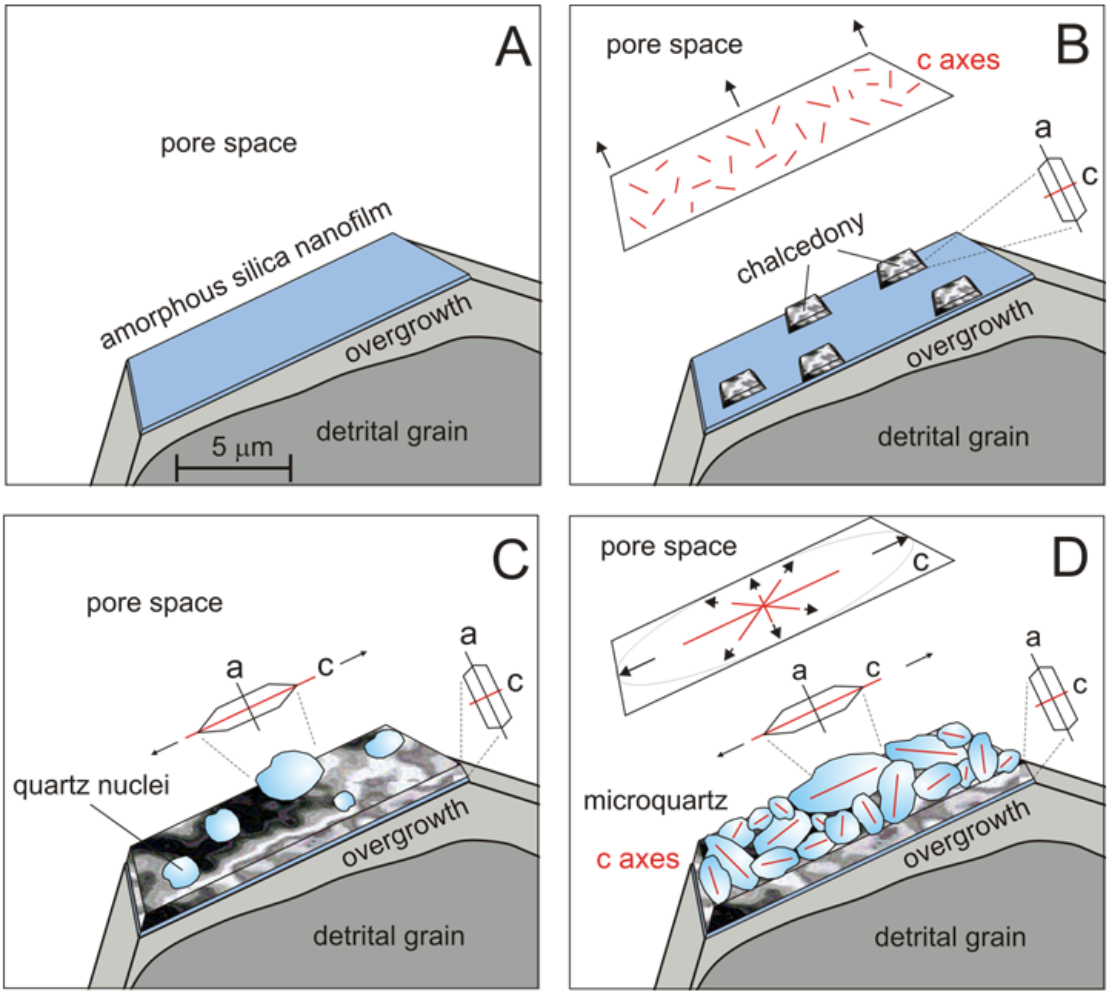

Figure 3.9 Model showing the sequence of growth events that resulted in *c* axes of microcrystalline quartz being parallel to, but rotated on, grain surfaces. A) At high amorphous silica concentrations in formation water, an amorphous silica nanofilm is deposited on top of a pre-existing quartz overgrowth. B) As silica saturation decreases following deposition of amorphous silica, fibrous crystals of chalcedony start to crystallize in the amorphous silica and grow into the pore space with their [11-20] directions perpendicular to the local surface. The *c* axes are always perpendicular to [11-20] and are thus parallel to the surface. Chalcedony [11-20] are azimuthally somewhat rotated on the surface so that *c* axes are randomly oriented within the nanofilm plane. C) Microcrystalline quartz nucleates on the chalcedony-coated substrate and uses the chalcedony crystal structure and orientation (*c*-axis parallel to grain surface) as a template. D) Microcrystalline quartz crystals grow along their c axes and subparallel

(within a few degrees) to the nanofilm plane. Continued growth of quartz crystals in their fast-growth *c*-axis directions is inhibited when microcrystalline quartz crystals impinge upon each other. There is no significant growth of quartz into the pore. Scale is reported in Part A. All thicknesses are exaggerated for clarity. Black arrows indicate the direction of growth.

3.7 Conclusions

Optic analysis, SEM, CL, EBSD, and TEM observations of the crystallography of microcrystalline quartz and other quartz-cement growth in the Heidelberg Formation reveal mechanisms of porosity preservation, and highlight the following conclusions:

1. Quartz cements of the Upper Cretaceous Heidelberg Formation reveal heterogeneous cement styles. Several silica polymorphs (amorphous silica, chalcedony, microcrystalline quartz) are contained in the cements, each of which displays different responses in CL, EBSD, and TEM.
2. In the Heidelberg Sandstone, parallel, isopachous, fine-scale bands of alternating bright and dark luminescence are reflected in different silica polymorphs.
3. Crystallographic information reveals an initial growth of amorphous silica, followed by chalcedony and lastly microcrystalline quartz. This sequence repeats itself, suggesting two discrete episodes each initially supersaturated with respect to amorphous silica.
4. Electron backscatter diffraction reveals that the detrital host grain and quartz overgrowths have the same crystallographic orientation; their relationship is syntaxial.
5. The microcrystalline quartz and the detrital grain have different crystallographic orientations. Microcrystalline quartz is crystallographically misoriented with respect to the detrital grain.
6. Misorientation profiles and pole figures show that there is a *systematic* misorientation between the detrital grain and the microcrystalline quartz, evidenced by the distribution of *c* axes sub-parallel to the parent-grain surface upon which microcrystalline quartz develops. This observation indicates that the non-syntaxial growth stages are not random and there is a distinct

crystallographic control on their growth. This control is related to the chalcedony precursor, which is length-fast ([11-20] preferred growth direction) and controls the growth axis of the subsequent microcrystalline quartz.

7. These data emphasize that the development of porosity-preserving microcrystalline quartz is the result of initial chalcedony growth on top of a nanofilm surface-coating layer of amorphous silica. The amorphous-silica nanofilm seems to be the key to the consequent porosity preservation. However, the misorientation of microquartz and the inhibition of quartz overgrowths are also a consequence of the [11-20] growth direction of the chalcedony that grows on the amorphous silica.

4 The origin of quartz cements revealed by spatially resolved oxygen isotope microanalysis, WDS, SEM-CL, TEM, and EBSD imaging; Heidelberg Formation, Germany

4.1 Abstract

Spatially resolved isotopic and trace element analysis of silica polymorphs in the Cretaceous Heidelberg Formation, Germany, and determination of crystal growth patterns utilizing SEM-CL, TEM and EBSD imaging have led to new evidence for mechanisms of silica cement growth. High precision, *in situ* oxygen isotope analyses of Cretaceous Heidelberg Formation detrital grains and quartz cements show three varieties of authigenic silica grow on detrital quartz grains. Detrital quartz has an average $\delta^{18}O$ composition of +9.4‰, syntaxial quartz overgrowths have an average composition of +20.3‰, and microcrystalline quartz has an average composition of +22.7‰. Chalcedony has a $\delta^{18}O$ composition greater than +27.4‰. Minor quartz overgrowths grew from meteoric water at about 80°C followed by concentric bands of silica cements that covered quartz grains and overgrowths alike. A thin layer of chalcedony was first deposited on both detrital quartz grains and quartz overgrowth cements followed by microcrystalline quartz; this cycle was then repeated. Trace element data support the petrological data and reveal two episodes of enrichment in aluminium and iron in the chalcedony. In contrast, aluminium concentrations in the microcrystalline quartz are below the detection limit for aluminium suggesting a low temperature of growth (< 70°C). If it is assumed that the closely-related chalcedony and microcrystalline quartz grew from the same water, then isotope data suggest that chalcedony grew at approximately 34°C while microcrystalline quartz grew at approximately 60°C from meteoric water. Analogous to groundwater silcretes, the Heidelberg Formation experienced two episodes of chalcedony and microcrystalline quartz growth from two episodes of influx of relatively cool meteoric water with high silica, iron, and aluminium concentrations.

4.2. Introduction

Quartz overgrowths are the most common authigenic silicates in sedimentary rocks and are the primary cause of porosity loss in sandstones (McBride, 1989; Worden and Morad, 2000). Quartz cement typically grows at temperatures > 80°C, develops as simple crystal extensions from detrital quartz grains and forms euhedral crystals. Microcrystalline quartz cement, often generated from biologically-derived silica (Vagle et al., 1994; Hendry and Trewin, 1995; Lima and De Ros, 2002), occurs as fine coatings of crystals on quartz grains. These prevent the growth of ordinary quartz overgrowths and lead to anomalously high porosity in deeply buried petroleum reservoirs (McBride, 1989; Vagle et al., 1994; Aase et al., 1996; Jahren and Ramm, 2000; and Bloch et al., 2002; Lima and De Ros, 2002). Microcrystalline quartz cement, 0.1-10 μm in size, coating the surface of grains in sandstones, has been previously identified in numerous studies (McBride, 1989; Vagle et al., 1994; Aase et al., 1996; Ramm et al., 1997; Jahren and Ramm, 2000; Lima and De Ros, 2002; Aase and Walderhaug, 2005). In the North Sea Basin, microcrystalline quartz occurs in sandstone reservoirs that contained biologically-derived amorphous silica (sponge spicules) (Vagle et al., 1994; Lima and De Ros, 2002). The growth mechanisms of microcrystalline quartz, and how it inhibits ordinary quartz cement, have only recently been investigated. Microcrystalline quartz cement growth on detrital quartz sand grains was recently studied and documented using electron backscatter diffraction (EBSD) (Haddad et al., 2006). Several authors have reported data on the microanalysis of detrital quartz and quartz overgrowths (Hervig et al., 1995; Williams et al., 1997; Lehmann et al., 2011) and cherts (Abruzzese et al., 2005), but little microanalysis data have been reported on the paragenetic sequence of silica polymorphs in sedimentary rocks from detrital quartz grains, quartz overgrowths, amorphous silica, chalcedony or microcrystalline quartz. Trace element analysis data have been reported by various authors for hydrothermal quartz (Rusk et al., 2008; Lehmann et al., 2009; Götte et al., 2011; and Lehmann et al., 2011) and agates (Götze et al., 2001). This study combines a variety of analytical techniques which, when integrated together to characterize the silica polymorphs, present the first study of spatially resolved isotope analysis and trace element analysis combined with

crystallographic analysis of detrital quartz, and the silica cements including quartz overgrowths, amorphous silica, chalcedony, and microcrystalline quartz.

The crystallography and growth mechanisms for porosity-preserving microcrystalline quartz and other quartz cements in the Heidelberg Formation, Germany, have here been examined using optical analysis, cathodoluminescence (CL), electron backscatter diffraction (EBSD), and transmission electron microscopy (TEM). Silica cements from the Upper Cretaceous Heidelberg Formation reveal heterogeneous cement styles. Normal quartz overgrowths are present on some quartz sand grains. Detrital grains, with and without quartz overgrowths, are covered by concentric bands of silica polymorph cements (Voigt et al., 2006).

The purpose of this paper is to examine the oxygen isotopic signature of the silica polymorphs and trace elements found in the Heidelberg Formation in the context of detailed mineralogical examination and, by integrating all of the previous described techniques, offer further evidence for understanding the origin of porosity-preserving microcrystalline quartz. The specific questions being addressed are:

1. Is there a link between stable oxygen isotope values and silica polymorph variations in microcrystalline quartz cemented sandstones?
2. Is there a link between trace element concentrations and silica polymorph variations?
3. What caused chalcedony and microcrystalline quartz growth in the Heidelberg Formation?

4.3 Geologic setting

The Cretaceous Heidelberg Sandstone is located in the Subhercynian Cretaceous Basin at the northern border of the Paleozoic Harz Mountains, Germany (Fig. 4.1) and consists primarily of marine, fine-grained, quartz-cemented sandstones (Voigt et al., 2006). The Heidelberg Formation is approximately 400-500 m thick and covers the eastern Subhercynian Cretaceous Basin between Quedlinburg and Blankenburg, Germany. Thrusting of the Harz Mountains onto its foreland led to flexuring of

Permian to Late Cretaceous strata that now form a steeply dipping sequence in front of the Harz Mountains (Franzke, 1990; Voigt et al., 2004).

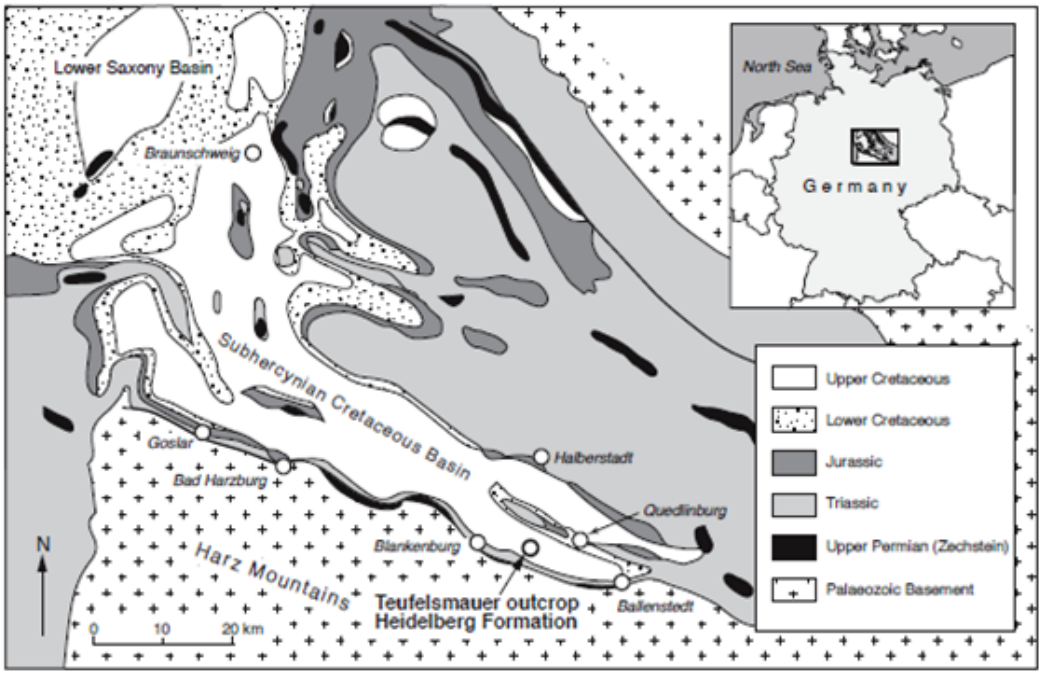

Figure 4.1 Geologic map of the Harz Mountains and Subhercynian Basin with the Heidelberg Formation, Teufelsmauer outcrop noted between Blankenburg and Quendlinburg, Germany.

4.4 Methods

4.4.1 Sample Preparation and Characterization

Samples from the Cretaceous Heidelberg Sandstone were provided by C. Fischer and S. Waldmann (University of Göttingen, Germany) and described by Waldmann (2006). Samples were injected with blue-dyed epoxy resin to hold the grains in place during sample preparation and were cast in 25mm diameter epoxy rounds with the quartz isotopic standard UWQ-1 (Kelly et al., 2007). The samples were imaged and analysed using facilities at ExxonMobil's Upstream Research Company, using a JEOL 6490LV scanning electron microscope (SEM) with Secondary Electron Imaging (SEI), Backscatter Electron Imaging (BSE), cathodoluminescence (CL), as well as petrological microscopes. Spatially-resolved SIMS analysis, Electron

Backscatter Diffraction (EBSD), Wavelength Dispersive Spectroscopy (WDS) and TEM analyses were performed at ExxonMobil's Corporate Strategic Research Company.

4.4.2 Isotope Analysis

Spatially-resolved SIMS analyses were performed using a Cameca nanoSIMS N50 with a spot size of 5-10μm. Analysis conditions were 16keV, 250pA Cs+ primary beam; 8 keV negative secondary ions; sample charge neutralization; 10μm x 10μm rastered analysis area; FC-EM detection (180~6E4 cps); and instrumental mass resolution ~5000 yielding a precision of ±0.15‰ (1SD). Ion microprobe spots were selected based on CL, SEI, and BEI images taken before the samples were put in the nanoSIMS. After analysis, each spot was investigated by SEM and CL to define the analysis point as being located in one of the following: detrital grain, quartz overgrowth, microcrystalline quartz, or microcrystalline quartz with chalcedony. Isotope data are reported relative to the V-SMOW standard.

4.4.3 Silica Polymorph Characterization

Quartz overgrowth cements are difficult to distinguish from detrital quartz grains by optical and SEI microscopy, but appear distinctly different in CL. High resolution secondary and backscattered electron images (SEI) were acquired using a JEOL 6330F FEG-SEM. Cathodoluminescence was used to identify and distinguish detrital quartz grains from syntaxial quartz overgrowths and microcrystalline quartz (Evans, et al., 1994). A JEOL 6490LV SEM, fitted with a Gatan cathodoluminescence detector (ChromaCL-006) was used for cathodoluminescence analysis. CL images were taken with an accelerating voltage of 10 kV (in contrast to 20 kV for BSE), 8nA beam current, and 16.5mm working distance. CL images were collected by accumulating a signal of 500 frames using a slow-scanning raster and red, green, and blue wavelength CL were collected and added using processing to produce a ChromaCL image. Areas for isotope analysis were selected based on overgrowth cement and microcrystalline quartz zones. Crystallographic orientation of the silica polymorphs was determined using electron backscattered diffraction (EBSD) analysis,

performed on polished thin sections using a LEO 1530 SEM fitted with an Oxford-HKL EBSD system. Samples were prepared using FIB-SEM analysed in a Philips CM200F TEM/STEM operated in the bright field imaging TEM mode at an accelerating voltage of 200kV.

4.4.4 Wavelength Dispersive Spectroscopy analysis

Wavelength dispersive spectroscopy analysis was performed using a JEOL 6400 SEM with wavelength dispersive spectrometers. The trace elements measured in the quartz overgrowth and concentric bands were: Al, Na, Mg, K, Ca, Ti, Fe, Cr, and Mn. Analysis times were 300 seconds on peak, 50 seconds on each background. Accelerating voltage was 15 kV, beam current 115 nA, probe size ~ 3 μm and spot size of 5-10 microns. The standards employed were SRM-1212 for Al, Na, K, and Ca, MgO for Mg, TiO_2 for Ti, Cr_2O_3 for Cr, and manganese metal for Mn. Data were quantified using Probe for EPMA software. Limits of detection (3 sigma) are: 12 ppm for Al, 24 ppm for Na, 19 ppm for Mg, 22 ppm for K, 26 ppm for Ca, 38 ppm for Ti, 216 ppm for Fe, 112 ppm for Cr, and 129 ppm for Mn. All analysis points were below detection for Cr and Mn and these elements are not discussed further.

4.5 Results

4.5.1 Light Optical and Electron Microscope Imaging

Transmitted-light optical analysis was performed in order to identify and locate quartz overgrowths and microcrystalline quartz on detrital host quartz grains. The location of the quartz overgrowths was based on the identification of euhedral crystals having sharp, clean edges. Optical images

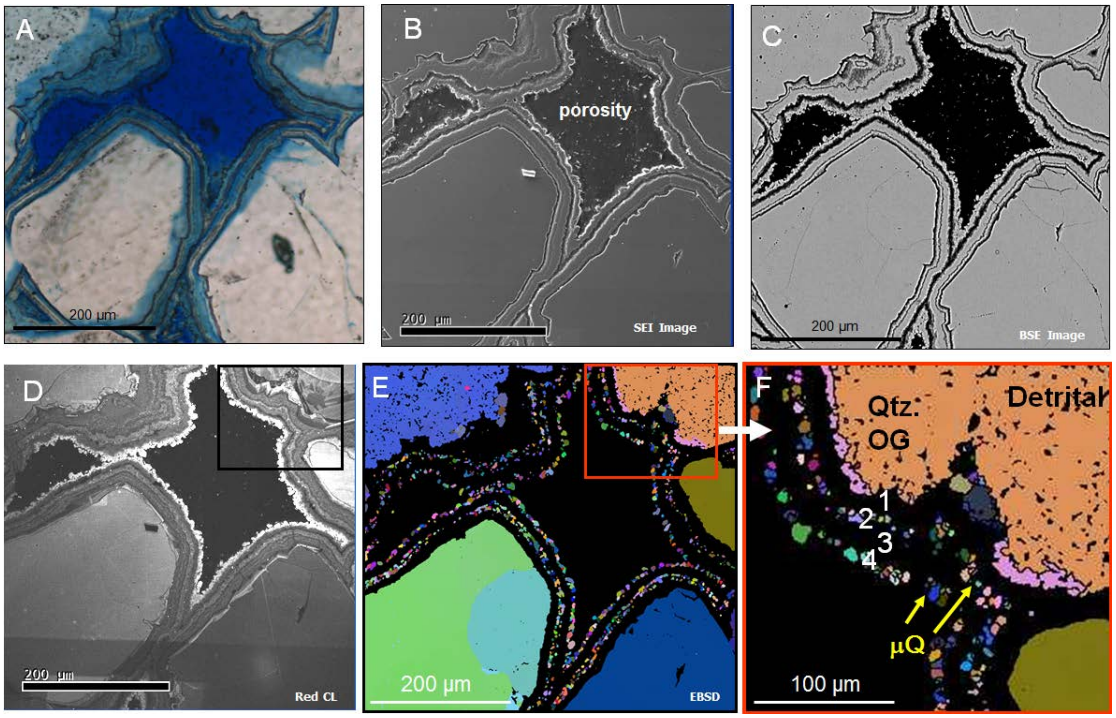

Figure 4.2 Petrographic images of silica cements in the Heidelberg Formation: (A) Light optical image of the angular cemented quartz grains and the concentric layers parallel to the detrital grain/overgrowth edges with porosity in blue. (B) Secondary electron image of the grain shown in Figure 2A. (C) Back-scattered electron microscope image of the grain shown in Figures 2A and b showing that there is only SiO_2 in the various cements. (D) Red cathodoluminescence image which differentiates the quartz overgrowth from the detrital grain (E) Euler map showing host grain orientation (green) and microcrystalline quartz (multiple colours) indicating that the crystallographic orientation of any of the microcrystalline quartz crystals adjacent to the host grain is crystallographically misoriented with respect to the host grain. (F) EBSD Euler map showing that the quartz overgrowth and detrital grain do not show any colour variation indicating there is no difference in the crystallographic orientation of the detrital quartz grain and quartz overgrowth. EBSD orientation map of the four isopachous layers which highlights the chalcedony layer (layers 1 and 3) upon which the microcrystalline quartz (layers 2 and 4) grows.

(Fig. 4.2A) show initially rounded quartz grains which now have strong angular facets caused by quartz overgrowth crystal faces. SEI cannot distinguish between the quartz overgrowths and the detrital host grains (Fig. 4.2B).

Transmitted-light optical images highlighted the presence of thin concentric layers parallel to the detrital grain or the overgrowth edge which contain areas of microporosity (revealed by the coloration introduced by the injection of blue epoxy during sample preparation) between the grains and microcrystalline quartz lining the

pores (Fig. 4.2A). Secondary electron imaging revealed an uneven surface at the site of the concentric bands, even though the sample was a polished section (Fig. 4.2B). This roughness may be due to the sample being microporous or the concentric bands having different resistance to polishing than quartz grains. Backscattered electron imaging showed that the grains, overgrowth and concentric bands are all composed of SiO_2 (Fig. 4.2C). Therefore, there are no compositional variations evident within the Heidelberg Formation cements.

4.5.2 Cathodoluminescence (CL) Analysis

Cathodoluminescence images (Fig. 4.2D) discriminate detrital grains that luminesce brightly, quartz overgrowths with zoned, somewhat variable luminescence, and the optically-defined concentric bands that contain dark luminescent layers and thinner, slightly more luminescent layers all of which coat the rim of the pore. The SEI image (Fig. 4.2B) shows several distinct bands beyond the detrital grain/overgrowth (Fig. 4.2D). CL reveals four bands suggesting that four discrete phases of silica polymorph growth occurred to create the concentric bands.

4.5.3 Electron Backscatter Diffraction and TEM analysis

As expected, quartz overgrowths have the same crystallographic orientation as their host detrital quartz grains, as confirmed by EBSD analysis. The Euler image (Figs. 4.2E-F) has the same colour (and thus same orientation) for the quartz grain and the quartz overgrowth.

Cathodoluminescence images differentiated four bands in the concentric layers; alternating light and dark bands; here called bands 1 to 4 (Figs. 4.2E-F). Bands 1 and 3, despite being composed only of silica, could not be indexed using EBSD (i.e. they could not have their crystallographic orientation defined) since they displayed no EBSD response (Figs. 4.2E-F). Examination of individual electron backscatter patterns (EBSPs) from specific points of electron beam analysis within the unindexed zones found there to be no well-developed Kikuchi patterns. This suggests that the unindexed bands are amorphous silica. However, further investigation with

transmission electron microscopy (Fig. 4.3) confirmed that these bands contain both nanometre size quartz crystals and amorphous silica and are therefore a form of chalcedony (Vagle et al., 1994). Further investigation with TEM confirmed that these bands contain nanometre size quartz crystallites and amorphous silica (Fig. 4.3).

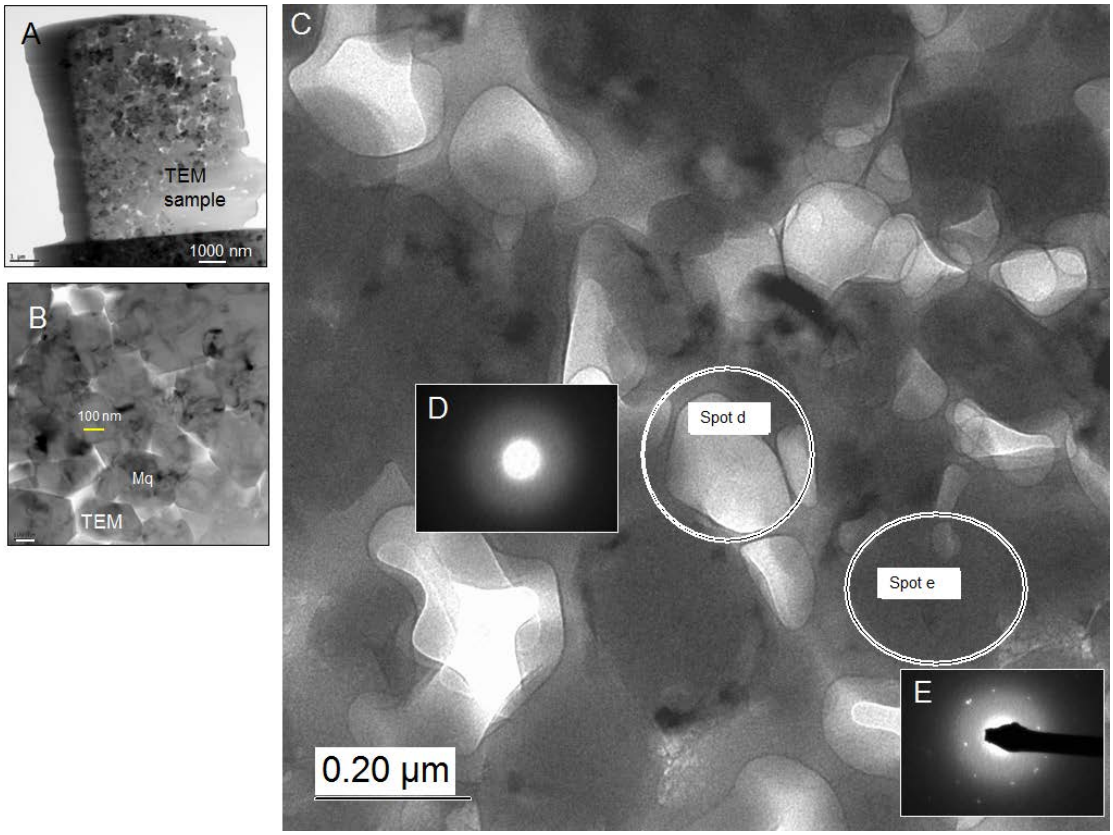

Figure 4.3 (A) Image of the TEM sample showing nanocrystals, the scale bar is 1,000 nm, (B) TEM sample showing crystallites that are in the 100 nm size range, the scale bar is 100 nm (C) TEM image of the chalcedony band revealing that it is composed of amorphous silica and nanocrystalline quartz. (D) Selected area diffraction pattern from amorphous silica with no diffraction spots indicating a non-crystalline or amorphous silica phase. (E) Selected area diffraction pattern from nanocrystalline quartz with characteristic diffraction spots indicating crystalline silica.

In summary BSEM, CL and EBSD reveal that the concentric bands of silica cement represent four growth events. An initial chalcedony layer (containing amorphous silica and nanometre quartz crystals) was followed by microcrystalline quartz. This sequence was then repeated. The concentric bands followed an initial period of normal quartz overgrowth development.

4.5.4 Stable isotope data

The CL image of the Heidelberg Formation reveals the burn marks after three scans in the nanoSIMS along a traverse from the detrital grains through the quartz overgrowths and into the microcrystalline quartz (Fig. 4.4).

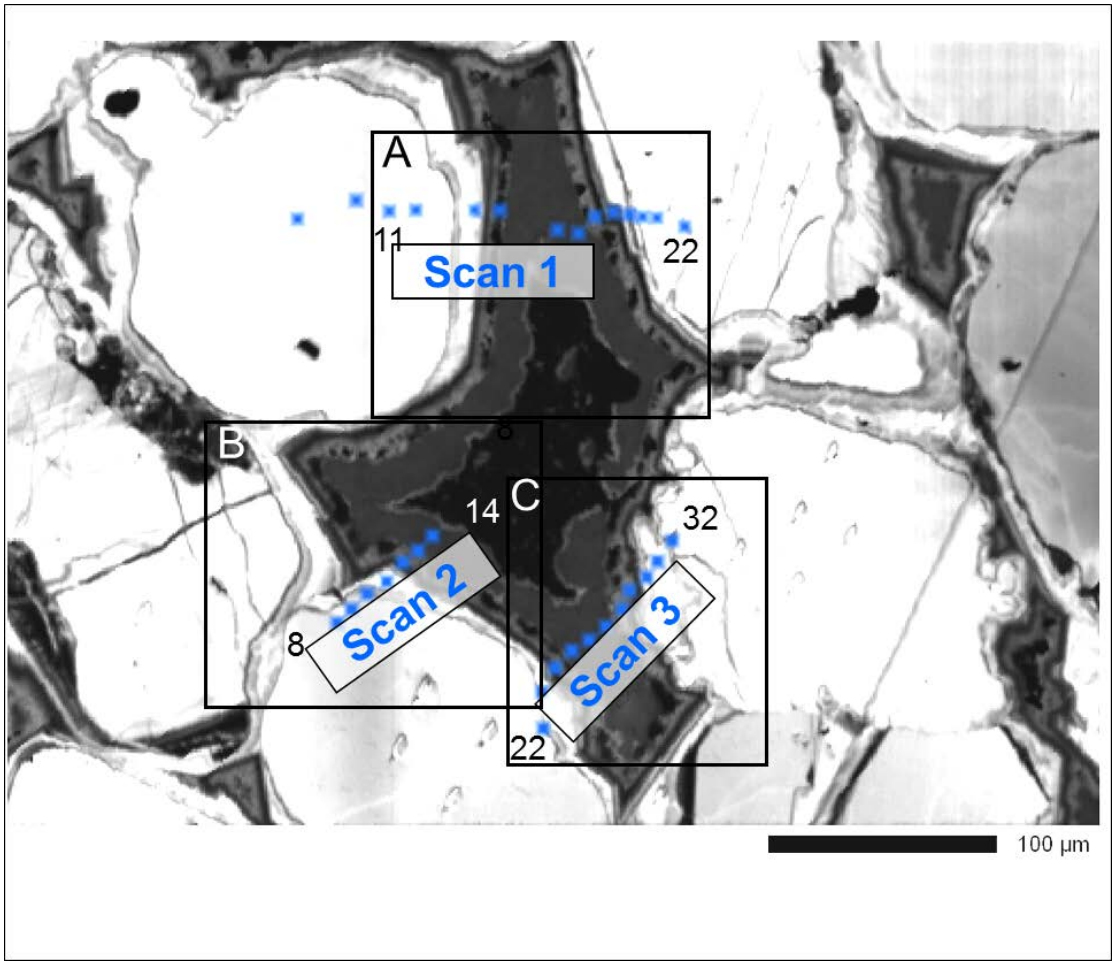

Figure 4.4 Cathodoluminescence (CL) index map of three nanoSIMS analysis scans of Heidelberg Formation sample.

The CL image for each scan, showing the nanoSIMS burn marks, has been added to link the stable isotope data to the type of silica (Figs. 4.5A, B, and C).

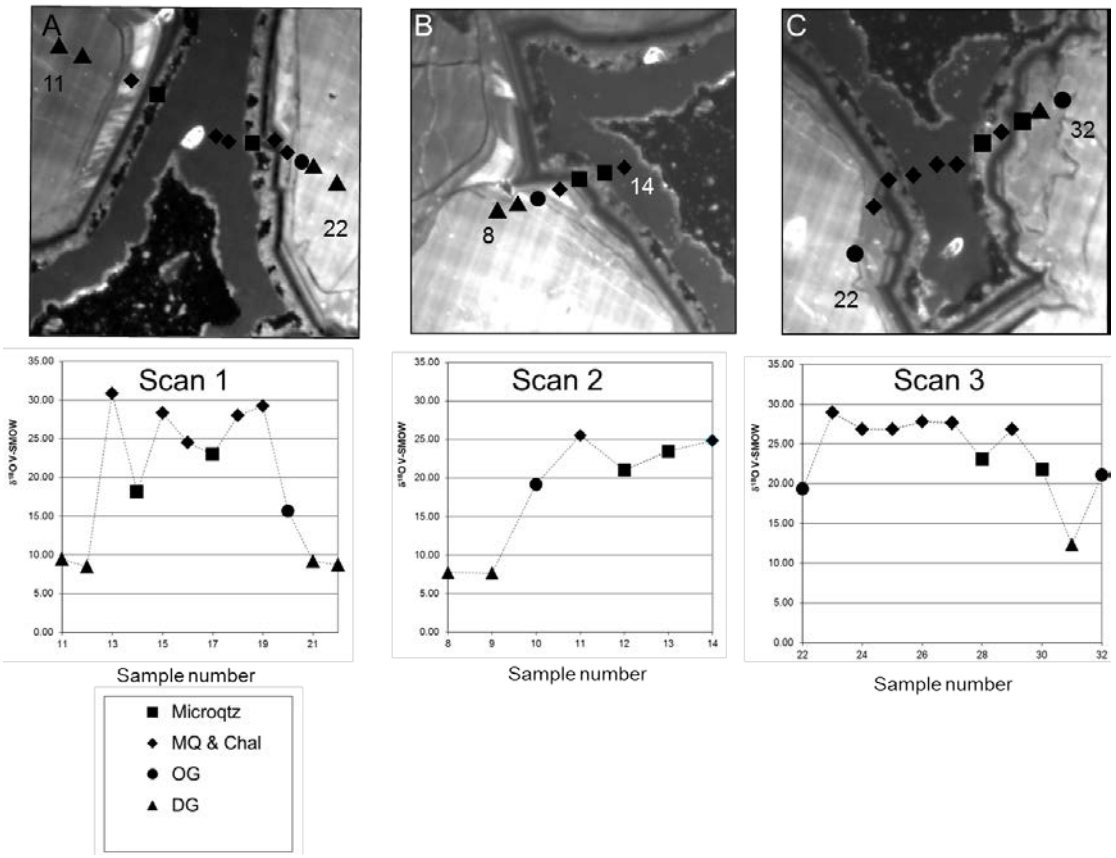

Figure 4.5 A) SEM-CL image indexed in Figure 4.4 showing analysis locations in the detrital grains (▲), quartz overgrowths (●), microcrystalline quartz (□), and chalcedony with microcrystalline quartz (◊). B) Scan 2, C) Scan 3. Directly beneath each SEM-CL image is the corresponding $\delta^{18}O$ V-SMOW versus sample number or location referenced to A, B, and C plotted by silica polymorph.

The quartz polymorphs were identified in CL as: detrital quartz grains (▲), quartz overgrowths (●), microcrystalline quartz (□), and a combination of chalcedony with microcrystalline quartz (◊).

	V-SMOW	DG	OG	MQ	MQ/Chal.	Cristobalite	Bio. Opal
Heidelberg Fm.	Average	**9.4**	**19.3**	**21.8**	**27.4**		
Literature Average		12.2	20.0	23.8	28.3	29.4	37.4
Heidelberg Fm.	Range	**7.7_12.4**	**15.6_21.9**	**18.1_23.5**	**24.9_30.9**		
Literature Range		4.2_24.1	12.6_32.4		24.9_32.4	27.9_30.4	

Table 4.1 Oxygen isotope values of scans 1, 2, and 3 in V-SMOW for detrital grains (DG), overgrowths (OG), microcrystalline quartz (MQ) and microcrystalline quartz with chalcedony (MQ/Chal.) for the Heidelberg Formation and from other silica samples (non-Heidelberg) from the references below, and for comparison cristobalite and biogenic opal from the same references. Data from the literature are derived from Blatt (1987); Vagle et al.,

(1994); Murata et al., (1977); Harwood et al., (2009); Pollington et al., (2011); Marchand et al., (2002); O'Neil and Hay (1972); Knauth and Epstein (1976); Abruzzese et al., (2005); Williams et al. (1997); and Harvig et al., (1995).

Stable isotope data are reported in Table 4.1. In the Heidelberg Formation, detrital quartz grains have an average $\delta^{18}O$ of +9.4‰, with a standard deviation of 1.6‰ and a range from +7.7‰ to +12.4‰. Quartz overgrowths have an average $\delta^{18}O$ of +20.3‰, with a standard deviation of 1.4‰ and a range from +19.0‰ to +21.9‰. Microcrystalline quartz has an average $\delta^{18}O$ of +22.7‰, with a standard deviation of 1.1 and a range from +21.0‰ to +23.5‰. Where microcrystalline quartz is intergrown with chalcedony (i.e. beyond the spatial resolution of the nanoSIMS), the average $\delta^{18}O$ is +27.4‰ with a standard deviation of 1.7‰ and a range from +24.5‰ to +30.8‰. Given that pure chalcedony has probably not been analysed, the mean value of +27.4‰ probably represents a mixture of microcrystalline quartz (with an average $\delta^{18}O$ of +22.7‰) and chalcedony; pure chalcedony possibly has an average $\delta^{18}O$ value in excess of +30‰.

4.5.5 Wavelength Dispersive Data (WDS)

Wavelength Dispersive (WDS) analysis was conducted on a sample from the Heidelberg sandstone in a traverse from a detrital quartz grain through a quartz overgrowth and into the consecutive pairs of chalcedony-microcrystalline quartz bands (Fig. 4.6). The WDS data are reported in parts per million (ppm) for the detrital quartz grain, quartz overgrowth, chalcedony, and microcrystalline quartz (Table 4.2). The detrital quartz grain and quartz overgrowth trace element concentrations are low compared to some of values from the bands extending from the edge of the overgrowth into the pore space. The trace elements with the highest concentrations are Fe, Al and Ca.

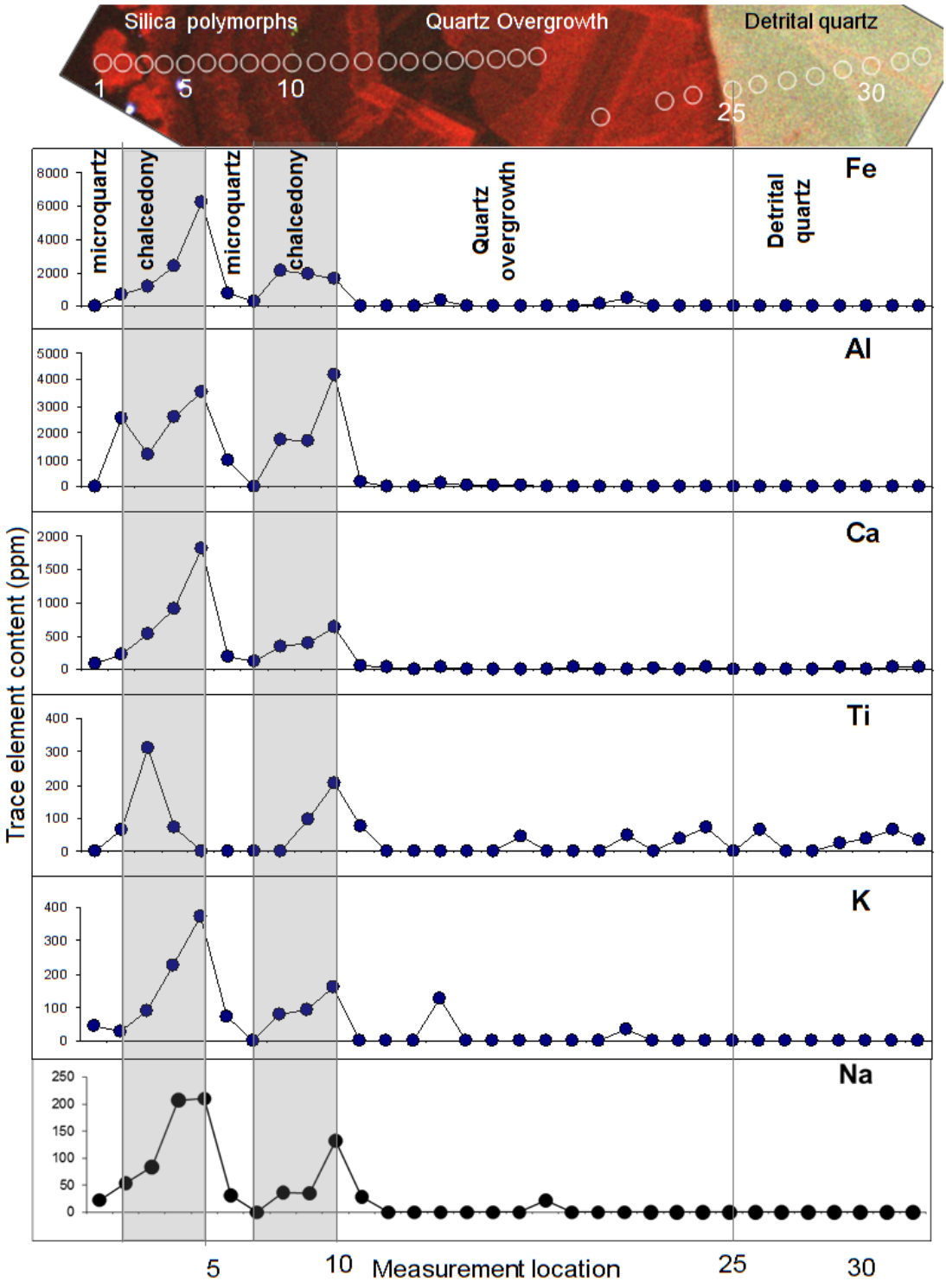

Figure 4.6 CL image showing analysis locations and Wavelength dispersive spectroscopy (WDS) analysis of trace elements in concentration (parts per million) along a profile from the detrital quartz grains to the quartz overgrowth through chalcedony and microcrystalline quartz bands into the pore centre showing the highest values of aluminium and iron in the first-deposited chalcedony which then decrease towards low concentrations in the microcrystalline quartz.

Tuefelsmauer OG to MQ		Al MDL	Fe MDL	Ca MDL	Ti MDL	K MDL	Na MDL	Mg MDL	Cr MDL	Mn MDL
Step Scan 2 Fine (2um)		12	216	26	38	22	24	19	112	129
Point		**Al (ppm)**	**Fe (ppm)**	**Ca (ppm)**	**Ti (ppm)**	**K (ppm)**	**Na (ppm)**	**Mg (ppm)**	**Cr (ppm)**	**Mn (ppm)**
1	MQ (band-4)	n.d.	n.d.	92	n.d.	44	23	98	n.d.	n.d.
2	Chalcedony (band-3)	2546	703	221	66	28	54	20	n.d.	n.d.
3	Chalcedony (band-3)	1206	1137	530	311	90	84	52	n.d.	n.d.
4	Chalcedony (band-3)	2609	2387	909	72	226	207	45	n.d.	n.d.
5	Chalcedony (band-3)	3547	6243	1820	n.d.	373	210	81	n.d.	n.d.
6	MQ & Chalcedony	967	743	191	n.d.	71	32	n.d.	n.d.	n.d.
7	MQ (band-2)	n.d.	261	119	n.d.	n.d.	n.d.	n.d.	n.d.	n.d.
8	Chalcedony (band-1)	1754	2087	346	n.d.	80	36	n.d.	n.d.	n.d.
9	Chalcedony (band-1)	1696	1922	385	95	92	35	n.d.	n.d.	n.d.
10	Chalcedony (band-1)	4183	1666	639	207	162	133	n.d.	n.d.	n.d.
11	OG	154	n.d.	49	74	n.d.	29	n.d.	n.d.	n.d.
12	OG	n.d.	n.d.	31	n.d.	n.d.	n.d.	n.d.	n.d.	n.d.
13	OG	n.d.	n.d.	n.d.	n.d.	n.d.	n.d.	n.d.	n.d.	n.d.
14	OG	108	315	28	n.d.	126	n.d.	n.d.	n.d.	n.d.
15	OG	38	n.d.	n.d.	n.d.	n.d.	n.d.	n.d.	n.d.	n.d.
16	OG	33	n.d.	n.d.	n.d.	n.d.	n.d.	n.d.	n.d.	n.d.
17	OG	29	n.d.	n.d.	44	n.d.	n.d.	n.d.	n.d.	n.d.
18	OG	13	n.d.	n.d.	n.d.	n.d.	22	n.d.	n.d.	n.d.
19	OG	n.d.	n.d.	42	n.d.	n.d.	n.d.	n.d.	n.d.	n.d.
20	OG	n.d.	134	n.d.	n.d.	n.d.	n.d.	n.d.	n.d.	n.d.
21	OG	n.d.	470	n.d.	46	34	n.d.	n.d.	n.d.	n.d.
22	OG	n.d.	n.d.	24	n.d.	n.d.	n.d.	n.d.	n.d.	n.d.
23	OG	n.d.	n.d.	n.d.	38	n.d.	n.d.	n.d.	n.d.	n.d.
24	OG	n.d.	n.d.	36	72	n.d.	n.d.	n.d.	n.d.	n.d.
25	DG	n.d.	n.d.	n.d.	0	n.d.	n.d.	n.d.	n.d.	n.d.
26	DG	n.d.	n.d.	n.d.	65	n.d.	n.d.	n.d.	n.d.	n.d.
27	DG	n.d.	n.d.	n.d.	n.d.	n.d.	n.d.	n.d.	n.d.	n.d.
28	DG	n.d.	n.d.	n.d.	n.d.	n.d.	n.d.	n.d.	n.d.	n.d.
29	DG	n.d.	n.d.	36	23	n.d.	n.d.	n.d.	n.d.	n.d.
30	DG	n.d.	n.d.	n.d.	39	n.d.	n.d.	n.d.	n.d.	n.d.
31	DG	n.d.	n.d.	37	65	n.d.	n.d.	n.d.	n.d.	n.d.
32	DG	n.d.	n.d.	28	35	n.d.	n.d.	n.d.	n.d.	n.d.
	MDL = minimum detection limit			*n.d. = not detected						

Table 4.2 Wavelength dispersive spectroscopy trace element data in parts per million from a traverse (Fig. 6) from the detrital grain (DG) through the quartz overgrowth (OG), Chalcedony (band-1), microquartz (MQ band-2), second chalcedony band Chalcedony (band-3), and second microquartz (MQ band-4) including a transition zone containing microquartz and chalcedony (MQ & Chalcedony). The detection limits are: Na 20 ppm, Mg 19 ppm, K 22 ppm, Ca 26 ppm, Ti 38 ppm, Fe 216 ppm, Cr 112 ppm, Mn 129 ppm, Al, 12 ppm.

The WDS profile from the overgrowth through the concentric silica bands show significant variations in iron and aluminium concentrations with the greatest concentrations at the base of the chalcedony bands, and concentrations decreasing approaching the overlying microcrystalline quartz bands (Fig. 4.6). The microcrystalline quartz bands have similar compositions to the detrital grain and quartz overgrowth (i.e. they have relatively low concentrations of trace elements).

4.6 Discussion

High precision, *in situ* oxygen isotope values from the Heidelberg Formation silica polymorphs fall within the ranges of previously published data for microcrystalline quartz and chalcedony (Table 4.1). This study reports the first use of *in situ* analysis of chalcedony with microcrystalline quartz using a five μm analysis spot size across the chalcedony precursor for porosity-preserving microcrystalline quartz, and provides a previously unattainable record of these silica polymorph histories. The wide range of $\delta^{18}O$ values for detrital grains is not unexpected given the potentially wide range of source terrains (each with their own geological history) that could contribute to the supply of quartz to the Heidelberg Fm. It is noteworthy that quartz overgrowths have lower $\delta^{18}O$ values than microcrystalline quartz which in turn have lower $\delta^{18}O$ values than chalcedony.

4.6.1 Range of possible controls on $\delta^{18}O$ in the silica cements of the Heidelberg Formation

There are potentially three end-member influences on the $\delta^{18}O$ values of the silica cements in the Heidelberg Formation:

1. Silica polymorph-dependent fractionation of ^{18}O between water and solid phase,
2. Variable temperatures of growth (e.g. for similar water $\delta^{18}O$ values),
3. Variable water $\delta^{18}O$ values (e.g. for similar temperatures).

These will be discussed in the following sections.

4.6.2 Effect of silica phase on fractionation

There has been a range of quartz-water oxygen isotope fractionation equations published. Clayton et al., (1972) and Matsuhisa et al., (1979) published equations of the type ($A \times 10^6/T^2 - B$) while Meheut (2007) published a third order polynomial describing the fractionation. While these three are different in detail, they give similar results (less than 1‰ difference at low temperatures).

The oxygen isotope fractionation between amorphous silica and water has also been published and is also of the type ($A \times 10^6/T^2 - B$) (Kita et al., 1985). The A and B constants are both slightly higher than those for quartz and so effectively cancel each other out. There seems to be negligible difference between the isotope fractionation of quartz and water and amorphous silica and water.

From this analysis, the specific type of silica polymorph does not seem to play a significant role in influencing the measured $\delta^{18}O$ of the silica cements. It seems that the identification of amorphous silica is not of significance to the interpretation of the stable oxygen isotopes.

4.6.3 Temperature versus water type and their controls on δ18O in the silica cements

It is not possible to directly measure the $\delta^{18}O$ of the water that facilitated the growth of the silica cements in the Heidelberg Formation. Similarly, it is not possible to define uniquely the temperature of growth of the silica cements in the concentric bands. Therefore a range of scenarios will be explored to assess their geological plausibility.

4.6.3.1 Quartz overgrowths

The quartz overgrowths have an average $\delta^{18}O$ of +19.3‰. Quartz cement is typically assumed to begin growing at temperatures greater than approximately 80°C (McBride, 1989; Ramm et al., 1997; Lander and Walderhaug, 1999; Walderhaug, 2000; and Worden and Morad, 2000). The portion of the Heidelberg Formation studied does not contain more than a few percent quartz cement so it can be concluded that it has not been exposed to temperatures much greater than about 80°C. Using this temperature, either the Clayton et al., (1972) or Matsuhisa et al., (1979) fractionation equations and the average quartz overgrowth $\delta^{18}O$ value reveals that the water that generated the overgrowth had a $\delta^{18}O$ of -4.4‰. This value is slightly higher than contemporary meteoric water (Duarte et al., 2011) but this difference

would be expected if there had been any water-rock interaction. For reference, if a less likely quartz overgrowth temperature of 100°C was used, then the calculated $\delta^{18}O$ of the water would be -2‰. It seems likely that diagenesis and growth of the small amount of quartz overgrowth occurred in the presence of meteoric water that presumably entered the permeable Heidelberg Formation, during a lowstand, sometime after deposition (perhaps when the formation was part of an active aquifer).

4.6.3.2 Chalcedony and microcrystalline quartz

Three types of water have been modelled that plausibly could have resulted in the growth of the concentric bands of silica cements; meteoric water (the type of water that seems to have been responsible for the quartz overgrowths), seawater and deep crustal water, perhaps associated with mineralization (noting the existence of the lead-zinc deposits in the nearby Harz Mountains; Liebmann, 1992). The meteoric water can be assumed to have a $\delta^{18}O$ value of about -5‰ (Gat, 1996), similar to the value for the water responsible for quartz overgrowths. Seawater can be assumed to have a $\delta^{18}O$ of 0‰. Deep crustal water can be assumed to have a $\delta^{18}O$ value of about +5‰ (Gat, 1996). These end-member values can then be used in the isotope fractionation equations to deduce the approximate temperature of mineral growth in the concentric bands.

Using Clayton et al., (1972), the microcrystalline quartz mean $\delta^{18}O$ value of +22.7‰ gives a temperature of 57°C for meteoric water, 87°C for seawater and 127°C for deep crustal water (Fig. 4.7). The mixed chalcedony-microcrystalline quartz mean $\delta^{18}O$ value of +27.7‰ yields a temperature of 35°C for meteoric water, 58°C for seawater and 89°C for deep crustal water.

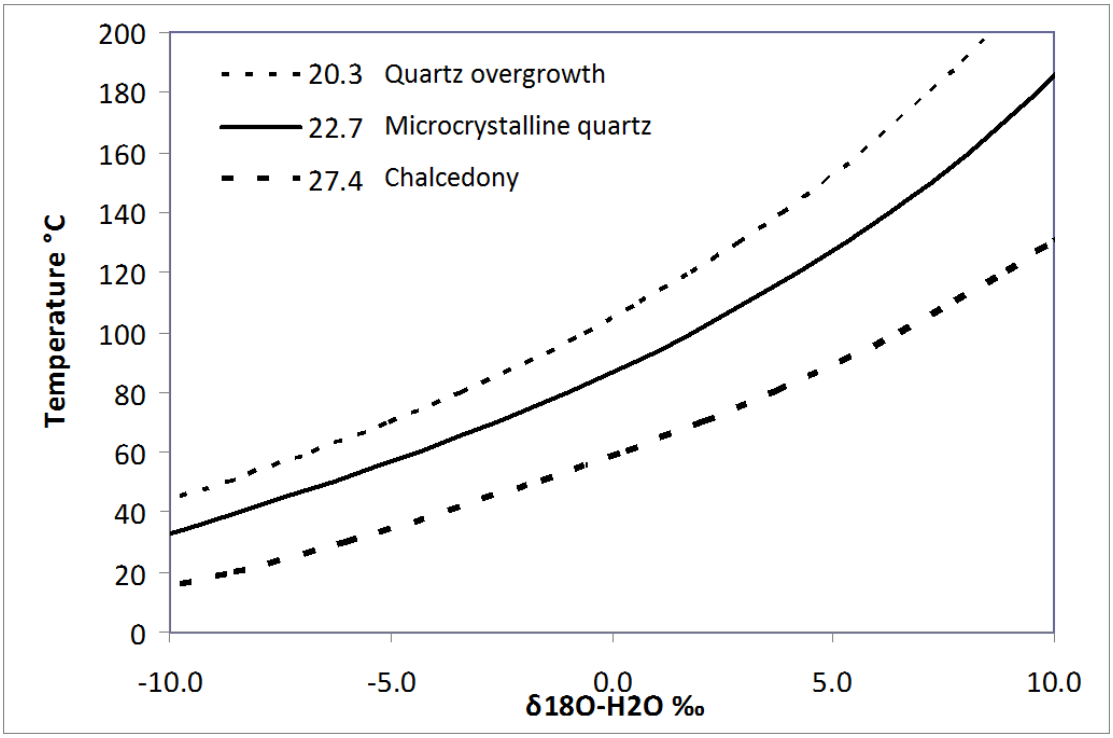

Figure 4.7 Calculated temperature curves for variable water $\delta^{18}O$ V-SMOW values in the range from -10‰ to +10‰ using a version of the silica-water oxygen isotope fraction curve (Clayton et al., 1972). The $\delta^{18}O$ values used are: quartz overgrowths, +20.3‰, microcrystalline quartz, +22.7‰, chalcedony, +27.4‰.

Again, using Clayton et al. (1972), the interpreted pure chalcedony value of $\delta^{18}O$ value of ~ +30‰ yields a temperature of 24°C for meteoric water, 45°C for seawater and 72°C for deep crustal water. On petrographic evidence (Fig. 4.2) chalcedony (bands 1 and 3) grew before microcrystalline quartz (bands 2 and 4) in two discrete events; it can be concluded that, if they grew from the same water, the chalcedony grew at a lower temperature than the microquartz that followed.

It is not impossible that the concentric bands of silica cement are due to an influx of deep crustal water (high $\delta^{18}O$ +5‰) which first grew chalcedony at ~ 89°C. The next event would have been microcrystalline quartz growth at 127°C requiring the water to become hotter with time. This sequence of events would then have been repeated, after a hiatus during which the host rock cooled down. This scenario seems unlikely since microcrystalline quartz is typically associated with relatively low temperatures of growth in sandstones (e.g. Vagle et al., 1994; Haddad et al., 2006).

Noting that the quartz overgrowth (Fig. 4.2) probably developed in meteoric water ($\delta^{18}O$ -4.4‰) at 80°C (see earlier) suggests that the meteoric water scenario for growth of the concentric bands of silica cements is more likely than the deep crustal fluid scenario. The implication is that there was an influx of cold meteoric water that gave rise to chalcedony growth at ~ 34°C followed by microcrystalline quartz growth from the same water, perhaps as it thermally equilibrated with the surrounding rock, at ~ 57°C.

4.6.4 Trace element data and silica cements

Trace elements in silica minerals can be present as part of a true solid solution, as material within aqueous fluid inclusions and as solid inclusions. Al, Fe^{3+} and Ti are considered to be able to form limited solid solution with quartz due to their similar ionic size and charge (Götze, 2009). While a limited quantity of monovalent cations are required to charge balance substitution of Al and Fe^{3+} in quartz, most group 1 and 2 cations (Na, K, Mg, Ca) are probably present within aqueous fluid inclusions. Submicroscopic solid inclusions can also account for elevated concentrations of metals in quartz (e.g. rutile needles or acicular hematite in quartz (Götze et al., 2009).

WDS analysis of the quartz overgrowth and microcrystalline quartz zone (Fig. 4.6) show that the first layer in each of the concentric bands has the highest concentrations of aluminium and iron (Figs. 4.2 and 4.6). On EBSD and TEM evidence this material is chalcedony containing both amorphous silica and nanocrystalline quartz. Aluminium concentrations are highest in the first deposited material and then tend to decrease towards the outer edge of the chalcedony bands. A layer of microcrystalline quartz was deposited on each of the chalcedony bands; microcrystalline quartz has very low concentrations of trace elements, including aluminium and iron. The repeated pattern of high aluminium and iron concentrations in chalcedony, followed by the lowest concentrations in microcrystalline quartz is further evidence of two discrete episodes of fluid influx.

Aluminium concentrations in quartz are reported to be a function of growth temperature. The specific concentration of aluminium has been proposed as a

geothermometer (e.g. Dennen et al., 1970). In microcrystalline quartz, aluminium is below detection (i.e. <12 ppm; Table 4.2, Fig. 4.6) suggesting a low temperature of growth. If it is assumed that the aluminium concentration in microcrystalline quartz is ≤11ppm then a temperature of ≤70ºC is implied (Dennen et al., 1970). By applying a maximum temperature of 70ºC to the microcrystalline quartz data and fractionation equation (Fig. 4.7) a water $\delta^{18}O$ value of <-4‰ is implied supporting the preferred interpretation of the microcrystalline quartz growing from meteoric water ($\delta^{18}O$ of -5‰) rather than deep crustal water ($\delta^{18}O$ of +5‰).

Aluminium data in chalcedony are difficult to interpret and are not easily related to temperature of growth (Götze et al., 2001). There are numerous precedents for elevated aluminium concentrations in other amorphous forms of silica such as opal and agate (Heaney and Davis, 1995; Merino et al., 1995; Götze et al., 2001).

The other trace elements in the silica cements, and especially the concentric bands (Figs. 4.2 and 4.6) are difficult to interpret but it is noteworthy that Ti, Fe, Na, Ca, K and Mg are all at elevated concentrations in the chalcedony compared to the quartz overgrowth and the microcrystalline quartz. It seems likely that cations of common salts (Na, K, Mg, and Ca) may be at elevated concentrations in chalcedony due to their entrapment in fluid inclusions (too small for fluid inclusion analysis). In contrast, the high concentrations of Ti may be present in solid inclusions, or possibly in solid solution, within chalcedony. Iron, like aluminium, is considered to be able to form a limited solid solution with silica (Götze, 2009) and maybe structurally bound within the chalcedony.

4.6.5 Model for microcrystalline quartz growth

Chalcedony band-1 has a slightly higher $\delta^{18}O$ value than chalcedony band-3 suggesting either lower temperature growth or a more negative $\delta^{18}O$ of the aqueous medium for the first phase of chalcedony formation (Fig. 4.5). Band 1 also has higher Al and lower Fe concentration than band 3 confirming the subtle differences in the two phases of chalcedony growth (Fig. 4.6). Band 2-microcrystalline quartz overlies band 1-chalcedony and has a slightly lower $\delta^{18}O$ value than band-4 microcrystalline

quartz (Fig. 4.6). The isotopic and trace element data suggest an initial event in which first chalcedony and then microcrystalline quartz grew followed by a repeating sequence from slightly different water (in terms of trace element chemistry and isotopes).

The SiO_2 concentration-temperature diagram for different silica polymorphs (Kastner et al., 1977) suggests that the amorphous silica (in chalcedony bands-1 and -3, Fig. 4.2F) required an elevated silica concentration of about 120 ppm for growth at about 34°C (interpreted from the stable isotope data) while the subsequent microcrystalline quartz growth required a silica concentration of about 20-24 ppm at 61°C (also interpreted from the stable isotope data and supported by the aluminium concentration data). The pre-existing quartz overgrowths (70°C from stable isotope data) required a silica concentration of up to about 40 ppm.

The water responsible for chalcedony growth, with high concentrations of silica, also had high concentrations of trace elements, specifically aluminium and iron. As amorphous silica began to precipitate on the quartz grains or overgrowths, the concentration of silica decreased and nanocrystalline quartz began to develop; overall this is the chalcedony layer seen in CL, BSEM, EBSD and TEM (Figs. 4.2-4.3). Larger EBSD-discernible quartz crystals began to grow (the microcrystalline quartz in Fig. 4.2) as silica saturation fell and the precipitation rate slowed down. This model illustrates that the growth of concentric bands of silica cements in the Heidelberg Formation required two influxes of relatively cold (< 34°C) meteoric water with high concentrations of silica, aluminium and other trace elements. Each influx precipitated chalcedony (amorphous silica and nanocrystalline quartz) and then heated up as microcrystalline quartz eventually precipitated (at 57°C) from waters with much lower silica and aluminium (and other trace element) concentrations.

It is noteworthy that the concentric bands of silica cement from the Heidelberg Formation reported here bear notable petrographic similarities to silcrete from the Fontainebleau Formation (Thiry and Marechal, 2001; Haddad et al., 2006) from the Cordillo Formation (Alexandre et al., 2004). Indeed the interpretation of the type of water (meteoric) and temperature of growth of silica cements in the Heidelberg Formation seems to suggest that these cements are related to warm groundwater flow.

In the Fontainebleau Formation it appears that silica precipitation occurred at the interface between groundwater and downward percolating recharge water (Thiry and Marechal, 2001). The cause of elevated silica concentrations required for silcrete formation remains unknown but metastable complexation has been proposed. The elevated concentrations of both silica and aluminium required for the growth of the chalcedony in the Heidelberg Formation may both result from destabilization of complexed SiO_2 and aluminium.

4.7 Conclusions

This is the first combined study of silica cements reported using WDS, spatially-resolved stable oxygen isotope analysis using nanoSIMS and high resolution mineralogical and crystallographic analysis using BSEM, EBSD, TEM and CL to provide a previously unattainable record of silica polymorph evolution to reveal the following:

1. A small volume of quartz overgrowths are present in the quartz arenitic Heidelberg Formation suggesting growth at approaching 80°C. Chalcedony, composed of amorphous silica and nanocrystalline quartz, grew as a coating on all surfaces (detrital grains and quartz overgrowths alike) followed by a layer of microcrystalline quartz. This cycle of chalcedony and microcrystalline quartz was then repeated due to a second influx of meteoric water.

2. There is a link between the stable oxygen isotope values and silica type in the Heidelberg Formation. Oxygen isotope values in the Heidelberg sandstones are different for the different types of silica: detrital quartz grains have an average $\delta^{18}O$ of +9.4‰. Quartz overgrowths have a higher $\delta^{18}O$ (average +20.3‰). Chalcedony mixed microcrystalline quartz has an average $\delta^{18}O$ of +27.4‰). Microcrystalline quartz has an average $\delta^{18}O$ of +22.7‰. Temperatures of formation of the silica polymorphs based on meteoric $\delta^{18}O$ water values are: quartz overgrowths, 70°C, chalcedony, 34°C and then microcrystalline quartz, 57°C (Table 4.3).

Silica Polymorph	$\delta^{18}O$ (‰)	T (°C) ($\delta^{18}O_{water}$ = -5.0(‰)	T (0C) (δ18Owater = 0(‰)	T (0C) (δ18Owater = +5(‰)
Quartz OG (min.)	**19.0**	78.2	115.4	167.7
Quartz OG (max.)	**21.9**	61.0	92.5	135.0
Microquartz (min.)	**21.0**	66.1	99.2	144.4
Microquartz (max.)	**23.5**	52.5	81.5	119.9
MQ + Chalcedony (min.)	**24.5**	47.5	75.1	111.2
MQ + Chalcedony (max.)	**30.8**	20.6	41.4	67.2
Averages				
Quartz OG	**20.3**	70.2	104.6	152.1
Microquartz	**22.7**	56.7	86.9	127.2
MQ + Chalcedony	**27.4**	34.3	58.3	88.9
Chalcedony	**30.0**	23.7	45.1	72.0

Table 4.3 Calculated temperatures of silica precipitation using the Clayton et al. (1972) quartz-water oxygen isotope fractionation equation and oxygen isotope data from quartz overgrowths, microcrystalline quartz and chalcedony. Temperatures of precipitation have been calculated for fractionation with meteoric water (-5‰), oceanic water (0‰) and magmatic water (+5‰).

3. There is a link between trace element concentrations and silica polymorph variations in the Heidelberg Formation. Microcrystalline quartz has aluminium concentrations below detection confirming the low temperature of growth. Trace element data from chalcedony provide evidence for two episodes of influx of fluid with high aluminium and iron concentrations into the Heidelberg Formation sandstone. The initial chalcedony layer has the highest concentrations of trace elements. Concentrations of aluminium and iron tend to decrease as chalcedony growth progressed during both of the fluid influxes (Fig. 4.6).

4. Chalcedony and microcrystalline quartz grew in the Heidelberg Formation as a result of meteoric water influx into the formation. The meteoric waters probably had high concentrations of silica and aluminium, possibly due to complexation. Silica and aluminium concentrations declined during growth of chalcedony (34°C), as the temperature began to rise resulting in microcrystalline quartz growth (57°C).

5 Orientation of microcrystalline quartz in the Fontainebleau Formation, Paris Basin and why it preserves porosity

5.1 Abstract

In sedimentary basins, deeply buried sandstones typically have low porosity due to cementation and compaction. There are several known causes of anomalously high porosity in sandstones, one of which is microcrystalline quartz coatings on sand grains that inhibit the growth of quartz cement. High resolution scanning electron microscopy, electron backscattered diffraction, fourier transform infrared spectroscopy and transmission electron microscopy has been used to study the microcrystalline quartz-cemented Oligocene Fontainebleau Formation, Paris Basin, France. Where the microcrystalline quartz is absent in the Fontainebleau Formation, the rock is tightly cemented by a large amount of syntaxial quartz overgrowths. Where microcrystalline quartz is present, a small and variable amount of syntaxial quartz cement formed initially but was followed by a layer of amorphous silica. The microcrystalline quartz sits on top of the amorphous silica. In contrast to the syntaxial quartz overgrowths, the microcrystalline quartz has a different lattice orientation to the underlying quartz grain. Instead, the microcrystalline quartz has its *c* axes parallel to whatever host surface it is sitting on, implying that its *a* axes (better defined as [11-20] directions) are perpendicular to the host surface. This is analogous to chalcedony. The *c* axes of individual microcrystalline quartz crystals are not parallel to each other on their growth surfaces, instead having about 30^{o} of rotational scatter on the growth surface. The amorphous silica has insulated the detrital quartz grain and any incipient syntaxial cement and helped to prevent further syntaxial growth. The subsequent growth of polynuclear, chalcedony-like microcrystalline quartz has also prevented further growth of quartz since the fast-growth *c* axes do not extend into the neighbouring pore but instead compete for space on the host grain surface. The combination of insulating amorphous silica and the orientation of microcrystalline

quartz hase been effective in preventing any further syntaxial quartz cement and so has preserved porosity.

5.2 Introduction

Finding new petroleum reservoirs with high porosity is increasingly important as demand for energy increases. In sandstones, the main cause of porosity-loss is quartz cement (McBride, 1989; Worden and Morad, 2000), which forms at temperatures > 80°C, and eventually occludes the pores between host grains. Thus, sedimentary researchers have assumed that when sandstones are buried to temperatures > 80°C, they rapidly lose porosity and potentially have limited reservoir potential. A subset of sandstones contain microcrystalline quartz cement (defined as 0.5 to 10.0 μm; Vagle et al., 1994) and exhibit anomalously high porosity deep in sedimentary basins (typically > 3500m). Microcrystalline quartz occurs as fine coatings of crystallites on quartz grains that prevent the growth of ordinary quartz cement (Aase et al., 1996; Bloch et al., 2002; Jahren and Ramm, 2000; Lima and De Ros, 2002; McBride, 1989; Vagle et al., 1994). Sedimentary microcrystalline quartz has been found in Devonian to Miocene sandstones (Haimson and Lee, 2004; Lima and De Ros, 2002) from regions as diverse as Brazil (Lima and De Ros, 2002), Colombia (Warren and Pulham, 2001), the United States (Haimson and Lee, 2004), the North Sea Basins (Aase et al., 1996; Hendry and Trewin, 1995; Ramm et al., 1997; Vagle et al., 1994; Weibel et al., 2010), Continental Europe (Worden et al., 2012), North Africa (Goldstein and Rossi, 2002), modern eolian deposits in the Uluru Formation in Australia (W. Heins, Personal communication), Saudi Arabia (Cagatay et al., 1996) and Japan (Hattori et al., 1996).

Quartz cement is typically syntaxial with the host grain, growing in optical and crystallographic continuity with the detrital quartz grain (McBride, 1989). In contrast, microcrystalline quartz does not grow in optical continuity with the host quartz grain (Chapter 2 - Worden et al., 2012; Haddad et al., 2006; Hendry and Trewin, 1995). Instead it grows as apparently randomly oriented crystals that are 0.5 to 10 μm in length (Vagle et al., 1994). Borrowing from tectonite fabrics, the Heidelberg microcrystalline quartz predominantly displays an “S” fabric or planar fabric (strong

c-axis orientation, but somewhat randomly oriented in the a-axes) and could be termed an S-diagenite, while the Fontainebleau microcrystalline quartz displays a linear or "L" fabric (some control on the linear a-axes), as well as, the "S" fabric and could be termed an LS-diagenite. Microcrystalline quartz is routinely associated with sandstone beds rich in biogenic silica, such as sponge spicules (Aase and Walderhaug, 2005; Hendry and Trewin, 1995) and seems to develop at the expense of silica bioclasts at temperatures of about 50°C (Vagle et al., 1994). Once detrital grains have a continuous coating of microcrystalline quartz, the overgrowth of optically- and crystallographically-continuous quartz cement is prevented. Therefore, early microcrystalline quartz inhibits ordinary quartz cement growth, preserves porosity and leads to anomalously high porosity in deeply buried sandstones. It has been suggested that elevated silica saturation, resulting from the very presence of microcrystalline quartz, inhibits quartz dissolution during burial and prevents quartz cementation (Hendry and Trewin, 1995). However, in the Heidelberg Sandstone, Germany, a combined electron backscatter diffraction/TEM/CL study revealed a twice-repeated growth sequence of amorphous silica, followed by chalcedony and then microcrystalline quartz (Chapter 3 - French et al., 2012; Chapter 2 - Worden et al., 2012). The Heidelberg microcrystalline quartz has a systematic misorientation between the detrital grain and the microcrystalline quartz, having c-axes sub-parallel to, but totally randomly oriented on, the parent-grain surface upon which microcrystalline quartz developed. The Heidelberg microcrystalline quartz thus has the same orientation pattern as chalcedony. The Heidelberg microcrystalline quartz has preserved porosity due to the layer of amorphous silica insulating the quartz grains and the chalcedony-like orientation of the microcrystalline quartz being unfavourable to *c*-axis growth into the pore.

In order to understand further the mechanism responsible for the growth of misoriented microcrystalline quartz, sandstone samples from the Oligocene Fontainebleau Formation in the Paris Basin, France (Thiry, 2001; Haddad et al., 2006) have been studied. High resolution electron microscope techniques were used to study the microcrystalline quartz and its relationship with the host grain. The crystallographic orientation of microcrystalline quartz crystals relative to their host quartz grains was assessed for the Fontainebleau Formation, to understand the mechanism of microcrystalline quartz growth and to determine the controls on the

misorientation of microcrystalline quartz. The following questions will be addressed in this study:

1) What silica phases are present in the Fontainebleau Formation?
2) What is the sequence of cementation events in the Fontainebleau Formation?
3) What controls the crystallographic orientation of the microcrystalline quartz?
4) How has microcrystalline quartz preserved porosity in the Fontainebleau Formation?
5) Is the Fontainebleau Formation microcrystalline quartz similar to the Heidelberg Formation microcrystalline quartz?

The results of this study will test if the Heidelberg microcrystalline quartz growth mechanism is an exception or a rule. This will provide additional insights into the growth mechanism for microcrystalline quartz by providing a second test example to elucidate the growth mechanism of microcrystalline quartz and porosity preservation in sandstone reservoirs.

5.3 Methods

5.3.1 Transmitted-light optics

Transmitted-light optical analysis identified and located quartz overgrowths and microcrystalline quartz on detrital host quartz grains. The location of the quartz overgrowths was based on the identification of euhedral grains, with sharp, clean edges and, to some extent, on the presence of dust rims. Microcrystalline quartz lining the pore spaces was identified with a petrographic microscope, but due to the small size, microcrystalline quartz is best characterized with the scanning electron microscope.

5.3.2 Scanning Electron Microscopy (SEM)

Scanning electron microscopy resolved microcrystalline quartz by its high resolution capabilities. High-resolution secondary electron images (SEI) and backscattered electron images (BEI) were acquired using a JEOL 6330F FEG-SEM and a JEOL 6490LV SEM.

5.3.3 Cathodoluminescence (CL)

Cathodoluminescence identified and distinguished detrital quartz grains from syntaxial quartz overgrowths and microcrystalline quartz (Evans et al., 1994). CL images were taken with an accelerating voltage of 10 kV (in contrast to 20 kV for BSE), 8 nA beam current, and 16.5 mm working distance. CL images were collected by accumulating a signal of 500 frames using a slow-scanning raster and red, green, and blue wavelength CL were collected and added using processing to produce a ChromaCL image. A JEOL 6490LV SEM, fitted with a Gatan cathodoluminescence detector (ChromaCL-006) was used for cathodoluminescence analysis.

5.3.4 Electron Backscatter Diffraction (EBSD)

The principles and techniques of EBSD have been explained in previous papers (e.g., Venables and Harland,1973; Dingley,1984; Schmidt and Olesen,1989; Adams et al., 1993; Wilkinson and Hirsch, 1997; Prior, 1999; Prior et al., 2009). This paper is the fifth investigation (following Haddad et al., 2006; Mörk and Moen, 2007; Chapter 2 - Worden et al., 2012; Chapter 3 - French et al., 2012) to utilize EBSD to address sandstone diagenetic questions. EBSD has the capability to resolve crystallographic orientations at a resolution as small as 200 nanometres to reveal microstructural information about the crystal structure and mineralogy of the material being analysed. EBSD analysis was performed on polished thin sections using a LEO 1530 SEM fitted with an Oxford-HKL EBSD system.

5.3.5 Transmission Electron Microscopy (TEM)

TEM is capable of imaging at markedly higher resolution than SEM and EBSD approaches (with selected area electron diffraction (SAED)), and has been used to characterize crystal structure and microstructures in various silica polymorphs (Wahl et al., 2002; Graetsch et al., 1987; Miehe et al., 1984; and Heaney et al., 1994). TEM was used in this study to distinguish the different silica polymorphs. A Focused Ion Beam Scanning Electron Microscope (FIB-SEM) was used to prepare samples for TEM analysis. The FIB-SEM uses a finely focused beam of ions (generally gallium) that can be operated at a high beam current for milling the sample. Beginning with the thin section, the sample is first examined with a petrographic microscope to identify the area of interest, then with EBSD to identify the non-diffracting zone, and finally with CL to focus on the area to sample. The sample is then ion milled, extracted from the thin section and mounted on a TEM grid. The TEM samples were prepared using a FEI NOVA 200 focused ion beam (FIB) SEM at Purdue University in the Birck Nanotechnology Center. Samples prepared using FIB-SEM were then analysed in a Philips CM200F TEM/STEM operated in the bright field imaging TEM mode at an accelerating voltage of 200kV.

5.3.6 Fourier Transform Infrared (FT-IR) spectroscopy

The utilization of infrared spectra to determine silica mineral phases by water content and speciation has been outlined previously by Langer and Flörke, 1974; Graetsch et al.,1985; and Kronenberg, 1994. Infrared spectra of the Fontainebleau sample were obtained using a liquid-nitrogen-cooled Nicolet Centaurus FT-IR microscope (Thermo Electron Corporation). Binocular lens (x 10) gave an optical image of the sample and rectangular apertures 300 x 300 μm were used for taking the measurement. Spectra were collected at 4 cm^{-1} resolution with 100 scans collected and averaged. Reflectance spectra were generated and converted to absorption spectra using OMNIC software (Thermo Electron Corporation). Peak positions were determined by taking positions of local maxima following linear baseline correction. The position of these peaks was within ± 3 cm^{-1} since a wavenumber resolution of 4 cm^{-1} was applied for the IR measurement.

5.4 Results

5.4.1 Transmitted light and SEM Analysis

Optical images of the sample (Fig. 5.1A) show cemented quartz grains that are subangular with some strong angular facets caused by quartz cementation.

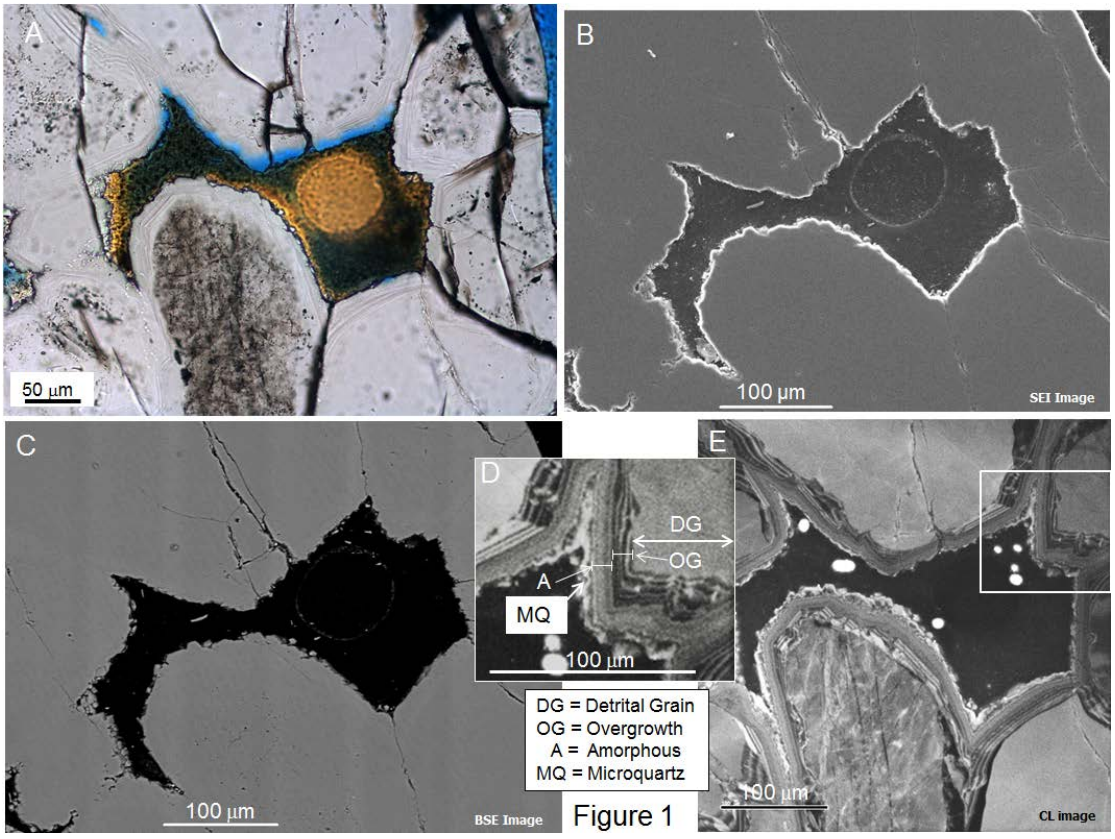

Figure 5.1 - Petrographic microscope image (A) in plane polarized light of the angular cemented quartz grains and the concentric layers of quartz overgrowths. Secondary electron image (B) of the same area shown in A, backscatter electron image (C) reveals that the grains and cements are composed of silica and cathodoluminescence images (D and E) show the concentric, isopachous layers of quartz cement, high resolution CL (D) distinguishes the detrital grain with bright luminescence (DG) from the quartz overgrowth with dark and bright alternating bands (OG), the amorphous silica layer or non-luminescing band (A), and the bright microcrystalline quartz (MQ).

The Secondary Electron Image (SEI) (Fig. 5.1B) shows that SEI cannot distinguish between quartz overgrowths and detrital host grains. It also highlights that microcrystalline quartz is the final layer of the diagenetic sequence. The backscattered

electron image (Fig 5.1C) has a uniform signal, suggesting that the overgrowth is pure silica (confirmed by secondary X-ray analysis using energy dispersive spectroscopy (EDS) in the SEM). High resolution secondary electron images (SEI) revealed that microcrystalline quartz crystals coat grains with their long growth axes (*c* axes) parallel to the host surface but microcrystalline quartz crystals are subtly misoriented relative to neighbouring crystals on that host surface.

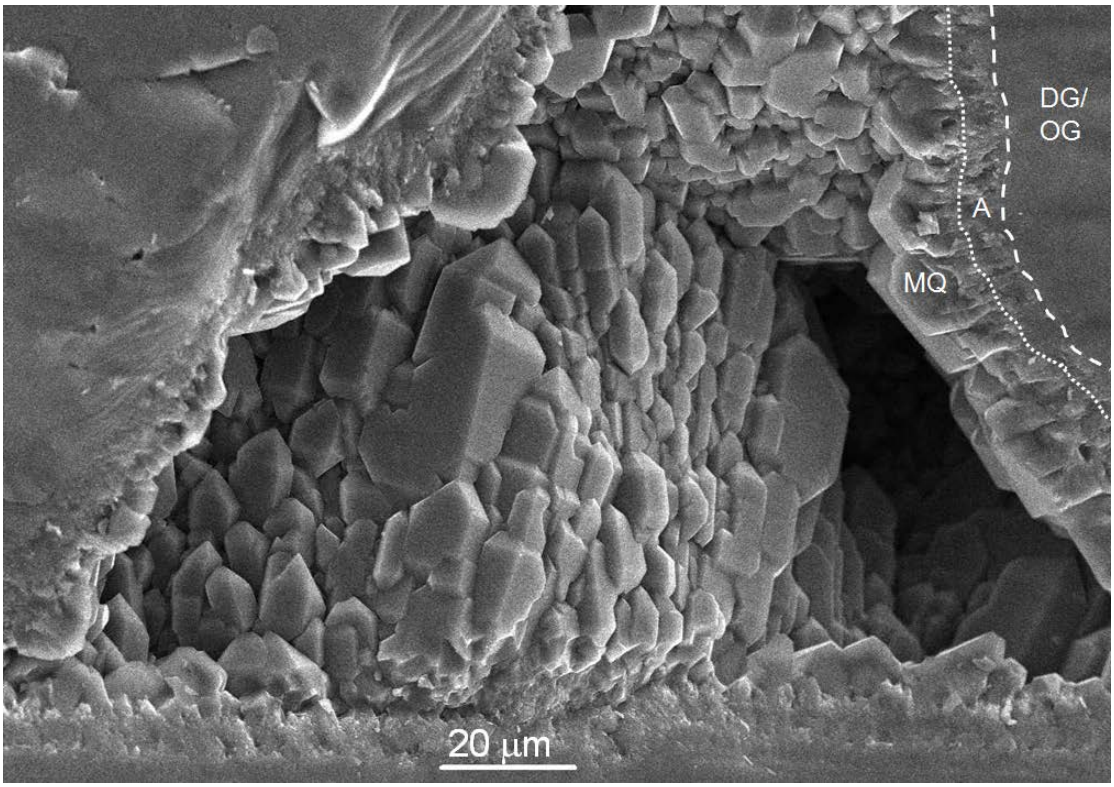

Figure 5.2 - High resolution secondary electron image (SEI) of microcrystalline quartz at 800x showing that the microcrystalline quartz grows parallel to the surface upon which it grows. Even without crystallographic orientation information, such as EBSD, this image reveals that the *c* axes of the microcrystalline quartz grew parallel to the surface although slightly rotated. In the upper right hand portion of the image, the detrital grain/quartz overgrowth surface (DG/OG) is shown with the dashed line with the amorphous silica (possibly including chalcedony) layer (A) growing on top and the microcrystalline quartz layer (MQ) growing with its [0001] surface parallel to the amorphous silica layer (A).

The detrital quartz grain/overgrowth (DG/OG) edge and an intermediate layer (A) can also be identified beneath the microcrystalline quartz (MQ).

5.4.2 Cathodoluminescence (CL) Analysis

Cathodoluminescence discriminates detrital grains that luminesce brightly, zoned overgrowths and material with highly variable banded luminescence, the brightly luminescent microcrystalline quartz which coats the edge of the pore, and the non-luminescent resin-filled porosity. High resolution CL images (Fig. 5.1C) allow differentiation of four types of silica: 1) detrital quartz grain, that is variably bright in CL and is also homogenous, 2) quartz overgrowths that are thin, alternating light and dark bands and form flat euhedral surfaces, 3) intermediate band(s) on top of the quartz overgrowths that are not as dark in CL as the overgrowths and also show some lighter and darker banding, 4) the last phase of moderately brightly luminescing microcrystalline quartz (as defined by Vagle et al.,1994 and Lima and De Ros, 2002), which has many small (0.5 to 5 μm) individual quartz crystals in a band between 2 and 4 μm thick (Figure 5.1D).

5.4.3 EBSD - Orientation Analysis

The EBSD crystal orientation image

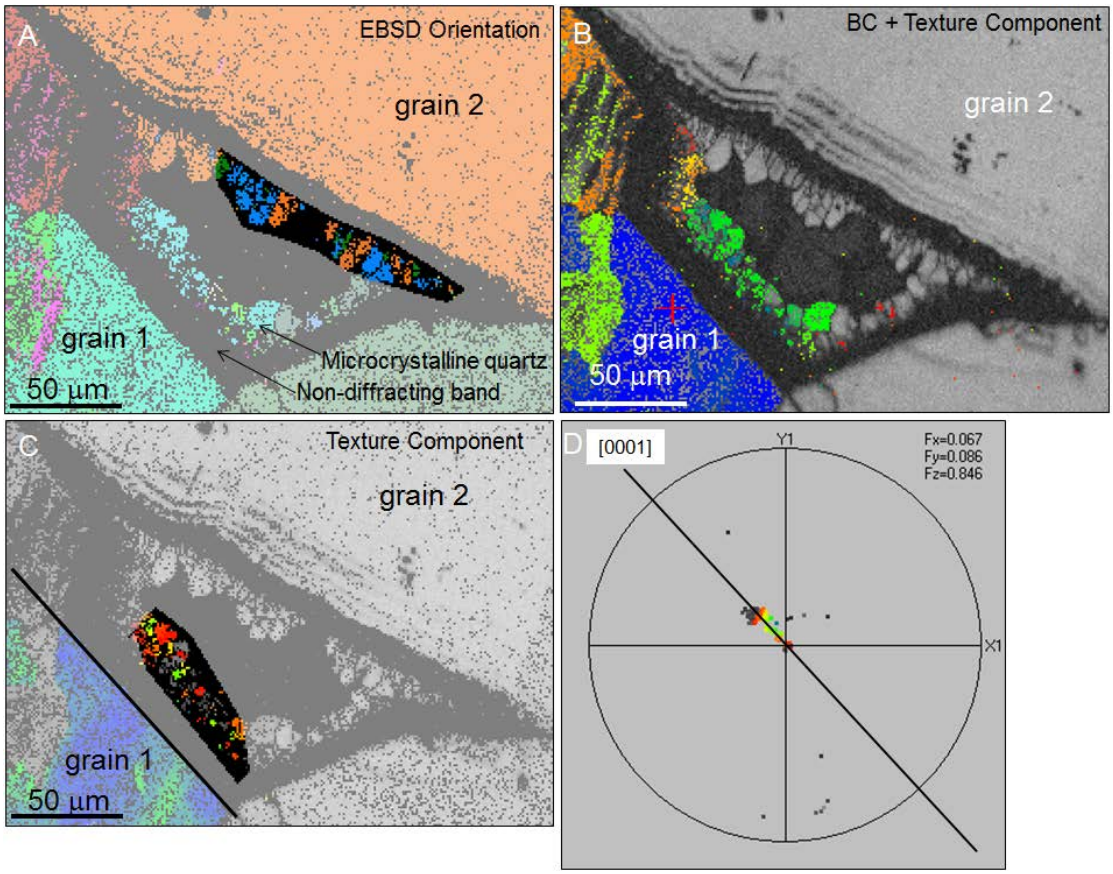

Figure 5.3 - A) Electron backscatter diffraction (EBSD) orientation image showing that the microcrystalline quartz grains have different crystallographic orientations than their adjacent host quartz grains (as represented by the different colours) and the un-indexible "zero-solution zone" in black) between the grains and the microcrystalline quartz. B) EBSD band contrast and texture component image showing the host grain orientation, grain 1, in blue and microcrystalline quartz in multiple colours indicating that the crystallographic orientation of the host grain and the adjacent microcrystalline quartz crystals are different. (C) Texture component image highlighting the microcrystalline quartz adjacent to grain 1 and its (D) pole figure of the c-axis [0001] orientation of the microcrystalline quartz on the surface of grain 1. The orientation of the microcrystalline quartz is spread in a girdle parallel to the host surface. The trace of a great circle of the microcrystalline quartz data, shown by the black line in D, matches the orientation of the face of the host grain (black line in C) indicating that the material on the surface of the host grain is controlling the growth of the microcrystalline quartz. Note that the rotation of the grains is relatively small in (D).

(Fig. 5.3A) reveals that the microcrystalline quartz has different crystallographic orientations (represented by the different colours) to the host detrital grains. The

EBSD orientation image (Fig 5.3A) also shows that the microcrystalline quartz has a variety of crystallographic orientations (similarly represented by the different colours) and that none of the microcrystalline quartz crystals adjacent to the host grains have inherited the crystallographic orientation of the host grain. This is also shown by the band contrast and texture component image (5.3B) using grain 1 as the index grain (in blue) versus the green colour of the adjacent microcrystalline quartz.

The EBSD orientation image (Fig. 5.3A) also shows that the intermediate band between the microcrystalline quartz and the detrital grain has yielded no crystallographic orientation data, i.e. it is a non-diffracting band. Following the approach explained by Haddad et al., (2006), these bands are non-diffracting because the point-by-point EBSD analysis from this area yielded no Kikuchi patterns (electron backscatter patterns). CL and backscatter images (Figs 5.1C and 5.1E) and qualitative secondary X-ray analysis (EDAX) revealed that this band is silica (SiO_2). There are two possible explanations for the non-diffracting SiO_2 bands: 1) the crystal size is below the ~1 μm spot size of the EBSD used for this analysis, or 2) this material is amorphous or poorly crystalline and does not have enough long-range crystal structure to diffract electrons. To resolve this region a transmission electron microscope for further investigation was utilized.

5.4.4 EBSD - Pole Figure Analysis

Pole figures of selected EBSD data are stereographic projections that represent the orientation of crystallographic planes (zones) and directions in sample coordinates (Fig. 5.3D). Microcrystalline quartz crystals adjacent to the northeast face of grain 1 (Fig. 5.3C) have their *c*-axis orientations [0001] spread in a narrow girdle parallel to the grain surface. The trace of the girdle is sub-parallel to the trace of the growth surface (shown as the black line in Fig. 5.3C). This analysis was repeated in multiple samples and in each case, the results were consistent showing that microcrystalline quartz *c* -axes lie parallel to their host grain surfaces but are misaligned having a ~ 30º rotational dispersal on that surface (i.e. they have subparallel c-axes on the surface they have grown on).

5.4.5 TEM Analysis of Non-Diffracting Bands

As with the EBSD analysis, small crystals were identified using selected area electron micro-diffraction of the crystal lattice in the microcrystalline quartz zone. In the sample taken adjacent to the overgrowth-detrital host grain in the EBSD zero-solution zone, the bright field TEM images (Figs. 5.4A and D) showed crystalline material

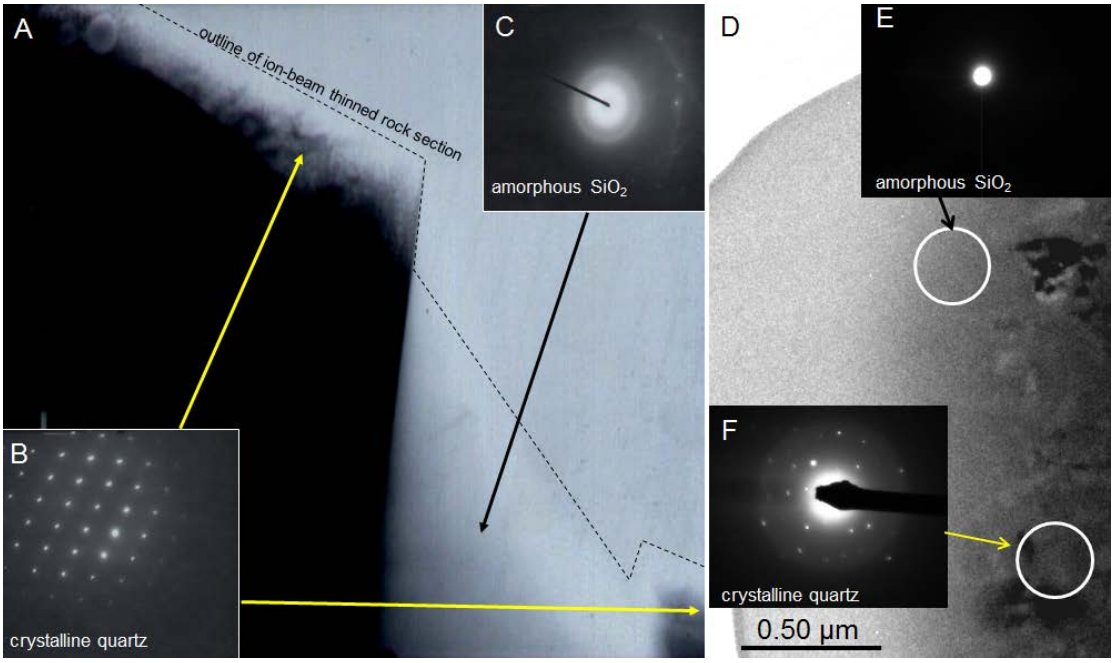

Figure 5.4 - Bright field TEM image (A and D) at a magnification of approximately 200,000 showing crystalline material, amorphous material and their respective microdiffractions. Microdiffractions (B and F) of the material in the adjacent circle or arrow showing crystalline diffraction patterns with some degree of rotation suggested in the diffraction spots. Microdiffractions (C and E) of the material in the adjacent circle or arrow showing only the transmitted beam (no diffracted intensities) as evidence for amorphous silica.

with a distinct diffraction pattern with a small degree of rotation of the diffraction spots (Figs. 5.4B and F). Given the crystal size, (Fig. 5.4F, Heaney, 1993), silica composition and rotation of crystals, this material resembles chalcedony. The bright field TEM images (Figs. 5.4A and D) also contained a material that did not diffract the electron beam (Fig. 5.4C and E), strong evidence for some of the material in this EBSD zero-solution zone being non-crystalline amorphous silica.

5.4.6 Fourier Transform Infrared (FT-IR) spectroscopy Analysis

Infrared absorption spectra from the layer that has no EBSD response on top of the quartz overgrowth and lies directly beneath the microcrystalline quartz in the Fontainebleau; Fig 5.1D, 5.5A)

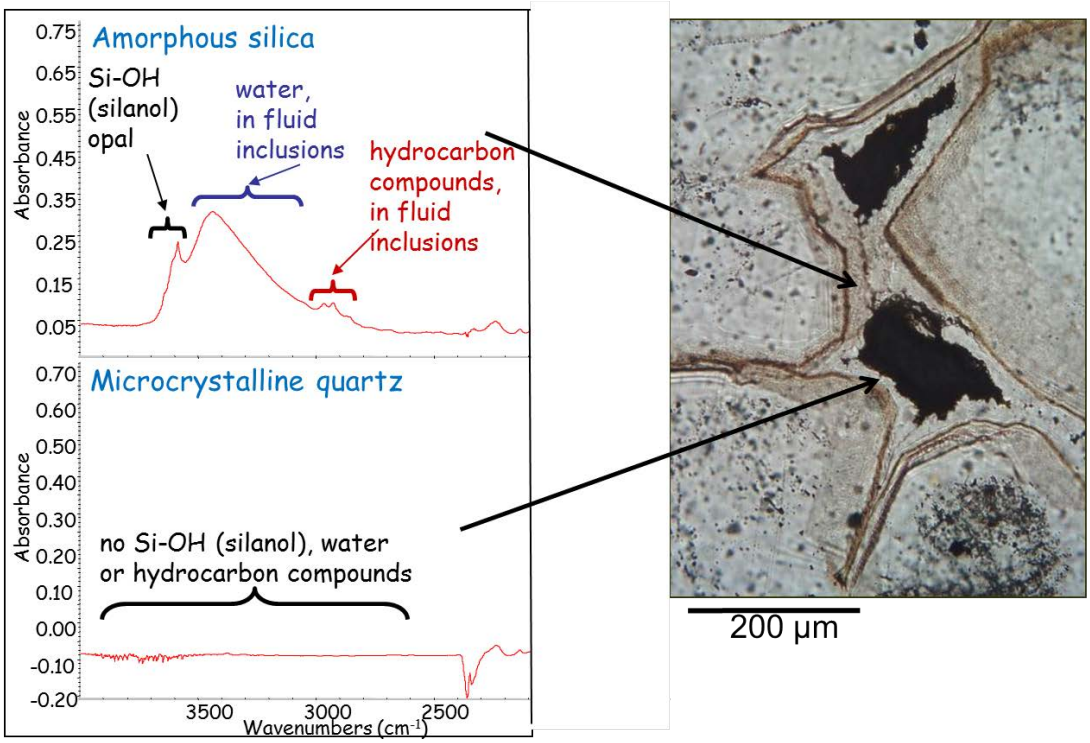

Figure 5.5 - FT-IR data of fluid inclusion trail in silica cement showing Si-OH (silanol) peak evidence for amorphous silica precursor, peak showing water in fluid inclusions and peak showing hydrocarbon compounds in fluid inclusions. FT-IR data of microcrystalline quartz showing no Si-OH (silanol), water or hydrocarbon compounds.

has a well-defined band at 3585 cm^{-1} indicative of the presence of Si-OH (silanol) bonds (Langer and Flörke, 1974; Kronenberg, 1994; Yamagishi et al., 1997). There is also a broad peak at ~ 3435 cm^{-1} indicating the presence of molecular H_2O trapped within this layer. Additionally, the complex bands between ~ 2950 and 3000cm^{-1} are due to the occurrence of $-CH_2-$ and $-CH_3$ hydrocarbon molecular units trapped within the layer. In contrast, the IR spectrum for the microcrystalline quartz cement shows no bands between 3800 and 2800 cm^{-1} indicating the complete absence of molecular water, silanol or hydrocarbons in the crystalline silica.

5.5 Discussion

5.5.1 Silica polymorphs in the Fontainebleau Formation

5.5.1.1 Quartz Overgrowths

Petrographic and SEM-CL observations (Figs. 5.1A, 5.1D and 5.1E) revealed that a small amount of early-formed (pre-microcrystalline quartz) syntaxial quartz overgrowth cements developed on the detrital quartz grains. The CL images (Figs. 5.1D and E), show that the quartz overgrowths are somewhat poorly developed and therefore represent an early stage of growth. In the sample studied, these embryonic quartz overgrowths did not occlude much of the porosity before being coated with an amorphous silica phase. The quartz overgrowths inherited the crystallographic orientation of the detrital host grains upon which they grew (Fig. 5.3A), as is typical of quartz overgrowths (Mörk and Moen, 2007; Worden and Morad, 2000).

5.5.1.2 Amorphous Silica

A surface layer coating the detrital grain and the embryonic quartz overgrowths, beneath the microquartz, was identified in CL (Figs. 5.1D and E) and EBSD (Fig. 5.3A) in the Fontainebleau Formation. The layer is silica but is not fully crystalline at the resolution possible using EBSD (~1 μm). Selected Area Electron Diffraction (SAED) analysis of this layer in the TEM showed that part of the surface material contains nanometre sized crystals of quartz (Fig. 5.4F) but much of it did not diffract the electron beam in the TEM (Figs. 5.4C and E). This suggests that the thin surface-coating film is dominated by truly amorphous, non-crystalline silica. TEM examination of numerous samples suggests that the amorphous silica-dominated layer is ubiquitous on sand grain surfaces in rocks where microcrystalline quartz is present.

The infrared spectra showed that the amorphous layer contains silanol (Si-OH), groups diagnostic of water-bearing amorphous, opaline silica, thus reinforcing the

crystallographic evidence from EBSD and TEM analysis. Previous investigations focusing on water content and speciation in silica minerals (Florke et al., 1982; Graetsch et al., 1985) have suggested that cryptocrystalline silica minerals easily incorporate water due to the highly disordered crystal structure present in such minerals. The presence of *molecular* water in the amorphous silica layer is probably associated with submicroscopic fluid inclusions trapped within this cement. It is not clear whether these represent primary features or are due to partial crystallization of the amorphous phase with the subsequent exsolution of spare water. The molecular hydrocarbon units evident in the infrared spectrum were not expected; they may also represent fluid trapped within inclusions in the amorphous silica layer. Note that destabilization (oxidation) of organo-silica complexes has been mooted as a possible contributory process in the creation of the silica cements in the Fontainebleau Formation (Thiry and Marechal, 2001) so that the organic signal detected by infrared microscopy may represent remnants of the organic complexes.

5.5.1.3 Microcrystalline Quartz

The orientation data (Fig. 5.3C) reveal that crystals of microcrystalline quartz have grown with their *c* axes parallel to, but rotationally dispersed by ~ 30°, on the amorphous silica-coated host grain surface. EBSD data from microcrystalline quartz suggest that the microcrystalline quartz grew with its [11-20] face projecting into the pore space. Formation of chalcedony typically occurs by preferential growth of crystals with [11-20] orthogonal to their growth surface, in contrast to quartz which typically grows with its c-axes into open pore spaces. Thus microcrystalline quartz has the same crystallographic orientation relationship as the silica polymorph chalcedony (Heaney et al., 1994).

5.5.2 Control on the Orientation of Microcrystalline Quartz

The simplest explanation for the orientation of the microcrystalline quartz in the Fontainebleau Formation is that it grew on chalcedony, within or on the amorphous silica, inheriting the chalcedony's *c*-axis orientations. The microcrystalline quartz then grew preferentially along the inherited *c* axes that were parallel to the growth

surface. The presence of chalcedony within the amorphous silica layer is further supported by the small degree of rotation of the selected area electron diffraction spots (Fig. 5.4F). That the microcrystalline quartz is not syntaxial and has c-axes parallel to growth surfaces is due to the combination of: (1) the insulating amorphous silica layer (Fig. 5.4) deposited on the detrital grain surface (or on the incipient quartz overgrowths if present); followed by (2) the inferred development of chalcedony within or on the amorphous silica.

5.5.3 Paragenesis of the Silica Polymorphs

Silica has been reported to evolve from amorphous silica (opal-A) to quartz, via a series of metastable intermediates such as opal-CT, chalcedony and microcrystalline quartz (Williams and Crerar, 1985, Williams et al., 1985). In the Fontainebleau Formation, amorphous silica coats the surface of many detrital grains. It seems unlikely that quartz would co-precipitate with amorphous silica since quartz grows significantly more slowly (Rimstidt and Barnes, 1980). The likely occurrence of chalcedony growing within, and perhaps on, the amorphous silica, and thus beneath the microcrystalline quartz, seems to explain the *c*-axis orientation of the microcrystalline quartz growing sub-parallel to the host grain surface. Thus the Fontainebleau Formation represents a classic growth series of opal-A, chalcedony and microcrystalline quartz.

5.5.4 Microcrystalline Quartz – Preservation of Porosity

The particular geometry of microcrystalline quartz crystals, which formed on top of amorphous silica, an inferred chalcedony layer, and is misoriented relative to the host grain, has ensured that the pore space within the adjacent pore is preserved. This is due to: 1) the *c*-axis (fastest growth axis) of the microcrystalline quartz is parallel to the surface and not directed into the pore, i.e. the majority of the microcrystalline quartz growth did not expand into the pore space and so did not occlude porosity; 2) the microcrystalline quartz growing parallel to the grain surface and along the fast *c*-axis, results in crystals that impinge on each other as they grow, limiting their growth length and size, preserving pore space; 3) the microcrystalline quartz grows on a

nanocrystalline substrate of chalcedony, generating small quartz crystals. In general, small crystals grow faster than large crystals (Ostwald ripening; Chang and Yortsos, 1994), and so the more energetically-favourable euhedral form, resulting in large slow growth crystals (Lander et al., 2008).

5.5.5 Comparison to the Heidelberg Formation Microcrystalline Quartz

There are clear similarities between the Fontainebleau Formation and Heidelberg Formation (Chapter 3 - French et al., 2012; Chapter 2 - Worden et al., 2012); but there are also differences. The main similarities between these geographically and stratigraphically distinct sedimentary rocks are:

(i) The Fontainebleau Formation and Heidelberg Formation both contain the two silica polymorphs (amorphous silica and microcrystalline quartz (CL, EBSD, and TEM)) which form on top of detrital quartz or quartz overgrowth surfaces (Figs. 5.1D, 5.2, 5.3A, and 5.4). Both are inferred to contain chalcedony in, or on, the amorphous silica layer.

(ii) Both sandstones have undergone a minor degree of early (pre-microcrystalline) quartz cementation with the early cement adopting the same orientation as the underlying sand grain.

(iii) Both have an amorphous silica layer indiscriminately covering both sand grains resulting in minor quartz cement.

(iv) In both cases, EBSD revealed that the microcrystalline quartz is crystallographically misoriented with respect to the detrital grain.

(v) Specifically EBSD showed that the misorientation is systematic, evidenced by the distribution of the c-axes sub-parallel to the parent-grain surface.

(vi) In both cases, the microcrystalline quartz growth had a chalcedony-like orientation possibly suggesting that the microcrystalline quartz grew on precursor chalcedony. This chalcedony has a length-fast [11-20] preferred growth direction and controls the growth axis of the subsequent microcrystalline quartz.

The main differences between the two quartz arenites are:

(i) The Heidelberg microcrystalline quartz experienced two events, each resulting in the repeated sequence: amorphous silica, chalcedony, and microcrystalline quartz. The Fontainebleau Formation has only one sequence of these silica polymorph cements. This is probably due to a single event (e.g. silica-rich fluid migration) in the Fontainebleau versus two fluid influx events in the Heidelberg Formation.

(ii) The Heidelberg Formation microquartz crystals have *c* axes parallel to their host surface and these *c* axes have grown with completely random rotational distribution on that surface (180° dispersal). In contrast, while the Fontainebleau Formation microquartz crystals also have *c* axes parallel to their host surface and these *c* axes have grown sub-parallel to each other with a rotational dispersal of only about 30°. The difference in rotational dispersal between the Heidelberg microcrystalline quartz and the Fontainebleau microcrystalline quartz is probably due to the type of parent chalcedony. In the Fontainebleau, the microcrystalline quartz dispersal is much smaller suggesting the parent chalcedony is a wall lining chalcedony that consists of parallel-fibrous bundles (Miehe et al., 1984). This yields parallel microcrystalline quartz with minor variation in rotation. In contrast, the rotation dispersal is much larger in the Heidelberg microcrystalline quartz suggesting the parent chalcedony is horizontal chalcedony, composed of spherulites with radiating fibres (Miehe et al., 1984). This yields more random orientation of the microcrystalline quartz.

Both of these sandstones are: 1) continentally-derived quartz arenites which are compositionally similar; 2) both are marine sandstones; 3) both sandstones have never developed beyond the early stages of quartz cementation as evidenced by the poorly developed quartz overgrowth cements; 4) both have been exposed to relatively shallow burial conditions so quartz overgrowth development has been minor; and 5) both have inferred ground water flow as the source of silica (Haddad et al., 2006; Chapter 3 - French et al., 2012, and Chapter 2 - Worden et al., 2012). These similarities translate to both sandstones having microcrystalline quartz growing under shallow burial conditions, with minor quartz overgrowth cements resulting from silica-rich groundwater flow. Conversely, the sandstones are different in age; the Fontainebleau is Oligocene, while the Heidelberg is Late Cretaceous. Additionally,

the sandstones have been buried to different depths; the Fontainebleau Formation has not been buried deeper than 100 metres (Haddad et al., 2006; Thiry and Marechal, 2001), while the Heidelberg Formation has been buried to depths somewhat greater than 100 metres (French et al., in press; Worden et al., 2012). These differences in age and burial depth may have resulted in the single sequence of amorphous silica-chalcedony-microcrystalline quartz in the Fontainebleau Formation versus a double sequence in the older and more deeply buried Heidelberg Formation sandstone. There may have been more time for a second episode of silica-rich fluid migration causing the second layer of amorphous silica, chalcedony and microcrystalline quartz. This exposure to longer time and deeper burial could have also influenced the fluid flow in the pores, i.e. if the rise and fall of the water table had an impact on the migration of the silica-rich fluid, it may have also influenced the orientation of the chalcedony, and the timing of growth, i.e., if the amorphous layer had any gaps it is possible that some quartz overgrowths may have begun to grow and influence the orientation of the microcrystalline quartz.

5.6 Conclusions

Optical analysis, SEM, CL, EBSD, FT-IR, and TEM observations of the crystallography of microcrystalline quartz and other silica cements in the Fontainebleau Formation reveal mechanisms of porosity preservation, and highlight the following conclusions:

1. Quartz cements of the Oligocene Fontainebleau Formation reveal heterogeneous cement styles. Several silica polymorphs (amorphous silica, inferred chalcedony, microcrystalline quartz) are contained in the cements, each of which displays different responses in CL, EBSD, and TEM.
2. Parallel, isopachous, fine-scale bands of alternating bright and dark luminescence are reflected by the different silica polymorphs. Paragenetically these are represented by an initial growth of amorphous silica, followed by inferred chalcedony and lastly microcrystalline quartz.

3. Electron backscatter diffraction reveals that the detrital host grain and minor early quartz overgrowths have the same crystallographic orientation; the relationship between the detrital host grain and the early quartz overgrowth is syntaxial (i.e. they have the same crystallographic orientation).
4. The microcrystalline quartz and the detrital host grain have different crystallographic orientations. Microcrystalline quartz is crystallographically misoriented with respect to the detrital grain.
5. Misorientation profiles and pole figures show that there is a *systematic* misorientation between the detrital grain and the microcrystalline quartz, evidenced by the distribution of *c* axes sub-parallel to the grain surface upon which microcrystalline quartz developed. This observation indicates that the non-syntaxial growth stages are not random and there is a distinct crystallographic control on their growth. This control could be related to an inferred chalcedony precursor which has length-fast [11-20] preferred growth direction which would control the growth axis of the subsequent microcrystalline quartz.
6. These results emphasize that the development of porosity-preserving microcrystalline quartz is the result of initial chalcedony growth on top of a surface-coating layer of insulating amorphous silica (FT-IR and TEM). **The amorphous silica layer seems to be the key to the consequent porosity preservation.** However, the misorientation of microcrystalline quartz, and the inhibition of quartz overgrowths, is also a consequence of the [11-20] growth direction of the inferred chalcedony that grows on amorphous silica.
7. The microcrystalline quartz in the Fontainebleau Formation is similar to the microcrystalline quartz in the Heidelberg Formation, namely both develop from a chalcedony precursor on top of amorphous silica. However, the rotational dispersal of the *c* axes of the microcrystalline quartz in the Fontainebleau Formation is less than found in the Heidelberg Formation. Additionally, there were two episodes of amorphous silica-chalcedony-microcrystalline quartz growth in the Heidelberg Formation versus only one in the Fontainebleau Formation.

6 Electron Backscatter Diffraction investigation of length-fast chalcedony in agate: implications for agate genesis and growth mechanisms

6.1 Abstract

Agates of volcanic origin contain a range of non-crystalline, microcrystalline, and crystalline silica minerals; with chalcedony and quartz arranged in concentric bands. Although agates are abundant worldwide, little is known about the genesis of their characteristic banding patterns. Current hypotheses suggest the bands result either from precipitation from convecting siliceous hydrothermal influxes or by in situ crystallization of a silica gel. This study combines the use of a variety of analytical techniques, including electron backscatter diffraction (EBSD), cathodoluminescence (CL) and Fourier Transform Infrared (FT-IR) spectroscopy, to characterise the silica minerals present and investigate their spatial and crystallographic relationships in the banding arrangement. Microstructural and spectroscopic observations reveal that chalcedony bands are composed of amorphous silica that also contain nanocrystalline and later-formed microcrystalline quartz. Nano- and micro-crystalline quartz grew with *a* axes perpendicular to the growth substrate, typical of length-fast chalcedony. The bands formed as a result of discrete influxes of siliceous fluid. Within these individual bands there is a sequence of minerals; chalcedony (with amorphous silica and nanocrystalline quartz) → chalcedony (with microcrystalline quartz) → quartz. This sequence is reflected in the degree of crystallinity, crystal orientations and water content and is analogous to a diagenetic cycle; the initial chalcedony portion of the band commences with amorphous silica with nanocrystalline quartz followed by fibrous microcrystalline quartz crystals; chalcedony then grades into larger equiaxial mesoquartz crystals. This paragenetic sequence suggests a viable model for the growth of chalcedony in agates.

6.1 Introduction

Agates are silica-rich rock species of volcanic origin commonly reported to form in vugs created by the vesiculation of the volcanic host (Moxon et al., 2006). Agates have been defined generally as banded chalcedony (SiO_2) (Götze et al., 2001) and are known to contain a variety of silica polymorphs; nanocrystalline and amorphous silica, chalcedony, and quartz (Heaney, 1993; Graetsch, 1994; Götze et al., 2001; Moxon and Rios, 2004). The silica polymorphs in agates are similar in type and sequence to those in silcretes and have also been identified in the genesis of microcrystalline quartz in petroleum sandstone reservoirs (Chapter 2 - Worden et al., 2012). Chalcedony is defined as microcrystalline (< 100 μm length) fibrous silica, following the classification system of Flörke et al. (1991) and Heaney (1993). Wall-lining chalcedony is characterized by its parallel fibrous microstructure and forms by nucleation onto the wall of the host cavity (Graetsch, 1994). The fibres in chalcedony are elongate along the *a* axes (specifically the [11-20] directions) toward the centre of agates, perpendicular to the banding pattern. As a consequence, chalcedony exhibits a length-fast optical character; resulting in lower refractive index in the direction of the fibre (Flörke et al., 1982). Chalcedony is normally length-fast with its *c*-axis oriented perpendicular to the fibres (Knauth, 1973). In some cases the fibres can be length-slow indicating that the *c*-axis intersects the fibres at angles of 90^o. Length-slow chalcedony forms in evaporite environments (Pittman and Folk, 1971; Knauth, 1973). In the repeated bands present in agates, chalcedony is often succeeded by fine-quartz or quartz. Fine-quartz is a microcrystalline variety of quartz with a granular texture and individual grains typically < 20 μm (Flörke et al., 1982).

The crystalline silica minerals in agate have relatively high silica purity, containing typically less than 1 wt. % non-volatile impurities while the amorphous and cryptocrystalline silica contains more volatiles (Flörke et al., 1991; Graetsch, 1994). The variable amounts of water (H_2O and Si-OH groups) can be used to define the silica polymorphs present (Graetsch et al., 1985). The segregation of the silica polymorphs, with their differing microstructural and compositional characteristics, creates the distinctive concentric banding patterns observed in typical banded agates.

Despite the worldwide occurrence of agates and numerous published investigations, understanding the formation of agates has proved problematic, especially in explaining the occurrence of the repeated bands throughout the body of an agate. The inability for agate to be produced synthetically under laboratory conditions has resulted in the proposal of numerous models to explain the banded texture; accounting for the rhythmic segregation of non-crystalline opal and chalcedony. There is still controversy in the literature that agates originate either from (1) the direct precipitation of silica minerals from hydrothermal fluids, or (2) the deposition of an amorphous silica gel which subsequently crystallizes or matures by diagenetic processes to form chalcedony. Numerous authors have suggested that agate banding forms as a result of crystallization from hydrothermal fluids (e.g. Flörke et al., 1982; Heaney and Davis, 1995). In these models, influxes of siliceous fluids with differing levels of silica saturation and trace element concentrations precipitate the various silica minerals present; e.g. quartz precipitates from water with relatively low silica concentration, resulting in the formation of low-defect crystals while amorphous silica precipitates from water with high silica saturations. In contrast, Wang and Merino (1995) and Merino et al. (1995) postulated that agates crystallize from gels of non-crystalline hydrous silica containing trace elements. Wang and Merino's model predicted that silica gels could crystallize in a banding manner (by self-organization) as observed in agates. The model proposed that chalcedony fibres develop due to morphological instability at the crystallization front caused by cations which accelerate crystal growth. Oscillations in trace element concentrations, as predicted by the model, could thus accommodate the formation of oscillating chalcedony and quartz bands.

As highlighted by the conflicting models outlined above, there are still a number of questions regarding the formation of agates which remain unresolved. Focusing on microstructural and crystallographic relationships with water content, this investigation aimed to provide a greater insight into understanding the controls on the banding patterns within agate; with possible implications for the genesis and growth mechanisms of the individual bands and the impact on the growth mechanism of microcrystalline quartz in petroleum reservoirs. The specific questions relating to the crystallography and composition of the silica phases within the concentric bands are addressed in this paper:

1. What minerals are present in agates and how does mineralogy relate to banding?
2. How does water content relate to mineralogy?
3. What are the crystallographic orientations of the different silica minerals within a given band?
4. How does the orientation of silica minerals in one band relate to the orientation in overlying or adjacent bands?
5. What implications do banding, mineralogy, composition and orientation have for band growth mechanisms?

To better help understand quartz growth in sedimentary reservoirs and in order to address the issues regarding the crystallographic texture of the silica polymorphs in agate banding and how they relate to each other, electron backscatter diffraction (EBSD) has been employed here successfully for the first time on agate. This technique resolved the orientation-dependent scattering of electrons at lattice planes within crystalline materials, resulting in distinctive diffraction patterns depending on the material present (Neumann, 2000). By employing techniques investigating backscatter electron (BSE) imaging, infrared (IR) spectroscopy, and cathodoluminescence (CL), the acquired EBSD data are used to relate the observations made with these other techniques.

6.2 Methods

6.2.1 Samples

Two agate samples were used in this study. An agate sample from Pleistocene gravel in the Citronelle Formation in Louisiana was the primary sample studied (Fig. 6.1A).

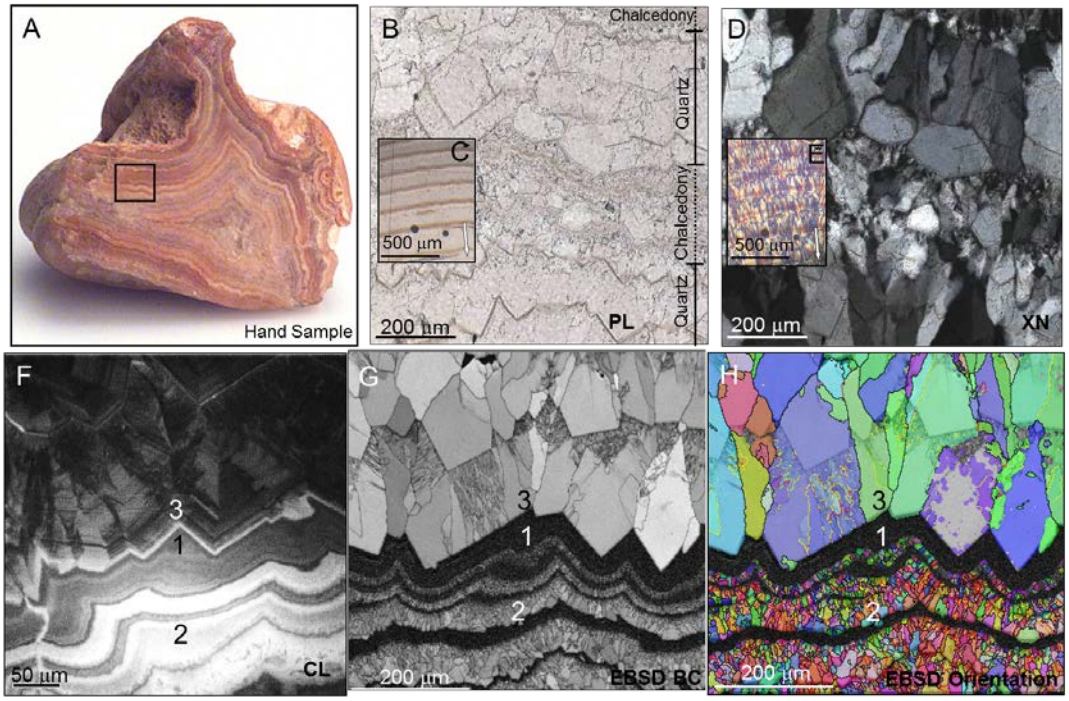

Figure 6.1 - A) Hand specimen of Citronelle Formation agate, B) petrographic microscope image in plane polarized light showing alternating chalcedony and quartz bands. Inset image C) is in plain polarized light at finer scale showing banding, arrow indicates growth direction of the agate, with the bands gradually widening, D) cross polarized light showing the banding and larger "host" quartz grains with the next generation of chalcedony, E) inset through crossed polars showing rhythmic banded fibres, F) cathodoluminescence image of the agate showing the alternating bands of quartz and chalcedony in the agate. Quartz (labelled zone 3) has euhedral terminations and displays sector and growth zoning in the CL and terminates with some bright luminescence. The chalcedony identified in light optics (Fig. 1B) has two sets of CL characteristics; some bands have dark luminescence (labelled zone 1) while other bands have brighter luminescence (labelled zone 2). The onset of the next quartz growth zone (zone 3) can be seen in the lower right corner of the image, G) EBSD band contrast image showing increase in brightness with increasing crystallinity. Euhedral quartz is labelled zone 3, in concord with the CL image. The chalcedony identified in light optics (Fig. 1B) has two sets of EBSD band contrast characteristics; some material is dark because it cannot be easily indexed (crystal structure identified using EBSD) and is therefore either not quartz or has crystal size below resolution by EBSD (labelled zone 1) while other material is composed of microcrystalline quartz (labelled zone 2), H) EBSD orientation image showing the crystallographic orientations of the quartz grains (zone 3), and chalcedony composed of alternating black zones (un-indexible) of non-quartz silica, and microcrystalline bands showing similar crystal orientations (by colour) along each fibre.

The provenance of this agate is from Paleozoic outcrops from the Lake Superior upland (Fisk 1939; Woodward et al., 1941). The second sample was a Lake Superior

Agate with a similar origin to the first agate sample, which formed within a basaltic host rock dated at 1.1 Ga (Moxon, 2002). The Citronelle Formation agate was cut into a thin section for petrographic, SEM, and EBSD examination. The Lake Superior Agate was made into a 100 μm doubly polished fluid inclusion wafer to allow FT-IR and EBSD analysis on the same sample region. To enable electron backscatter diffraction and cathodoluminescence analysis both samples were SYTON polished using a colloidal silica solution (Fynn and Powell, 1979; Lloyd, 1987) to remove any mechanical damage to the surface. The samples were carbon coated using the EMITECH K950X (<10 nm thickness).

6.2.2 Transmitted-light optics

Transmitted-light optical analysis using a Zeiss Axiophot binocular microscope was used to characterize the samples and identify the silica polymorphs based on crystal size and their distribution throughout the sample.

6.2.3 Cathodoluminescence (CL)

Cathodoluminescence microscopy identified and distinguished crystalline quartz grains from fine bands of chalcedony. A JEOL 6490LV SEM, fitted with a Gatan cathodoluminescence detector (ChromaCL-006) was used for cathodoluminescence analysis. CL images were taken with an accelerating voltage of 10 kV (in contrast to 20 kV for BSE), 8 nA beam current, and 16.5 mm working distance. CL images were collected by accumulating a signal of 500 frames using a slow-scanning raster and red, green, and blue wavelengths.

6.2.4 Electron backscatter diffraction (EBSD)

The principles and techniques of EBSD have been explained previously (Venables and Harland, 1973; Dingley, 1984; Lloyd, 1987; Schmidt and Olesen, 1989; Lloyd and Freeman, 1991; Adams et al., 1993; Wilkinson and Hirsch, 1997; Prior, 1999; Prior et al., 2009). EBSD has the capability to resolve the crystallographic

orientations at a resolution as small as 200 nanometres to reveal microstructural information about the crystal structure and mineralogy of the material being analysed. This technique has guided interpretations regarding the mechanisms of chalcedony and microcrystalline crystal growth. EBSD analysis was performed on the Citronelle Formation Agate on polished thin sections using a LEO 1530 SEM fitted with an Oxford-HKL EBSD system and for the Lake Superior Agate, a CamScan X500 crystal probe field emission gun SEM. Working conditions were 20 kV accelerating voltage, 30 nA beam current and ~ 25 mm working distance. EBSD patterns were auto-indexed using the CHANNEL 5 software from Oxford Instruments HKL A/S. The software was used to display maps and pole figure data.

6.2.5 Fourier Transform Infrared (FT-IR) spectroscopy

The utilization of infrared spectra to determine silica mineral phases by water content and speciation has been outlined previously (Langer and Flörke, 1974; Graetsch et al., 1985; Kronenberg, 1994). Infrared spectra of the Lake Superior Agate sample were obtained using a liquid-nitrogen-cooled Nicolet Centaurus FT-IR microscope (Thermo Electron Corporation). Binocular lens (x 10) gave an optical image of the sample and rectangular apertures 300 x 300 μm were used for taking the measurement. Spectra were collected at 4 cm^{-1} resolution with 100 scans collected and averaged. Reflectance spectra were generated and converted to absorption spectra using OMNIC software (Thermo Electron Corporation). Peak positions were determined by taking positions of local maxima following linear baseline correction. The position of these peaks was within ± 3 cm^{-1} since a wavenumber resolution of 4 cm^{-1} was applied for the IR measurement.

6.3 Results

6.3.1 Transmitted-light optics

At high magnification of the Citronelle Formation sample (Fig. 6.1A) the alternating bands of chalcedony and microcrystalline quartz were identified (Fig. 6.1B, D) with

quartz characterized by euhedral terminations followed by a much more finely crystalline and less well organised zone of chalcedony. At the low magnification, transmitted-light optical analysis revealed clear and pale brown bands using plane polarized light, the bands repeating at about 0.2 mm (Fig. 6.1C). In cross polarized light, there was a birefringent fibrous fabric perpendicular to the bands (Fig. 6.1E). The fibres show a length-fast optical character indicative of chalcedony due to the lower refractive index in the direction of the fibre (Flörke et al., 1991). The chalcedonic parallel fibrous aggregates exhibit rhythmic extinction, resulting in a distinctive wrinkle-band texture diagnostic of wall-lining chalcedony (Fig. 6.1E). The thickness of individual bands shows a gradual width increase trend along the sample. Bands on the outer edge of the sample relative to the growth inwards are approximately 0.05 mm wide, increasing to over 0.4 mm at the inner edge of the sample.

6.3.2 Cathodoluminescence (CL)

Cathodoluminescence imaging revealed a marked contrast in the degree of luminescence between the crystalline bands and the chalcedony bands (Fig. 6.1F). Quartz crystals have euhedral terminations and display sector and growth zoning in CL. The euhedral quartz terminates with very bright luminescence and is then succeeded by chalcedony (identified in light optics, Fig. 6.1B). Chalcedony has two sets of CL characteristics; some bands have dark luminescence while other bands have brighter luminescence. Subtle variations in the CL character of the darker bands in the chalcedony can be identified. The euhedral outline of the quartz has been succeeded by the CL-banded chalcedony.

6.3.3 Electron backscatter diffraction (EBSD)

6.3.3.1 Microstructure and orientation of bands

The band-contrast (BC) image (Fig. 6.1G) discriminates euhedral quartz layers from banded chalcedony which has discrete variations in grey scale. The band-contrast image reflects the degree of crystallinity with the non-crystalline layer yielding a

black BC response, the microcrystalline quartz layer yielding a brighter BC response, and the euhedral quartz crystals yielding the brightest BC response. Three distinct types of silica can be defined by crystallinity, crystal size and morphology:

1) In the chalcedony layer (see Fig 6.1B), there is a silica band dominated by material that could not be crystallographically indexed (zero-solution zone) (Fig. 6.1G). This part of the agate exhibits the darkest band-contrast response. The parts of chalcedony that were dark in the BC image are thus amorphous silica possibly mixed with sub-EBSD resolution, nanocrystalline quartz crystals. These bands were the first to form in the sequence and so are labelled zone 1 (see also CL image Fig. 6.1F),
2) Also in the chalcedony layer (see Fig. 6.1B), are parallel-aligned, fibrous and elongate crystals of microcrystalline quartz grading from 0.5 to 5 μm in length with axial ratios approximately 1:5 (Fig. 6.1G). These quartz fibres show a gradual increase in width toward the tip of the individual crystallites in the direction of growth. The fibres are elongate parallel to the growth direction of the bands.
3) In the quartz layer (Fig 6.1B) larger polygonal euhedral quartz crystals grow up to 100 to 200 μm in diameter (Fig. 6.1G). The quartz exhibits the highest band-contrast response in the agate.

CL and band-contrast imaging thus confirm that there are quartz bands within the agate. They also show that the chalcedony bands contain both microcrystalline quartz and bands (with dark luminescence) that are predominantly composed of amorphous silica but which contain quartz crystals at the limit of EBSD resolution (sub-μm; i.e. nanocrystalline quartz).

6.3.3.2 Characterizing the zero-solution zone

In the Citronelle Formation Agate, EBSD analysis (Fig. 6.1H) revealed layers within the chalcedony that could not be indexed *(i.e.* are crystallographically-unresolved) which are opal-A and opal-CT intergrown within the chalcedony bands by analogy as

reported in previous studies in agates (Godovikov et al., 1987; Blankenburg, 1988; Götze et al., 1998; Moxon and Rios, 2004; Götze et al., 2009). The zero-solution, amorphous silica zones labelled 1 in Figures 6.1G and 6.1H result from the initial EBSD maps being unable to yield crystallographic orientation data from these areas. The software was unable to index these regions because the crystallographic data recorded were so weak (and see Haddad et al., 2006). Qualitative secondary X-ray analysis (EDAX) identified these banded components as silica (SiO_2). There are a number of possible explanations for this pattern: (1) the silica is quartz with abnormally high dislocation density, possibly due to deformation (as undeformed crystals are present in adjacent bands, this possibility is unlikely; (2) the diffraction patterns decay over time due to crystal lattice damage caused by the electron beam. Although there was some damage to the sample when the beam was focused on a region for longer time periods, such loss in diffraction pattern quality was also evident in quartz. This suggests that the time-dependent damage is similar to quartz and only shows appreciable damage after time periods significantly longer than the data acquisition time; and (3) the final possibility is that the SiO_2 present is a cryptocrystalline phase and does not have a long-range crystal structure capable of diffracting electrons and is therefore amorphous.

6.3.3.3 Orientation of bands

To gain insight into the growth relationships of microcrystalline quartz in the chalcedony bands and its crystallographic relationship with the quartz bands, the orientation of quartz crystals in the agate was examined. The crystal-orientation map (Fig. 6.1H) uses colour to qualitatively represent crystallographic orientations and reveals that chalcedony crystals exhibit a common orientation along the length of the individual crystals. The change in colour between neighbouring crystals indicates that the crystals have different crystallographic orientations relative to each other.

6.3.3.4 *c*-axis dispersal of the microcrystalline quartz bands in the chalcedony

Directions of *c* axes of the microcrystalline quartz portion of the chalcedony from the Citronelle Formation agate

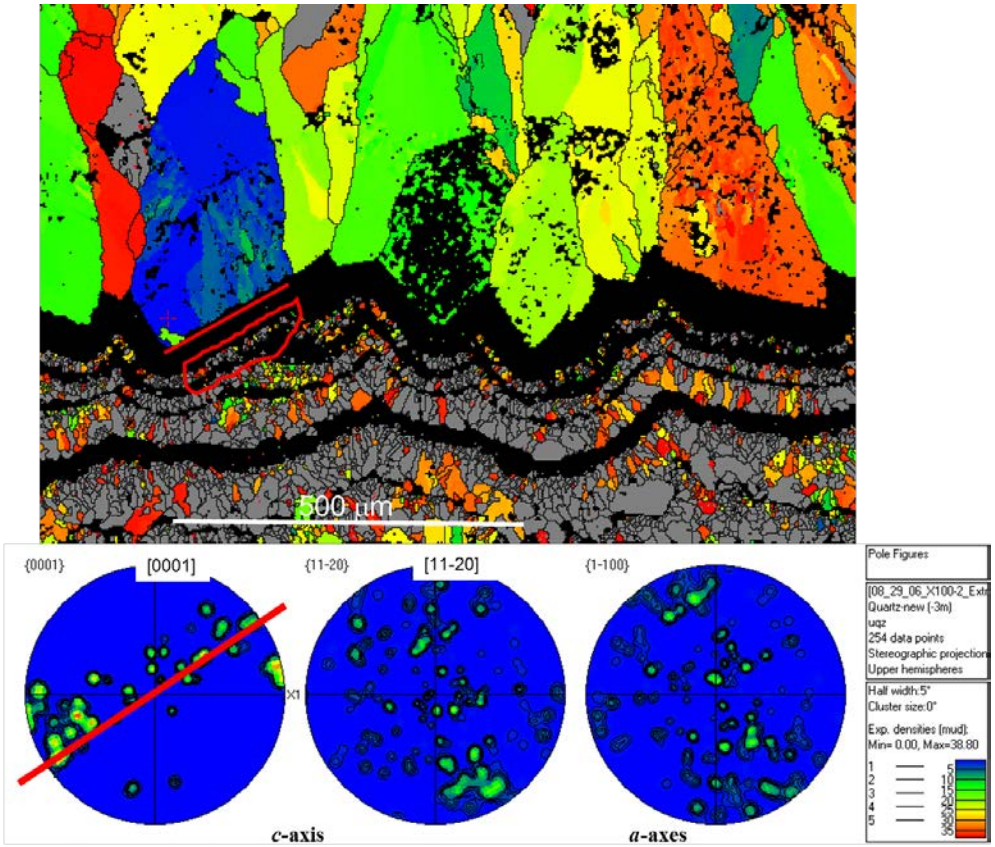

Figure 6.2 - A) electron backscatter diffraction (EBSD) orientation map of the Citronelle Formation Agate showing microcrystalline quartz host grain orientation and chalcedony (multiple colours) indicating that the crystallographic orientations of the host microcrystalline quartz grains and the adjacent chalcedony crystals are different. B) Pole figure of the *c*-axis orientation of the microcrystalline quartz on the surface of the host grain. The orientation of the microcrystalline quartz in the chalcedony is spread in a girdle parallel to the host surface. The trace of a great circle of these microcrystalline quartz data, shown by the red line, matches the orientation of the face of the host grain (red line) indicating that the material on the surface of the host grain is controlling the growth of the microcrystalline quartz.

(Fig. 6.2A) were plotted on a stereogram (Fig. 6.2B). The orientations of the *c*-axis from the chalcedony are arranged in a great circle rotating within the plane of the quartz grain facet. This pattern indicates that fibres of the chalcedony have grown with their *c*-axes parallel with, but randomly distributed (with some possible minor orientation control) (rotated) on, the host quartz crystal surface. In the Citronelle Formation agate, in succeeding bands

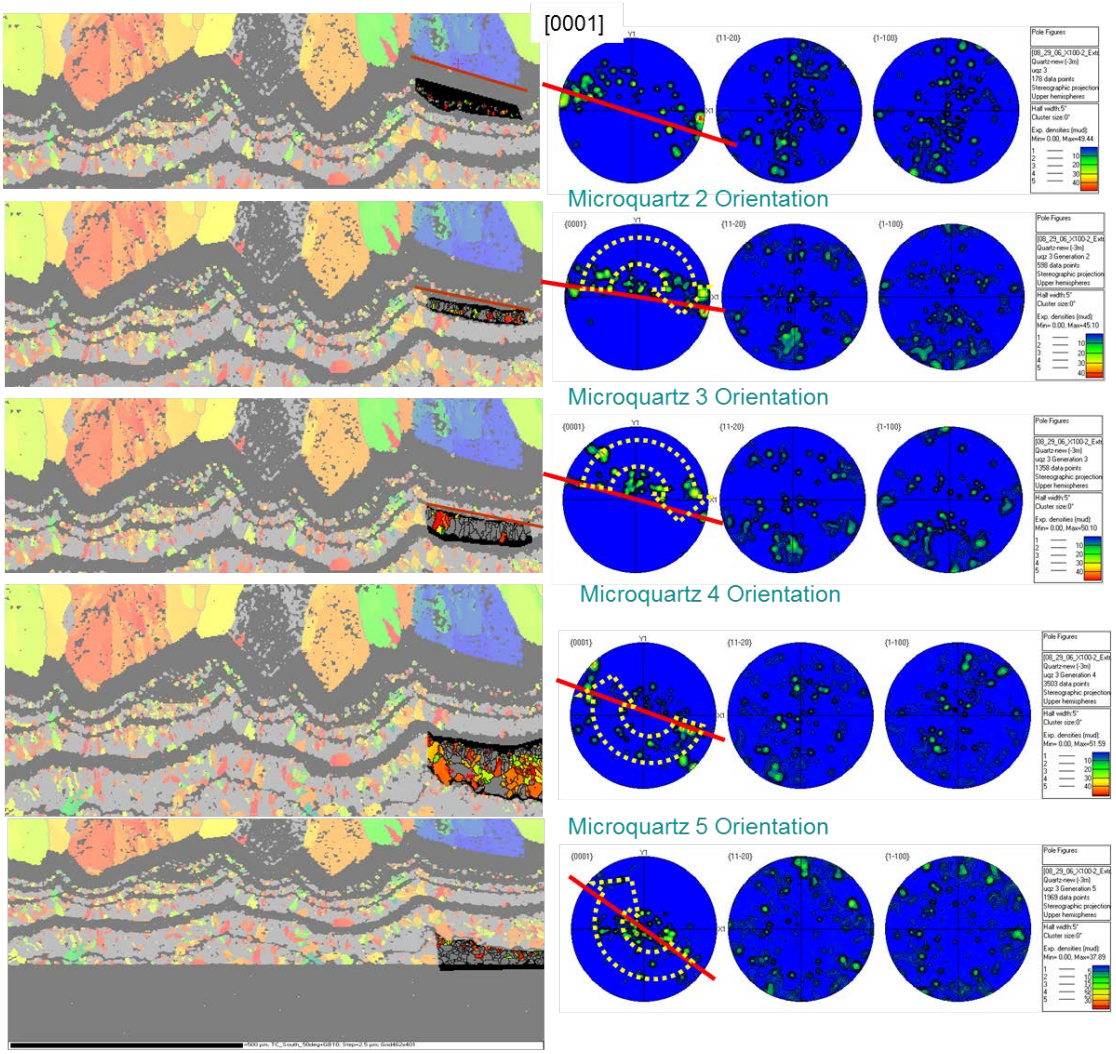

Figure 6.3 - EBSD orientation and pole figures from the Citronelle Formation Agate showing four generations of microcrystalline quartz within chalcedony bands. Each generation developed with its *c*-axis parallel to the growth surface.

(Fig. 6.3) on a different host quartz crystal surface, the chalcedony has *c* axes parallel to the underlying quartz crystal surface. This was observed in every case examined.

6.3.3.5 Orientation data from the amorphous, microcrystalline and quartz bands

Pole figures of EBSD data from the Lake Superior agate, representing crystallographic orientations of the three types of silica (chalcedony with amorphous silica and nanocrystalline quartz, chalcedony with microcrystalline quartz, and quartz) have been plotted on separate stereographic projections

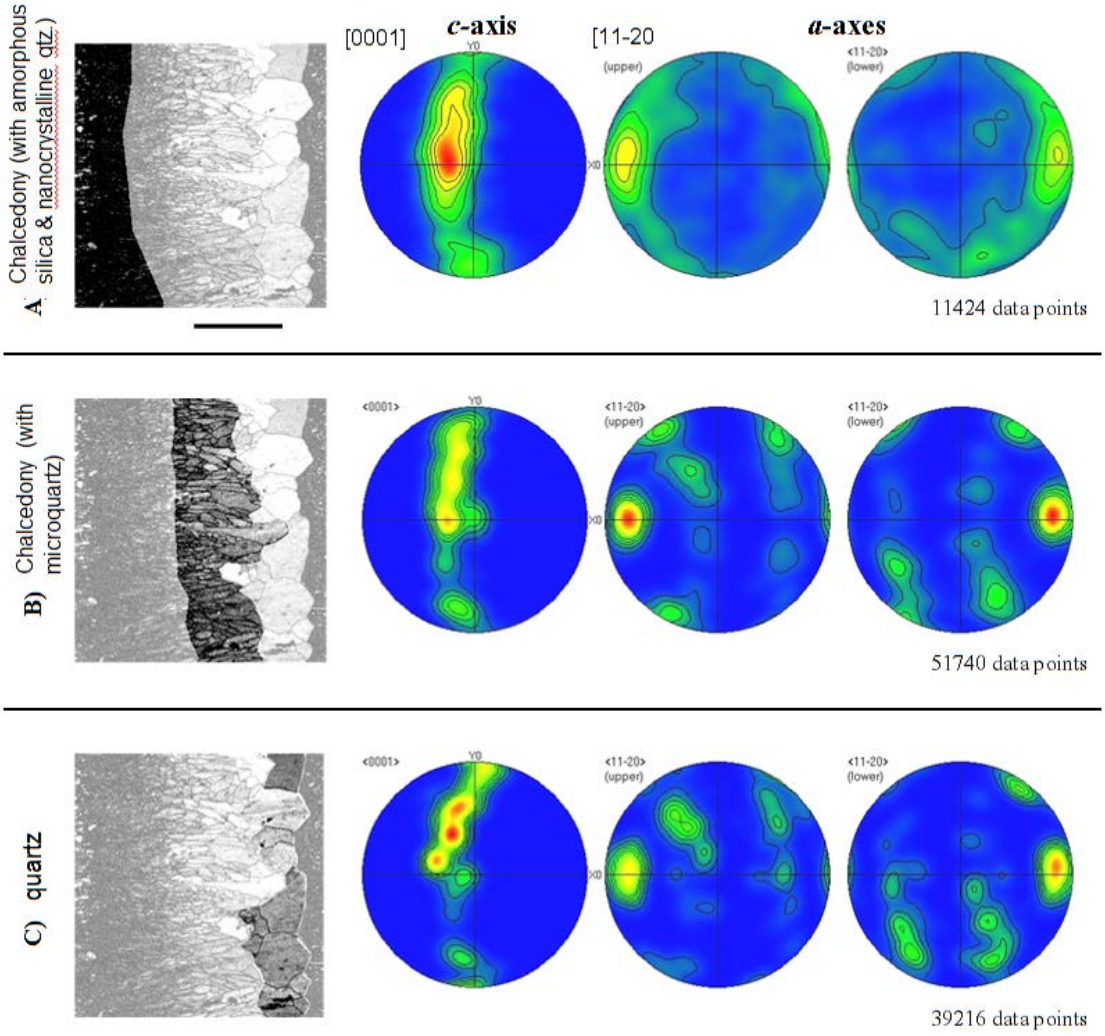

Figure 6.4 - Band contrast images highlighting the three types of silica in the Lake Superior Agate and pole figure representations of EBSD data. Note that *a*-axis data are plotted upper hemisphere (*left*) and lower hemisphere (*right*). Data from each component are represented on contoured stereographic projections showing crystallographic orientations; plotted for [0001] (*c*-axis) and the two [11-20] growth zones (*a* axes). A) Orientation data from chalcedony (with amorphous silica and nanocrystalline quartz) band showing a degree of data dispersal although preferred lineation of *a*-axes is evident. B) Orientation data from chalcedony (with microcrystalline quartz) band showing tight data cluster in *a*-axes and a dispersed (rotated) *c*-axis girdle. (C) Orientation data from the quartz band also showing tight data cluster for the *a* axes and a dispersed *c*-axis girdle.

(Fig. 6.4). All figures (6.4A to C) reveal a distinct clustering of orientation data in the *a* axes ([11-20] directions) parallel to band growth direction with dispersal (rotation) of data in the *c*-axis plot. This suggests that all the band components share a related crystallographic orientation with a distinct alignment of *a*-axes. Thus the Citronelle

(Figs. 6.2-6.3) and the Lake Superior (Fig. 6.4) agate samples show identical crystallographic orientation patterns.

6.3.4 Fourier Transform Infrared (FT-IR) spectroscopy

Infrared spectroscopy is dependent on the response of short range molecular scale energetic vibrations such as O-H stretching and bending. This generates characteristic spectra for particular mineral phases depending on the molecules present, for example different water species (Langer and Flörke, 1974). Infrared spectra with broad bands centred around 3430 cm^{-1} are generally considered to be related to molecular water (H_2O_{mol}) such as water in fluid inclusions. A sharp peak present at ~3585 cm^{-1} has been attributed to silanol (Si-OH) species (Langer and Flörke, 1974; Kronenberg, 1994; Yamagishi et al., 1997).

Infrared absorption spectra (3800-2800 cm^{-1}) for the three band components (defined using EBSD) in the individual bands were identified in the Lake Superior Agate (Fig. 6.5). Amorphous silica-dominated part of the chalcedony bands displays a broad peak at ~ 3435cm^{-1} with a prominent peak at 3585 cm^{-1}; indicating the presence of both H_2O_{mol} and Si-OH group water. Microcrystalline quartz parts of the chalcedony exhibit the same peak locations as present in amorphous silica bands but the Si-OH peak at 3585 cm^{-1} is less well defined. The spectra also display relatively less absorbance, indicating lower total water content than the amorphous silica. The absorbance spectra for quartz bands show no response in the 3800-2800 cm^{-1} range indicating no molecular water or silanol group water are present in this region.

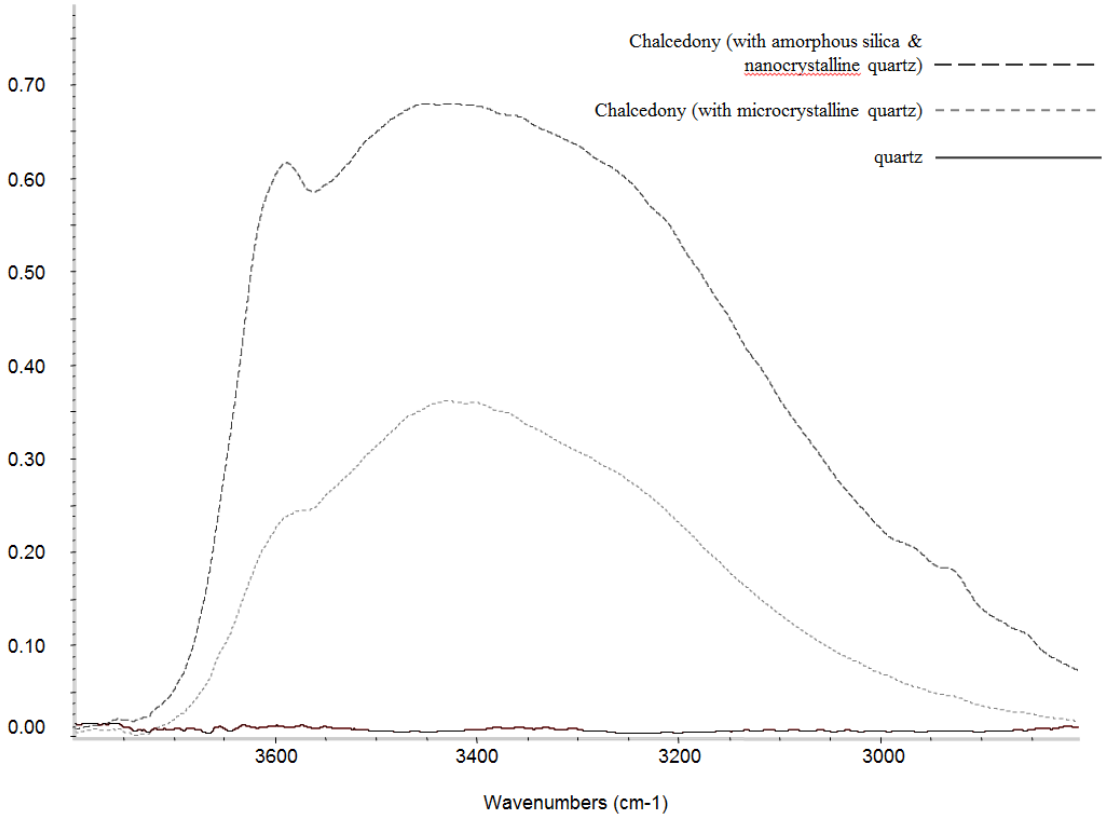

Figure 6.5 - Absorption spectra (2800 to 3800 cm^{-1}) showing variation between the three silica minerals present within each individual bands in the Lake Superior Agate. Peaks at ~ 3430 and 3585 cm^{-1} relate to H_2O_{mol} and Si-OH groups respectively.

6.4 Discussion

6.4.1 Mineralogy and banding in agates

Light optics allowed differentiation of the agate into bands of chalcedony and mesocrystalline, euhedral quartz. CL, EBSD and FT-IR allowed further differentiation of chalcedony bands into: 1) discrete bands of amorphous silica (containing nanocrystalline quartz) or chalcedony-A, and 2) chalcedony with microcrystalline quartz or chalcedony-MQ by crystal size, crystallographic orientation, and water content.

Previous authors noted that a problem in validating agate banding as forming from a viscous silica fluid or gel was the lack of amorphous silica with a nanocrystalline phase concordant with observations of siliceous sinters (Heaney, 1993; Inagaki et al., 2003). However, the EBSD data presented here show unequivocally that an amorphous or poorly crystalline phase is present in the bands. The progressive pattern observed in the bands; chalcedony-A (chalcedony with amorphous silica and nanocrystalline quartz) → chalcedony-MQ (chalcedony with microcrystalline quartz) → quartz, shares characteristics of silica diagenetic processes related to degrees of supersaturation with respect to silica (Williams et al., 1985; Williams and Crerar, 1985).

A number of studies have investigated the relative rates of nucleation and growth of silica polymorphs at different silica concentrations in sedimentary environments (Williams and Crerar, 1985). It has been proposed that varying degrees of silica saturation in the solution dictate the type of silica polymorph precipitated (Flörke et al., 1982; Heaney and Davis, 1995). Flörke et al. (1982) concluded that the different crystallite sizes and water content in the individual band components represented precipitation of the microcrystalline silica species from discrete fluid influxes with varying levels of silica supersaturation. However, the CL and band-contrast results from this study indicate that although the silica minerals observed are microstructurally-distinct, there is an apparent gradation between the polymorphs. This does not correlate with the conclusion that the banding pattern chalcedony-A (chalcedony with amorphous silica) → chalcedony-MQ (chalcedony with microcrystalline quartz) → quartz) forms due to discrete, compositionally-distinct hydrothermal fluid influxes which exhibit progressively less silica saturation (Flörke et al., 1982). From the results showing grading of CL, band-contrast and water content it is possible to infer that the differing band components form by precipitation from a single fluid influx in which the solution gradually decreases its extent of silica supersaturation. Heaney and Davis (1995) speculated that a solution initially supersaturated with respect to silica would be partly polymerized and rapidly precipitate amorphous silica and chalcedony. The authors indicated that rapid growth of chalcedony fibres at the crystal front would result in a gradual depletion of silica in the solution. Assuming that this hypothesis is correct, the decreasing concentration of silica would facilitate the progressively slower growth of increasingly larger crystals

with fewer crystal defects. The results (Figs. 6.4 and 6.5), showing increasing crystal size and decreasing water content through the individual bands, appear to support this crystal growth process. On this basis, the solution eventually would have a sufficiently low silica concentration to allow the slow growth of defect-free quartz crystals. The lack of IR response for water (H_2O_{mol} and Si-OH groups) indicates no presence of fluid inclusions or structurally held water in the quartz suggesting defect-free crystal growth from a monomeric solution. This is supported by the high-band-contrast signal indicating high crystallinity.

6.4.2 Water content and mineralogy

Variations in the infrared spectra indicating water content (H_2O_{mol} and Si-OH groups) of the agate band components (Fig. 6.5) show concordance with the band-contrast response (Fig. 6.1H). The low-band-contrast chalcedony-A (with amorphous silica and nanocrystalline quartz) displays the highest water content; the intermediate band-contrast signal indicative of chalcedony-MQ (chalcedony with microcrystalline quartz) shows a relative decrease in water content; and quartz (high-band-contrast) is coincident with no water present. This implies that the amount of water (H_2O_{mol} present as fluid inclusions and Si-OH groups in the amorphous silica as well as at structural disparities) present in SiO_2 minerals is dependent on the degree of crystallinity of the polymorph. It is possible that the decrease in water may simply be due to reducing surface area as a consequence of increasing crystal size. Previous investigations focusing on water content and speciation in silica minerals (Florke et al., 1982; Graetsch et al., 1985) have suggested that amorphous silica and nanocrystalline quartz easily incorporate water due to the highly disordered crystal structure present in such minerals. They noted that with increasing structural order and crystal size, water content decreased as it could no longer be accommodated in the evolving crystal structures. The IR responses from the sample in this study (Fig. 6.5) concur with these previous observations on water content in silica polymorphs, indicating a gradual decrease in water content with increasing crystallinity in the individual bands. The results also show that the ratio between the H_2O_{mol} and Si-OH peaks is constant for the amorphous silica with nanocrystalline quartz and microcrystalline quartz (Fig. 6.5) showing that increasing crystallinity does not lead to

relatively more fluid inclusions (H_2O_{mol}) at the expense of silanol in amorphous silica or at structural disparities (Si-OH). This suggests that the silanol is not simply converted into aqueous fluid inclusions during a progressive transformation process.

6.4.3 Crystallographic orientation

Directions of the *c* axes of the microcrystalline quartz within the chalcedony bands (chalcedony-MQ) studied here were plotted on a stereogram (Fig. 6.3) and as with the microcrystalline quartz from the Heidelberg Formation in Germany (Chapter 2 - Worden, et al., 2012), the orientations of the *c* axes from the microcrystalline quartz are arranged in a "great circle" rotating within the plane of the host mesoquartz grain facet. This pattern indicates that crystals of the microcrystalline quartz within the chalcedony have grown with their *c* axes parallel with, but somewhat randomly distributed (rotated) on, the host (underlying) surface.

The surface controlled growth of the microcrystalline quartz within the chalcedony continues with each successive band of chalcedony (Fig. 6.3), with the orientation of the *c*-axes of each band of microcrystalline quartz within the chalcedony arranged in a "great circle" rotating parallel to the plane of the previous surface indicating that the crystals of microcrystalline quartz have grown with their *c* axes parallel with, but dominantly randomly distributed (rotated) on, the previous host surface. Given that the *c*-axis of each band of microcrystalline quartz is parallel to the grain surface, the [11-20] directions are perpendicular to the previous chalcedony-MQ band surface (Fig. 6.3).

The EBSD data reveal that all of the components of the individual bands share a similar crystallographic orientation (Figs. 6.3-6.4). The pole figures corresponding to the EBSD data show *c*-axis growth parallel to the growth surface which is apparent in all the band components regardless of the crystal morphology and degree of crystallinity present. This is surprising, especially in the chalcedony-A (chalcedony with amorphous silica and nanocrystalline quartz) because although the data reveal (Fig. 6.4) that the crystallites formed in the amorphous matrix, they share one common crystallographic orientation (c axes parallel to the growth surface *a* axes).

The orientation data become more clustered in the chalcedony-MQ and quartz bands, possibly reflecting the relative increase in crystallinity.

Relating the pole figures to the banding arrangement reveals that the general band growth direction is parallel to the *a*-axis orientations. This evidence suggests that the alignment dictates the growth direction of the bands. The nanocrystalline quartz in the amorphous silica and the microcrystalline quartz (Fig. 6.2 – 6.4) exhibit elongate crystallites parallel to the strong *a* axes lineation, suggesting growth in this orientation. Such a controlled growth mechanism for chalcedony has been hypothesized in previous investigations (Heaney, 1993). The textures determined in the results of this study support the published growth mechanism proposals for chalcedony.

6.4.4 Possible band growth mechanisms

The influx of a supersaturated silica fluid into the cavity resulted in precipitation onto the wall or earlier influx deposit (Fig. 6.6A).

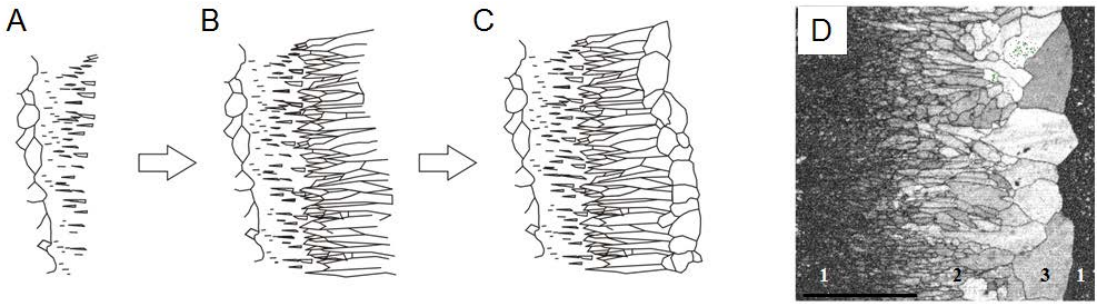

Figure 6.6 - Schematic diagram showing proposed growth mechanism of individual bands in both agates: A) rapid precipitation of chalcedony-A (with amorphous silica containing some nanocrystalline quartz), B) growth of chalcedony-MQ (with microcrystalline quartz), C) growth of defect free quartz crystals, and D) EBSD band contrast image showing increase in brightness with increasing crystallinity (numbers denote silica mineral defined in text; 1) chalcedony-A (with amorphous silica and nanocrystalline quartz), 2) chalcedony-MQ (with microcrystalline quartz), and 3) quartz).

The high degree of supersaturation with respect to silica led to rapid formation of hydrous amorphous silica and nanocrystalline quartz, trapping water as fluid inclusions and in structural defects (Williams and Crerar, 1985). Silica saturation

decreased at the crystal growth front as rapid deposition outpaced diffusion to the crystallization front (Heaney and Davis, 1995), allowing the formation of crystals. The interpreted presence of trace elements in the fluid created elongate chalcedony fibres (Fig. 6.6B) (Heaney and Davis, 1995). Gradually silica saturation became sufficiently low to allow growth of defect free quartz crystals (Heaney and Davis, 1995); Fig. 6.6C). These stages of the model can be represented in the band contrast image (Fig. 6.6D). Different proportions of chalcedony (here observed to be split into amorphous silica and microcrystalline quartz) and mesoquartz in sets of bands throughout the sample suggest a combination of different rates of influx, or compositional differences (silica saturation and trace element concentrations) occurred during agate growth.

Previous work on the Heidelberg Formation, Germany (Chapter 2 - Worden et al., 2012, Chapter 3 - French et al., 2012) studying silica polymorph growth in sandstone reservoirs indicated that the misorientation of microcrystalline quartz coatings on sand grains was controlled by the orientation of nanocrystalline quartz in an amorphous layer (collectively analogous to the chalcedony described here). The implication is that microcrystalline quartz inherited its *c*-axis orientation from pre-existing chalcedony adjacent to amorphous silica in the Heidelberg sandstone similar to the growth of quartz following chalcedony in agates.

agate					Heidelberg Fm microquartz			
this study					Worden et al., 2012, French et al., 2012			
silica type	layer thickness	crystal size	orientation of quartz	silica type	layer thickness	crystal size	orientation of quartz
chalcedony-amorphous with nanocrystalline quartz	10-50 µm	<1 µm	for nanoquartz: a-axes ⊥ to growth surface, c-axes ∥ to growth surface (randomly rotated)	amorphous silica	50-100 nm	no crystals	no orientation
chalcedony-microcrystalline quartz	10-50 µm	5-10 µm	a-axes ⊥ to growth surface, c-axes ∥ to growth surface (randomly rotated)	chalcedony	50-100 nm	20-50 nm	a-axes ⊥ to growth surface, c-axes ∥ to growth surface (randomly rotated)
mesoquartz	200 µm	200 µm	a-axes ⊥ to growth surface, c-axes ∥ to growth surface (randomly rotated)	microcrystalline quartz	10-20 µm	10-20 µm	a-axes ⊥ to growth surface, c-axes ∥ to growth surface (randomly rotated)

Table 6.1 Comparison of silica polymorphs in agates in this study and silica polymorphs in the Heidelberg Formation.

Table 6.1 shows a comparison of the silica polymorphs found in the agates in this study and the silica polymorphs found in the Heidelberg Formation by silica type, layer thickness, crystal size, and orientation of quartz. The orientation of the a axes perpendicular to the growth surface and the orientation of the c axes parallel to the growth surface for the crystalline silica polymorphs found in the agates in this study are the same orientations as those found in the Heidelberg sandstone. Thus agate is morphologically and crystallographically the same as microcrystalline quartz coats in the Heidelberg and Fontainebleau sandstones although the agate layer thicknesses are > 20 times greater than in microcrystalline quartz coats in sandstones.

6.5 Conclusions

The crystallographic, textural, and compositional relationships of silica polymorphs present within banded agate have been examined using EBSD, CL and FT-IR to reveal the following:

1. Two agates with similar origins were studied and have identical patterns of growth of silica polymorphs: amorphous silica, nanocrystalline quartz, chalcedony and quartz.
2. The boundaries between individual bands within the agate are sharply contrasting, reflected in crystallography (degree of crystallinity, morphology) and composition (water content); indicating formation from aqueous silica-rich fluid influxes.
3. Crystallographic information reveals that the degree of crystallinity and morphology of the silica minerals within the individual bands changes in a systematic fashion analogous to a diagenetic cycle; the initial chalcedony part of the band commences with amorphous silica followed by fibrous microcrystalline quartz crystals; chalcedony then grades into larger equiaxial mesoquartz crystals.
4. CL revealed gradual changes in luminescence and signal response across individual bands. These changes are coincident with the evolving silica polymorphs present. Pole figures from EBSD revealed there is a strong crystallographic control throughout all bands in the agate regardless of crystallinity or microtexture. This suggests that the crystal orientation in agate

is dictated by a process that is independent of the silica mineral polymorph present as the substrate.

5. The combination of the initial precipitation of amorphous silica followed by [11-20] growth for chalcedony and rotated *c*-axes of microcrystalline quartz (parallel to the host surface) in the agate studied here is identical to the growth patterns in the Heidelberg sandstone.

7 Summary of research questions and scope for further work

7.1 Summary of research questions

Nine questions regarding microcrystalline quartz growth were investigated in this research and evidence to answer each question was collected using the analytical tools described in Chapter 1. These questions were categorized into two overarching questions to answer the fundamental research of this thesis: 1) **What is microcrystalline quartz**, and 2) **How does microcrystalline quartz grow**?

What is microcrystalline quartz and what are the associated silica polymorphs?

1. What are the silica polymorphs in quartz cements?
2. What is the paragenesis of the silica polymorphs?
3. What is the crystallographic orientation of porosity-preserving microcrystalline quartz?
4. What are the similarities and differences between the microcrystalline quartz in the Heidelberg Formation and the microcrystalline quartz in the Fontainebleau Formation?
5. What are the similarities and differences between the silica polymorphs in agates and in the Heidelberg and Fontainebleau sandstones?

How does microcrystalline quartz grow and how do the associated silica polymorphs grow?

6. How do trace elements affect the growth of silica polymorphs?
7. Is there a link between stable oxygen isotope values and silica polymorph variations in microcrystalline quartz cemented sandstones?
8. How does the temperature of formation vary related to original water source and what are the controls on the $\delta^{18}O$ in the silica cements?
9. How does porosity-preserving microcrystalline quartz grow?

7.1.1. What are the silica polymorphs in quartz cements?

The following silica polymorphs: amorphous silica, chalcedony, and microcrystalline quartz, which grow on top of syntaxial quartz overgrowths, are contained in the Heidelberg and Fontainebleau quartz cements, each of which displays different responses in CL, EBSD, FT-IR, and TEM.

7.1.1.1 Syntaxial Quartz Overgrowths

Petrographic, SEM-CL, and EBSD observations in the Heidelberg and Fontainebleau Formation sandstones (Chapters 3 and 5) revealed that a small amount of early-formed (pre-microcrystalline quartz) syntaxial quartz overgrowth cements developed on the detrital quartz grains. The CL images (Chapter 3 Fig. 3.3D and Chapter 5 Figs. 5,1D and E), show that the quartz overgrowths are poorly developed and therefore represent an early stage of growth. These embryonic quartz overgrowths did not occlude much of the porosity before being coated with an amorphous silica phase. The quartz overgrowths inherited the crystallographic orientation of the detrital host grains upon which they grew (Chapter 3 Fig. 3.4 and Chapter 5 Fig. 5.3A), as is typical of quartz overgrowths (Mörk and Moen, 2007; Worden and Morad, 2000).

Table 7.1 Nomenclature and characteristics of non- and microcrystalline silica minerals (adapted from Lee, 2006 and Flörke et al., 1991) mapped with this study

this study	silica type	layer thickness	crystal size	orientation of quartz	Crystal Structure	Variety	Sub-variety	Morphology	"Crystal" size	Total water (H_2O_{tot})	H_2O_{slow}/H_2O_{tot}	Additional References
Agate: Chapter 6	mesoquartz	200 µm	200 µm	a-axes ⊥ to growth surface, c-axes ∥ to growth surface (randomly rotated)	crystalline quartz	megaquartz	macroquartz	crystalline	>50 µm	0.5 - 2.5 wt.%	~0	Hesse, 1989; Hendry & Trewin, 1995
							mesoquartz		20 - 50 µm			
Heidelberg Formation: Chapters 2 and 3	microcrystalline quartz	10-20 µm	10-20 µm	a-axes ⊥ to growth surface, c-axes ∥ to growth surface (randomly rotated)		fine-quartz		granular	20 - 5 µm			Hesse, 1989; Graetsch, 1994; Knauth, 1994
Agate: Chapter 6	chalcedony-microcrystalline quartz	10-50 µm	5-10 µm	a-axes ⊥ to growth surface, c-axes ∥ to growth surface (randomly rotated)		chalcedony	wall-lining	parabolic fiber bundles	>1 µm			Langer & Flörke, 1974; Heaney, 1993; Graetsch, 1994; Knauth, 1994; Cady et al., 1996, 1998; Moxon et al., 2006
Heidelberg Formation: Chapters 2 and 3	chalcedony	50-100 nm	20-50 nm	a-axes ⊥ to growth surface, c-axes ∥ to growth surface (randomly rotated)				(length-fast)	(typically 50 - 350 nm)			
Agate: Chapter 6	chalcedony-amorphous with nanocrystalline quartz	10-50 µm	<1 µm	for nanoquartz: a-axes ⊥ to growth surface, c-axes ∥ to growth surface (randomly rotated)	microcrystalline quartz		horizontally banded	radiating spherulites	~100 - 200 nm			
							quartzine	parabolic fiber bundles	~100 - 200 nm			
								(length-slow)				
					microcrystalline opal	opal-C	lussatine	platy (length-fast)	10 - 100 nm	1 - 3 wt.%	0.02	Jones and Segnit, 1971; Langer & Flörke, 1974; Murata and Larsen, 1975; Williams et al., 1985; Graetsch, 1994; Knauth, 1994; Cady et al., 1996, 1998; Alexandre et al., 2004; Lynne et al., 2005
						opal-CT	lussatite	fibrous (length-slow)	10 - 100 nm	3 - 10 wt.%		
							massy opal	bumpy microspheres, clustered nanospheres, aligned nanospheres, beaded blades, sharply bladed lepispheres	1 - 10 µm spheroids			
					non-crystalline opal	opal-A	Precious opal	Botryoidal, amalgamated microspheres	1 - 8 µm spheres	10 - 12 wt.%	0.1 - 0.7	Darragh et al., 1966; Langer & Flörke, 1974; Graetsch, 1994; Herdianita et al., 2000, Lynne et al., 2005
							Potch opal	Nano- and microspheres				
Heidelberg Formation: Chapters 2 and 3	amorphous silica	50-100 nm	no crystals	no orientation								

Table 7.1 Comparison of the silica polymorphs in this study with those reported in the literature.

7.1.1.2 Amorphous Silica

An approximately 50-100 nm thin film was revealed at the highest resolution in a SEM in the Heidelberg Formation between the detrital host grain and a multitude of microcrystalline quartz crystals (Chapter 3, Figs. 3.6A-C). Chemical analysis, carried out using EDS, indicated that the surface-coating nanofilm is silica (SiO2). However, static probing of the surface-coating film during EBSD analysis revealed no diffraction patterns, indicating either that the crystal size was below the detection limit of this particular EBSD, i.e., smaller than 0.2 μm, or that the surface-coating film layer was noncrystalline (i.e., amorphous). To investigate further the surface-coating film between the host detrital grain and the microcrystalline quartz, samples were prepared using a FIB-SEM and examined with a TEM. A selected-area electron diffraction (SAED) pattern in the TEM demonstrates that part of the surface material consists of nanometre-size crystals of quartz (Chapter 3, Fig. 3.7C). However, there was also a surface-coating material that did not diffract the electron beam (Chapter 3, Fig. 3.7B), suggesting that the thin surface-coating film contains amorphous silica. TEM examination of numerous grains suggests that this amorphous material is ubiquitous on the sandstone grain surfaces.

Similarly, in the Fontainebleau Formation a surface layer coating the detrital grain and the embryonic quartz overgrowths, beneath the microquartz, was identified in CL (Chapter 5, Figs. 5.1D and E) and EBSD (Fig. 5.3A) The layer is silica but is not fully crystalline at the resolution possible using this EBSD (~1 μm). Selected Area Electron Diffraction (SAED) analysis of this layer in the TEM showed that part of the surface material contains nanometre sized crystals of quartz (Chapter 5, Fig. 5.4F) but much of it did not diffract the electron beam in the TEM (Chapter 5, Figs. 5.4C and E). This suggests that the thin surface-coating film is dominated by truly amorphous, non-crystalline silica. TEM examination of numerous samples suggests that the amorphous silica-dominated layer is ubiquitous on sand grain surfaces in rocks where microcrystalline quartz is present in both the Heidelberg and Fontainebleau Formations.

FT-IR studies of the Fontainebleau Formation sample revealed that the amorphous layer contains silanol (Si-OH), groups diagnostic of water-bearing amorphous, opaline silica, thus reinforcing the crystallographic evidence from EBSD and TEM analysis. Previous investigations focusing on water content and speciation in silica minerals (Florke et al., 1982; Graetsch et al., 1985) have suggested that cryptocrystalline silica minerals easily incorporate water due to the highly disordered crystal structure present in such minerals. The presence of *molecular* water in the amorphous silica layer is probably associated with submicroscopic fluid inclusions trapped within this cement. It is not clear whether these represent primary features or are due to partial crystallization of the amorphous phase with the subsequent exsolution of spare water. The molecular hydrocarbon units evident in the infrared spectrum were not expected; they may also represent fluid trapped within inclusions in the amorphous silica layer. Note that destabilization (oxidation) of organo-silica complexes has been mooted as a possible contributory process in the creation of the silica cements in the Fontainebleau Formation (Thiry and Marechal, 2001) so that the organic signal detected by infrared microscopy may represent remnants of the organic complexes.

7.1.1.3 Chalcedony

Chalcedony, less than 0.5 μm in size and with the [11-20] perpendicular to the grain surface, was identified as one of the silica polymorphs in the Heidelberg Formation by examining the band between the amorphous silica and the microcrystalline quartz. The *c* axes of the Heidelberg microcrystalline quartz, measured on a specific face of a host quartz grain facing into a pore, were plotted on stereograms (Chapter 3, Figs. 3.5A-D). The *c* axes are spread on a great circle (the white line on the figure representing a plane through that great circle) parallel to the plane of the quartz grain face, within a ± 15° scatter. This evidence indicates that crystals of microcrystalline quartz have grown with their *c* axes parallel to, but rotated on, the host surface, which is coated with an ~ 50-100 nm film. This observation is consistent with the presence of the silica polymorph chalcedony. When nucleating within amorphous silica, competitive crystal growth of chalcedony ensures that favourably oriented grains grow along [11-20], and into the pore space, resulting in the alignment of [11-20] orthogonal to the surface upon which the amorphous silica had deposited. As

explained above, EBSD data of microcrystalline quartz strongly suggests that the microcrystalline quartz grew on the chalcedony, inheriting its *c*-axis orientation first and then growing fast along the *c*-axis and parallel to the detrital host grain surface. This interpretation is supported further by high-resolution EBSD data revealing small crystals of chalcedony 0.2-0.5 μm in size (Chapter 3, Fig. 3.4D) on which the microcrystalline quartz grows (Heaney et al. 1994). Additionally, the indication of rotation of the selected area electron diffraction spots (Chapter 3, Fig. 3.7C) is also strong evidence for chalcedony.

Light optic analysis in the agates allowed differentiation of the agates into bands of chalcedony and mesocrystalline, euhedral quartz. CL, EBSD and FT-IR allowed further differentiation of chalcedony bands into: 1) discrete bands of amorphous silica (containing nanocrystalline quartz) or chalcedony-A, and 2) chalcedony with microcrystalline quartz or chalcedony-MQ by crystal size, crystallographic orientation, and water content.

7.1.1.4 Microcrystalline Quartz

In the Heidelberg Formation, a layer of microcrystalline quartz crystals (as defined by Vagle et al., 1994 and Lima and De Ros, 2002) with a thickness of approximately 1 μm has grown over syntaxial quartz overgrowth cement (Chapter 3, Figs. 3.3A and B). In the Fontainebleau Formation, high resolution secondary electron images (SEI) revealed microcrystalline quartz crystals < 10 μm in size in a band between 15 and 26 μm thick, coating grains with their long growth axes (*c* axes) parallel to the host surface (Chapter 5, Fig. 5.2). In the agates, in the chalcedony layer (Chapter 6, Fig. 6.1B), are parallel-aligned, fibrous and elongate crystals of microcrystalline quartz grading from 0.5 to 5 μm in length with axial ratios approximately 1:5 (Fig. 6.1G). These quartz fibres show a gradual increase in width toward the tip of the individual crystallites in the direction of growth. The fibres are elongate parallel to the growth direction of the bands.

7.1.2 What is the paragenesis of the silica polymorphs?

Amorphous silica has been reported to transform to quartz via a series of metastable intermediates: Opal A → Opal CT → chalcedony → microcrystalline quartz (Williams and Crerar, 1985; Williams et al., 1985). In the Heidelberg Formation and Fontainebleau Formation, amorphous silica coats the surfaces of many detrital grains. The likely occurrence of chalcedony growing within, and perhaps on, the amorphous silica, and thus beneath the microcrystalline quartz, seems to explain the *c*-axis orientation of the microcrystalline quartz growing sub-parallel to the host grain surface. The occurrence of chalcedony within amorphous silica bands suggests that the amorphous phase has undergone partial recrystallization to chalcedony during the geological history of these rocks, and therefore that the amorphous material is a precursor to the microcrystalline quartz and chalcedony. Similarly, the occurrence of chalcedony growing within and above the amorphous silica and beneath the microcrystalline quartz explains the *c*-axis orientation of the microcrystalline quartz growing subparallel to the surface of the host grain. The experimental work in Chapter 3 corroborates this conclusion. The paragenesis of the silica polymorphs in the Heidelberg and Fontainebleau Formations, representing a classic growth series from amorphous silica → chalcedony → microcrystalline quartz, is similar to the amorphous silica transformation noted by Williams and Crerar (1985) and Williams et al. (1985). Similarly, in the agates there is a progressive pattern observed in the bands; chalcedony-A (chalcedony with amorphous silica and nanocrystalline quartz) → chalcedony-MQ (chalcedony with microcrystalline quartz) → quartz, shares characteristics of silica diagenetic processes related to degrees of supersaturation with respect to silica (Williams et al., 1985; Williams and Crerar, 1985).

7.1.3. What is the crystallographic orientation of porosity preserving microcrystalline quartz?

In the Heidelberg Formation, a layer of microcrystalline quartz with a thickness of approximately 1 μm has grown over syntaxial quartz overgrowth cement (Chapter 3, Figs. 3.3A and B). To gain insight into the orientation of the microcrystalline quartz

crystals and their crystallographic relationship with the host grain, EBSD analysis was performed on polished thin sections. The analyses confirm that the microcrystalline quartz, unlike syntaxial quartz overgrowths, is misoriented with respect to the host grain. This attribute is represented by the multiple colour variations of the microcrystalline quartz crystals, relative to the detrital host grain in the EBSD images (Chapter 3, Figs. 3.4A and B).

The concept of the misorientation of microcrystalline quartz relative to the host grain has been reported in one previous paper (Haddad et al. 2006), but the control on the misorientation has not been previously reported. It has been shown for the microcrystalline quartz from the Heidelberg Formation that there is a distinct control on the misorientation of the grains. Quartz, including microcrystalline quartz, typically grows faster in the *c*-axis direction. Length-fast chalcedony is microcrystalline fibrous quartz which grows faster in the [11-20] direction (Miehe et al., 1984; Frondel, 1982). The microcrystalline quartz in the Heidelberg Formation inherited the crystallographic orientation of the chalcedony precursor it grew upon.

The simplest explanation for the orientation of the microcrystalline quartz in the Fontainebleau Formation is that it grew on chalcedony, within or on the amorphous silica, inheriting the chalcedony's *c*-axis orientations. The microcrystalline quartz then grew preferentially along the inherited *c* axes that were parallel to the growth surface. The presence of chalcedony within the amorphous silica layer is further supported by the small degree of rotation of the selected area electron diffraction spots (Chapter 5, Fig. 5.4F). That the microcrystalline quartz is not syntaxial and has *c* axes parallel to growth surfaces is due to the combination of: (1) the insulating amorphous silica layer (Chapter 5, Fig. 5.4) deposited on the detrital grain surface (or on the incipient quartz overgrowths if present); followed by (2) the inferred development of chalcedony within or on the amorphous silica.

7.1.4. What are the similarities and differences between the microcrystalline quartz in the Heidelberg Formation and microcrystalline quartz in the Fontainebleau Formation?

There are clear similarities between the Fontainebleau Formation and Heidelberg Formation (Chapter 3 and Chapter 5); but there are also differences. The main similarities between these geographically and stratigraphically remote sedimentary rocks are:

(i) The Fontainebleau Formation and Heidelberg Formation both contain the two silica polymorphs (amorphous silica and microcrystalline quartz (CL, EBSD, and TEM)) which forms on top of detrital quartz or quartz overgrowth surfaces (Chapter 5, Figs. 5.1D, 5.2, 5.3A, and 5.4). Both are inferred to contain chalcedony in, or on, the amorphous silica layer.

(ii) Both sandstones have undergone a minor degree of early (pre-microcrystalline) quartz cementation with the early cement adopting the same orientation as the underlying sand grain.

(iii) Both have an amorphous silica layer indiscriminately covering both sand grains resulting in minor quartz cement.

(iv) In both cases, EBSD revealed that the microcrystalline quartz is crystallographically misoriented with respect to the detrital grain.

(v) Specifically EBSD showed that the misorientation is systematic, evidenced by the distribution of the c-axes sub-parallel to the parent-grain surface.

(vi) In both cases, the microcrystalline quartz growth had a chalcedony-like orientation possibly suggesting that the microcrystalline quartz grew on precursor chalcedony. This chalcedony has a length-fast [11-20] preferred growth direction and controls the growth axis of the subsequent microcrystalline quartz.

The main differences between the two quartz arenites are:

(i) The Heidelberg microcrystalline quartz experienced two events, resulting in the repeated sequence: amorphous silica, chalcedony, and microcrystalline quartz. The Fontainebleau Formation has only one sequence of these silica polymorph cements. This is probably due to a single event (e.g. silica-rich fluid migration) in the Fontainebleau versus two fluid influx events in the Heidelberg Formation.

(ii) The Heidelberg Formation microcrystalline quartz crystals have *c* axes parallel to their host surface and these *c* axes have grown with random rotational distribution on that surface (180° dispersal). In contrast, while the Fontainebleau

Formation microcrystalline quartz crystals also have c-axes parallel to their host surface and these *c* axes have grown sub-parallel to each other with a rotational dispersal of only about 30°. The difference in rotational dispersal between the Heidelberg microcrystalline quartz and the Fontainebleau microcrystalline quartz is probably due to the type of parent chalcedony. In the Fontainebleau, the microcrystalline quartz dispersal is much smaller suggesting the parent chalcedony is a wall lining chalcedony that consists of parallel-fibrous bundles (Miehe et al., 1984). This yields parallel microcrystalline quartz with minor variation in rotation. In contrast, the rotation dispersal is much larger in the Heidelberg microcrystalline quartz suggesting the parent chalcedony is horizontal chalcedony, composed of spherulites with radiating fibres (Miehe et al., 1984). This yields more random orientation of the microcrystalline quartz.

Both of these sandstones are: 1) continentally-derived quartz arenites which are compositionally similar; 2) both are marine sandstones; 3) both sandstones have never developed beyond the early stages of quartz cementation as evidenced by the poorly developed quartz overgrowth cements); and 4) both have had inferred ground water flow as the source of silica (Haddad et al., 2006; Chapter 3 and Chapter 5). These similarities translate to both sandstones having microcrystalline quartz growing under shallow burial conditions, with minor quartz overgrowth cements resulting from silica-rich groundwater flow. Conversely, the sandstones are different in age; the Fontainebleau is Oligocene, while the Heidelberg is Late Cretaceous. Additionally, the sandstones have been buried to different depths; the Fontainebleau Formation has not been buried deeper than 100 metres (Haddad et al., 2006; Thiry and Marechal, 2001), while the Heidelberg Formation has been buried to depths somewhat greater than 100 metres (Chapter 2 and Chapter 3). These differences in age and burial depth may have resulted in the single sequence of amorphous silica-chalcedony-microcrystalline quartz in the Fontainebleau Formation versus a double sequence in the older and more deeply buried Heidelberg Formation sandstone. There may have been more time for a second episode of silica-rich fluid migration causing the second layer of amorphous silica, chalcedony and microcrystalline quartz. This exposure to longer time and deeper burial could have also influenced the fluid flow in the pores, i.e. if the rise and fall of the water table had an impact on the migration of the silica-rich fluid, it may have also influenced the orientation of the chalcedony, and the

timing of growth, i.e., if the amorphous layer had any gaps it is possible that some quartz overgrowths may have begun to grow and influence the orientation of the microcrystalline quartz.

7.1.5 What are the similarities and differences between the silica polymorphs in agates and in the Heidelberg and Fontainebleau Formations?

The silica polymorphs in two agates from the Citronelle Formation and Lake Superior were studied to understand the similarities and differences between chalcedony in agates and microcrystalline quartz in sandstones. Previous work on the Heidelberg Formation, Germany (Chapter 2 and Chapter 3) and the Fontainebleau Formation (Haddad et al., 2006 and Chapter 5) studying silica polymorph growth in sandstone reservoirs indicated that the misorientation of microcrystalline quartz coatings on sand grains was controlled by the orientation of nanocrystalline quartz in an amorphous layer (collectively analogous to the chalcedony described in Chapter 6). The implication is that microcrystalline quartz inherited its *c*-axis orientation from pre-existing chalcedony adjacent to amorphous silica in the Heidelberg and Fontainebleau sandstones similar to the growth of quartz following chalcedony in agates. Table 7.1 shows a comparison of the silica polymorphs found in the agates in the Citronelle Formation and Lake Superior (Chapter 6) and the silica polymorphs found in the Heidelberg and Fontainebleau Formations by silica type, layer thickness, crystal size, and orientation of quartz. The orientation of the *a* axes perpendicular to the growth surface and the orientation of the *c* axes parallel to the growth surface for the crystalline silica polymorphs found in the agates in Chapter 6 are the same orientations as those found in the Heidelberg and Fontainebleau sandstones. Thus agate is morphologically and crystallographically the same as microcrystalline quartz coats in sandstones although in the agate the bands are repeated multiple times suggesting multiple episodes of fluid influx in the agates versus one episode in the Fontainebleau Formation and two episodes in the Heidelberg Formation.

The crystallographic, textural, and compositional relationships of silica polymorphs present within the Citronelle Formation and Lake Superior agates and the Heidelberg

and Fontainebleau sandstones have been examined using EBSD and CL reveal the following:

1. Two agates with similar origins and the two sandstones with similar silica sources were studied and have identical patterns of growth of silica polymorphs: amorphous silica, nanocrystalline quartz, chalcedony and quartz.
2. The boundaries between individual bands within the agate and in the sandstones are sharply contrasting, reflected in crystallography (degree of crystallinity, morphology) and composition (water content); indicating formation from aqueous silica-rich fluid influxes.
3. Crystallographic information reveals that the degree of crystallinity and morphology of the silica minerals within the individual bands changes in a systematic fashion analogous to a diagenetic cycle; the initial chalcedony part of the agate band commences with amorphous silica followed by fibrous microcrystalline quartz crystals; chalcedony then grades into larger equiaxial mesoquartz crystals, similarly, in the sandstones, the first layer to form on the detrital quartz surface is amorphous silica followed by chalcedony which grades into larger microcrystalline quartz crystals.
4. CL revealed gradual changes in luminescence and signal response across individual bands. These changes are coincident with the evolving silica polymorphs present. Pole figures from EBSD revealed there is a strong crystallographic control throughout all bands in the agate, as well as in the sandstones, regardless of crystallinity or microtexture. This suggests that the crystal orientation in agate is dictated by a process that is independent of the silica mineral polymorph present as the substrate.
5. The combination of the initial precipitation of amorphous silica followed by [11-20] growth for chalcedony and rotated *c*-axes of microcrystalline quartz (parallel to the host surface) in the agate studied here is identical to the growth patterns in the Heidelberg and Fontainebleau sandstones.

There are clear similarities between the chalcedony found in the Citronelle Formation and Lake Superior agates and the microcrystalline quartz in the Fontainebleau Formation and Heidelberg Formation (Chapters 2, 3 and 5); but there are also differences. The main similarities between these geographically and stratigraphically remote sedimentary rocks are:

i. The Fontainebleau Formation and Heidelberg Formation both contain the two silica polymorphs (amorphous silica and microcrystalline quartz (CL, EBSD, and TEM)) which forms on top of detrital quartz or quartz overgrowth surfaces (Chapter 5, Figs. 5.1D, 5.2, 5.3A, and 5.4). Both are inferred to contain chalcedony in, or on, the amorphous silica layer, similar to the agates.
ii. Both have an amorphous silica layer indiscriminately covering both sand grains resulting in minor quartz cement, similar to the agates.
iii. In both cases, EBSD revealed that the microcrystalline quartz is crystallographically misoriented with respect to the detrital grain.
iv. Specifically EBSD showed that the misorientation is systematic, evidenced by the distribution of the c-axes sub-parallel to the parent-grain surface.
v. In both cases, the microcrystalline quartz growth had a chalcedony-like orientation possibly suggesting that the microcrystalline quartz grew on precursor chalcedony. This chalcedony has a length-fast [11-20] preferred growth direction and controls the growth axis of the subsequent microcrystalline quartz.

The main differences between the two quartz arenites and the agates are:

i. The Heidelberg microcrystalline quartz experienced two events, each resulting in the repeated sequence: amorphous silica, chalcedony, and microcrystalline quartz. The Fontainebleau Formation has only one sequence of these silica polymorph cements. This is probably due to a single event (e.g. silica-rich fluid migration) in the Fontainebleau versus two fluid influx events in the Heidelberg Formation. The agates have multiple sequences of the silica polymorphs, suggesting that there were multiple fluid influx events.
ii. The Heidelberg Formation microcrystalline quartz crystals and the agates chalcedony with microcrystalline quartz have *c* axes parallel to their host surface and these *c* axes have grown with completely random rotational distribution on that surface (180° dispersal). In contrast, while the Fontainebleau Formation microcrystalline quartz crystals also have c-axes parallel to their host surface and these *c* axes have grown sub-parallel to

each other with a rotational dispersal of only about 30°. The difference in rotational dispersal between the Heidelberg microcrystalline quartz and the Fontainebleau and agate microcrystalline quartz is probably due to the type of parent chalcedony. In the Fontainebleau, the microcrystalline quartz dispersal is much smaller suggesting the parent chalcedony is a wall lining chalcedony that consists of parallel-fibrous bundles (Miehe et al., 1984). This yields parallel microcrystalline quartz with minor variation in rotation. In contrast, the rotation dispersal is much larger in the Heidelberg and agate microcrystalline quartz suggesting the parent chalcedony is horizontal chalcedony, comprised of spherulites with radiating fibres (Miehe et al., 1984). This yields more random orientation of the microcrystalline quartz.

7.1.6 How do trace elements affect the growth of silica polymorphs?

Two possible mechanisms for the trace element control on microquartz growth are:
1) Metal ions interact with silicic acid to form colloidal silica and increase the precipitation rate of quartz and therefore help to grow microquartz, and 2) Surface defects caused by ionic substitution increase the silica precipitation rate and therefore promotes growth of microcrystalline quartz.
Consistent misorientation differences due to ionic substitution have been shown in chalcedony by Merino et al.,(1995). Additionally, the incorporation of trace elements disrupting the lattice sufficiently to cause screw dislocations and crystal defects which provide growth surfaces has been advocated by Heaney (1993). The misorientation seen in microcrystalline quartz in several examples studied could be due to defect sites caused by the trace element substitution. In conclusion, the defect sites caused by trace element substitution promote rapid growth which could initiate the growth of microcrystalline quartz.

EDS and WDS data on microcrystalline quartz studied indicate varying trace amounts of aluminium ranging from 50 to 10,000 ppm and iron 100 to 13,000 ppm. There is also evidence for coupled substitution of aluminium and sodium, maintaining charge balance when substituting for silicon in the quartz overgrowths, which has also been

documented in chalcedony by Graetsch, 1987 and in agate by Heaney, 1995. Aluminium and iron dominate the trace elements in amorphous silica and chalcedony. Other trace elements noted in the amorphous silica and chalcedony are: sodium, titanium, magnesium and potassium.

Trace elements in silica minerals can be present as part of a true solid solution, as material within aqueous fluid inclusions or as solid inclusions. Al, Fe^{3+} and Ti are considered to be able to form limited solid solution with quartz due to their similar ionic size and charge (Götze, 2009). While a limited quantity of monovalent cations are required to charge balance substitution of Al and Fe^{3+} in quartz, most group 1 and 2 cations (Na, K, Mg, Ca) are probably present within aqueous fluid inclusions. Submicroscopic solid inclusions can also account for elevated concentrations of metals in quartz (e.g. rutile needles or acicular hematite in quartz (Götze et al., 2009).

WDS analysis of the quartz overgrowth and microcrystalline quartz zone (Chapter 4, Fig. 4.6) show that the first layer in each of the concentric bands has the highest concentrations of aluminium and iron (Chapter 4, Figs. 4.2 and 4.6). On EBSD and TEM evidence this material is chalcedony containing both amorphous silica and nanocrystalline quartz. Aluminium concentrations are highest in the first deposited material and then tend to decrease towards the outer edge of the chalcedony bands. A layer of microcrystalline quartz was deposited on each of the chalcedony bands; microcrystalline quartz has very low concentrations of trace elements, including aluminium and iron. The repeated pattern of high aluminium and iron concentrations in chalcedony, followed by the lowest concentrations in microcrystalline quartz is further evidence of two discrete episodes of fluid influx.

Aluminium concentrations in quartz are reported to be a function of growth temperature. The specific concentration of aluminium has been proposed as a geothermometer (e.g. Dennen et al., 1970). In microcrystalline quartz, aluminium is below detection (i.e. < 12 ppm; Chapter 4, Table 4.2 and Fig. 4.6) suggesting a low temperature of growth. If it is assumed that the aluminium concentration in microcrystalline quartz is ≤ 11ppm then a temperature of ≤ 70ºC is implied (Dennen et al., 1970). By applying a maximum temperature of 70ºC to the microcrystalline quartz data and fractionation equation (Chapter 4, Fig. 4.7) a water $\delta^{18}O$ value of < -

4‰ is implied supporting the preferred interpretation of the microcrystalline quartz growing from meteoric water ($\delta^{18}O$ of -5‰) rather than deep crustal water ($\delta^{18}O$ of +5‰).

Aluminium data in chalcedony are difficult to interpret and are not easily related to temperature of growth (Götze et al., 2001). There are numerous precedents for elevated aluminium concentrations in other amorphous forms of silica such as opal and agate (Heaney and Davis, 1995; Merino et al., 1995; Götze et al., 2001).

The other trace elements in the silica cements, and especially the concentric bands (Chapter 4, Figs. 4.2 and 4.6) are difficult to interpret but it is noteworthy that Ti, Fe, Na, Ca, K and Mg are all at elevated concentrations in the chalcedony compared to the quartz overgrowth and the microcrystalline quartz. It seems likely that cations of common salts (Na, K, Mg, and Ca) may be at elevated concentrations in chalcedony due to their entrapment in fluid inclusions (too small for fluid inclusion analysis). In contrast, the high concentrations of Ti may be present in solid inclusions, or possibly in solid solution, within chalcedony. Iron, like aluminium, is considered to be able to form a limited solid solution with silica (Götze, 2009) and maybe structurally bound within the chalcedony.

7.1.7 Is there is link between stable oxygen isotope values and silica polymorph variations in microcrystalline quartz cemented sandstones?

High precision, *in situ* oxygen isotope values from the Heidelberg Formation silica polymorphs fall within the ranges of previously published data for microcrystalline quartz and chalcedony (Table 4.1). This study reports the first use of *in situ* analysis of chalcedony with microcrystalline quartz using a 5 μm analysis spot size across the chalcedony precursor for porosity-preserving microcrystalline quartz, and provides a previously unattainable record of these silica polymorph histories. The wide range of $\delta^{18}O$ values for detrital grains is not unexpected given the potentially wide range of source terrains (each with their own geological history) that could contribute to the supply of quartz to the Heidelberg Fm. It is noteworthy that quartz overgrowths have

lower $\delta^{18}O$ values than microcrystalline quartz which in turn have lower $\delta^{18}O$ values than chalcedony.

7.1.7.1 Range of possible controls on $\delta^{18}O$ in the silica cements of the Heidelberg Formation

There are potentially three end-member influences on the $\delta^{18}O$ values of the silica cements in the Heidelberg Formation:

1. Silica polymorph-dependent fractionation of ^{18}O between water and solid phase,
2. Variable temperatures of growth (e.g. for similar water $\delta^{18}O$ values),
3. Variable water $\delta^{18}O$ values (e.g. for similar temperatures).

These will be discussed in the following sections.

7.1.7.2 Effect of silica phase on fractionation

There has been a range of quartz-water oxygen isotope fractionation equations published. Clayton et al., 1972 and Matsuhisa et al., 1979 published equations of the type ($A \times 10^6/T^2 - B$) while Meheut, 2007 published a third order polynomial describing the fractionation. While these three are different in detail, they give similar results (less than 1‰ difference at low temperatures).

The oxygen isotope fractionation between amorphous silica and water has also been published and is also of the type ($A \times 10^6/T^2 - B$) (Kita et al., 1985). The A and B constants are both slightly higher than those for quartz and so effectively cancel each other out. There seems to be negligible difference between the isotope fractionation of quartz and water and amorphous silica and water.

From this analysis, the specific type of silica polymorph does not seem to play a significant role in influencing the measured $\delta^{18}O$ of the silica cements. It seems that the identification of amorphous silica is not of significance to the interpretation of the stable oxygen isotopes.

7.1.8 How does the temperature of formation vary related to original water type and what are the controls on the $\delta^{18}O$ in the silica cements?

It is not possible directly to measure the $\delta^{18}O$ of the water that facilitated the growth of the silica cements in the Heidelberg Formation. Similarly, it is not possible to define uniquely the temperature of growth of the silica cements in the concentric bands. Therefore a range of scenarios will be explored and assessed for their geological plausibility.

7.1.8.1 Quartz overgrowths

The quartz overgrowths have an average $\delta^{18}O$ of +19.3‰ (Chapter 4). Quartz cement is typically assumed to begin growing at temperatures greater than approximately 80°C (McBride, 1989; Ramm et al., 1997; Lander and Walderhaug, 1999; Walderhaug, 2000; and Worden and Morad, 2000). The Heidelberg Formation does not contain more than a few percent quartz cement so it can be concluded that it has not been exposed to temperatures much greater than about 80°C. Using this temperature, either the Clayton et al., (1972) or Matsuhisa et al., (1979) fractionation equations and the average quartz overgrowth $\delta^{18}O$ value reveals that the water that generated the overgrowth had a $\delta^{18}O$ of -4.4‰. This value is slightly higher than contemporary meteoric water (Duarte et al., 2011) but this difference would be expected if there had been any water-rock interaction. For reference, if a less likely quartz overgrowth temperature of 100°C was used, then the calculated $\delta^{18}O$ of the water would be -2‰. It seems likely that diagenesis and growth of the small amount of quartz overgrowth occurred in the presence of meteoric water that presumably entered the permeable Heidelberg Formation, during a lowstand, sometime after deposition (perhaps when the formation was part of an active aquifer).

7.1.8.2 Chalcedony and microcrystalline quartz

Three types of water that plausibly could have resulted in the growth of the concentric bands of silica cements have been modelled; meteoric water (the type of water that seems to have been responsible for the quartz overgrowths), seawater and deep crustal water, perhaps associated with mineralization (noting the existence of the lead-zinc deposits in the nearby Harz Mountains; Liebmann, 1992). The meteoric water can be assumed to have a $\delta^{18}O$ value of about -5‰ (Gat, 1996), similar to the value for the water responsible for quartz overgrowths. Seawater can be assumed to have a $\delta^{18}O$ of 0‰. Deep crustal water can be assumed to have a $\delta^{18}O$ value of about +5‰ (Gat, 1996). These end-member values can then be used in the isotope fractionation equations to deduce the approximate temperature of mineral growth in the concentric bands.

Using Clayton et al., (1972), the microcrystalline quartz mean $\delta^{18}O$ value of +22.7‰ gives a temperature of 57°C for meteoric water, 87°C for seawater and 127°C for deep crustal water (Fig. 7). The mixed chalcedony-microcrystalline quartz mean $\delta^{18}O$ value of +27.7‰ yields a temperature of 35°C for meteoric water, 58°C for seawater and 89°C for deep crustal water. Again, using Clayton et al. (1972), the interpreted pure chalcedony value of $\delta^{18}O$ value of ~ +30‰ yields a temperature of 24°C for meteoric water, 45°C for seawater and 72°C for deep crustal water. On petrographic evidence (Chapter 4, Fig. 4.2) chalcedony (bands 1 and 3) grew before microcrystalline quartz (bands 2 and 4) in two discrete events; it can be concluded that, if they grew from the same water, the chalcedony grew at a lower temperature than the microcrystalline quartz that followed.

It is not impossible that the concentric bands of silica cement are due to an influx of deep crustal water (high $\delta^{18}O$ +5‰) which first grew chalcedony at ~ 89°C. The next event would have been microcrystalline quartz growth at 127°C requiring the water to become hotter with time. This sequence of events would then have been repeated, after a hiatus during which the host rock cooled down. This scenario seems unlikely since microcrystalline quartz is typically associated with relatively low temperatures of growth in sandstones (e.g. Vagle et al., 1994; Haddad et al., 2006).

Noting that the quartz overgrowth (Chapter 4, Fig. 4.2) probably developed in meteoric water ($\delta^{18}O$ -4.4‰) at 80°C (see earlier) suggests that the meteoric water scenario for growth of the concentric bands of silica cements is more likely than the deep crustal fluid scenario. The implication is that there was an influx of cold meteoric water that gave rise to chalcedony growth at ~ 34°C followed by microcrystalline quartz growth from the same water, perhaps as it thermally equilibrated with the surrounding rock, at ~ 57°C.

7.1.9 What is the growth mechanism for porosity preserving microcrystalline quartz?

The observations revealed in this study led to a conceptual model for a sequence of diagenetic transformations, from the initial deposition of the amorphous silica surface-coating nanofilm (Chapter 3, Fig. 3.9A) on the host grain, to the growth of chalcedony with its [11-20] direction (fast growth axis, e.g., Florke et al., 1982) perpendicular to the surface of the host grain (Chapter 3, Fig. 3.9B) to the nucleation or recrystallization and growth of microcrystalline quartz (Fig. 3.9C). The microcrystalline quartz inherits the *c*-axis orientation of the chalcedony on which it grows, which is parallel to the surface of the host grain (Chapter 3, Fig. 3.9D) because chalcedony grows into the pore space along its fast growth direction, orthogonal to the *c*-axis (Heaney et al., 1994).

During the formation of quartz overgrowths in sandstones, relatively large quartz crystals (50-100 μm) grow into pore spaces after burial, inheriting the exact crystallographic orientation of the detrital host grain upon which they have grown (Waugh, 1970). Syntaxial quartz overgrowths extend into the pore space and effectively occlude most of the porosity in sandstones buried to depths where temperatures have exceeded ~ 80°C (Worden and Morad, 2000). In contrast, misoriented microcrystalline quartz crystals (0.1-10 μm) preserve porosity by coating the surface of the detrital sandstone grain during early diagenesis (Aase et al., 1996; Aase and Walderhaug, 2005). A film of amorphous silica initially coats the grain surfaces, growing from fluids which are saturated with respect to amorphous silica.

Once precipitation of amorphous silica starts, the silica concentration of the fluid must decrease. As silica saturation decreases, chalcedony begins to crystallize (Williams et al., 1985), growing with its [11-20] direction perpendicular to the amorphous layer. This requires the *c*-axis to be parallel to the amorphous layer, but the *c* axes of the collection of chalcedony crystals are rotated on that layer. Initial growth of microcrystalline quartz occurs on the chalcedony. The amorphous silica may subsequently undergo further crystallization to become an intergrowth of nano-sized quartz crystals or chalcedony and remnant amorphous silica. This combination of amorphous nano-film, length-fast chalcedony, and *c* axes of microcrystalline quartz parallel to the host surface inhibits the growth of large crystals of quartz into available space, thus preserving porosity for the storage and migration of petroleum in the subsurface. Understanding that an amorphous-silica precursor is necessary for porosity-preserving growth of microcrystalline quartz is the first step in developing a predictive model for preserving porosity in deep, high-temperature sandstone reservoirs. The development of an intermediate chalcedony phase is likely to be important, because it favours the systematic misorientation of microcrystalline quartz.

The first band of chalcedony (band-1) in the Heidelberg Formation has a slightly higher $\delta^{18}O$ value than the second band of chalcedony (chalcedony band-3) suggesting either lower temperature growth or a more negative $\delta^{18}O$ of the aqueous medium for the first phase of chalcedony formation (Chapter 4, Fig. 5). Band 1 also has higher Al and lower Fe concentration than band 3 confirming the subtle differences in the two phases of chalcedony growth Chapter 4, Fig. 4.6). The second band in the Heidelberg (band 2-microcrystalline quartz) overlies band 1-chalcedony and has a slightly lower $\delta^{18}O$ value than band-4 microcrystalline quartz (Chapter 4, Fig. 4.6). The isotopic and trace element data suggest an initial event in which first chalcedony and then microcrystalline quartz grew followed by a repeating sequence from slightly different water (in terms of trace element chemistry and isotopes).

The SiO_2 concentration-temperature diagram for different silica polymorphs (Kastner et al., 1977) suggests that the amorphous silica (in chalcedony bands-1 and -3, Chapter 4, Fig. 4.2F) required an elevated silica concentration of about 120 ppm for growth at about 34°C (interpreted from the stable isotope data) while the subsequent microcrystalline quartz growth required a silica concentration of about 20-24 ppm at

61°C (also interpreted from the stable isotope data and supported by the aluminium concentration data). The pre-existing quartz overgrowths (70°C from stable isotope data) required a silica concentration of up to about 40 ppm.

The water responsible for chalcedony growth, with high concentrations of silica, also had high concentrations of trace elements, specifically aluminium and iron. As amorphous silica began to precipitate on the quartz grains or overgrowths, the concentration of silica in the fluid decreased and nanocrystalline quartz began to develop; overall this is the chalcedony layer seen in CL, BSEM, EBSD and TEM (Chapter 4, Figs. 4.2-3). Larger EBSD-discernible quartz crystals began to grow (the microcrystalline quartz in Chapter 4, Fig. 4.2) as silica saturation fell and the precipitation rate slowed down. This model illustrates that the growth of concentric bands of silica cements in the Heidelberg Formation required two influxes of relatively cold (< 34°C) meteoric water with high concentrations of silica, aluminium and other trace elements. Each influx precipitated chalcedony (amorphous silica and nanocrystalline quartz) and then heated up as microcrystalline quartz eventually precipitated (at 57°C) from waters with much lower silica and aluminium (and other trace element) concentrations.

It is noteworthy that the concentric bands of silica cement from the Heidelberg Formation reported here bear notable petrographic similarities to silcrete from the Fontainebleau Formation (Thiry and Marechal, 2001; Haddad et al., 2006) and from the Cordillo Formation (Alexandre et al., 2004). Indeed the interpretation of the type of water (meteoric) and temperature of growth of silica cements in the Heidelberg Formation seems to suggest that these cements are related to warm groundwater flow. In the Fontainebleau Formation it appears that silica precipitation occurred at the interface between groundwater and downward percolating recharge water (Thiry and Marechal, 2001). The cause of elevated silica concentrations required for silcrete formation remains unknown. The elevated concentrations of both silica and aluminium required for the growth of the chalcedony in the Heidelberg Formation may both result from destabilization of complexed SiO_2 and aluminium.

7.2 Scope for further work

Three additional questions were posed initially, but not pursued extensively during the research and would be the focus for future work:

7.2.1. How does silica source (saturation) affect the growth of microcrystalline quartz?

Microcrystalline quartz is hypothesized to form from supersaturated concentrations of silica in reservoirs under two possible conditions: 1) internal silica source: highly soluble silica e.g. sponges, diatoms, or radiolarian co-deposited with the sandstone. Moderate temperature during shallow burial dissolves the silica and creates the microcrystalline quartz coating. Previous work has identified sponge spicules as a source of silica and subsequent microcrystalline quartz in the Brea Formation in the Miller Field, the Fulmar Formation in the Puffin, Fulmar, Deep Graben, Curlew/Paul, Franklin, Shearwater, Martha, Elgin, Thomas and Molly Fields in the North Sea. Other silica-secreting organisms, such as diatoms and radiolaria and silica secreting plants such as Equisetum genus (horsetails) and Gramineae grasses could also generate high silica concentrations and provide soluble silica sources to generate microcrystalline quartz in proximal sandstone reservoirs. These organic sources proximal to sandstone reservoirs could potentially be predicted using climate models to identify areas with upwelling conditions. Inorganic silica sources such as chemical weathering of opaline organic remains in sediments, feldspars, volcanic tuffs and ashes, as well as, hot springs and deposition from meteoric circulation could also provide highly concentrated silica sources for subsequent microcrystalline quartz growth. 2) An alternative solution is an external silica source which brings high concentration silica fluid into a porous sandstone. If the microcrystalline quartz coating occurs near a fault, the fault could act as a conduit for silica-rich fluids flowing into the reservoir. Previous work on the Fontainebleau Formation in the Paris Basin by Haddad et al., 2006 indicated that the silica source is from meteoric fluids mixing with formation waters. The source of silica for the microcrystalline quartz in the Heidelberg Formation in Germany is also postulated to be sourced similarily, as well, so this alternative is not likely for these two sandstones based on current data.

Evidence comparing the quartz overgrowths to the Heidelberg microcrystalline quartz and the overgrowth in kinetic modelling by Lander et al., (2008) suggests that quartz overgrowths form in a growth-dominated regime while microcrystalline quartz forms in a nucleation dominated regime. Silica concentration differentiates these two regimes with the supersaturated silica concentration depending on nucleation and growth, which can potentially be estimated through chemical kinetic modelling. Additionally, the presence of volcanogenic sediments and zeolites (De Ros et al., 1997) and also diagenesis associated with the smectite-illite reaction (Abercrombie et al., 1994) are potential sources of silica for microcrystalline quartz.

7.2.3. Does the model for microcrystalline quartz growth apply in a hydrocarbon reservoir (e.g. Fulmar Formation, North Sea)?

The microcrystalline quartz studied in this research was primarily from outcrop samples. Although the Miller Field in the North Sea was studied in this research (see Appendix I), the small size of the microcrystalline quartz made EBSD work to understand the orientation of the Miller microcrystalline quartz untenable. Samples from other North Sea fields containing microcrystalline quartz could be studied to test the model proposed for microcrystalline quartz growth and determine if the model is consistent in hydrocarbon reservoirs.

7.2.3. Can chalcedony be conclusively identified as associated with microcrystalline quartz (i.e. test for chalcedony with TEM analysis)?

Focused ion beam samples of possible chalcedony were made for the Heidelberg Formation and Fontainebleau Formation. Additional high resolution TEM work to identify chalcedony conclusively could be undertaken in the future to add additional evidence to confirm that chalcedony is associated with microcrystalline quartz in the Heidelberg and Fontainebleau Formations.

7.2 References

Aase, N.E., Bjorkum, P.A., and Nadeau, P.H., 1996, The effect of grain-coating microquartz on preservation of reservoir porosity: American Association of Petroleum Geology, Bulletin, v. 80, p. 1654-1673.

Aase, N.E., and Walderhaug A., 2005, The effect of hydrocarbons on quartz cementation: diagenesis in the Upper Jurassic sandstones of the Miller Field, North Sea, revisited: Petroleum Geoscience, v.11, p. 215-223.

Abercrombie, H.J., Hutcheon, I.E., and Bloch, J.D., 1994, :Silica activity and the smectite-illite reaction. Geology, v. 22, p. 539-542.

Abruzzese M. J., Waldbauer J. R. and Chamberlain C. P., 2005, Oxygen and hydrogen isotope ratios in freshwater chert as indicators of ancient climate and hydrologic regime. Geochim. Cosmochim. Acta 69, p. 1377-1390.

Adams, B.L., Wright, S.I., and Kunze, K., 1993, Orientation imaging: The emergence of a new microscopy: Metallurgical Transactions, v. 24A, p. 819-931.

Alexandre A., Meunier J-D., Llorens E., Hill S. M., and Savin S. M., 2004, Methodological improvements for investigating silcrete formation: petrography, FT-IR and oxygen isotope ratio of silcrete quartz cement, Lake Eyre Basin (Australia). Chem. Geol. 211, p. 261-274.

Blankenburg, H-J.,1988, Achat, Liepzig, Germany, VEB Deutscher Verlag für Grundstoffinustrie.

Blatt, H., 1987, Oxygen Isotopes and the Origin of Quartz: Journal of Sedimentary Petrology, v. 57, p. 373-377.

Bloch, S., Lander, R.H., and Bonnell, L., 2002, Anomalously high porosity and permeability in deeply buried sandstone reservoirs: Origin and predictability: The American Association of Petroleum Geologists Bulletin, v. 86, no. 2, p. 301–328.

Bryxina, N. A. & Sheplev, S. V., 1999, Auto-oscillation in agate crystallization. Math. Geol., 31, p. 297-309.

Cagatay, M.N., Saner, S., AlSaiyed, I., and Carrigan, W.J., 1996, Diagenesis of the Safaniya Sandstone Member (mid-Cretaceous) in Saudi Arabia: Sedimentary Geology, v. 105, no. 3–4, p. 221–239.

Chang, J.C., and Yortsos, Y.C., 1994, Lamination during silica diagenesis - effects of clay content and Ostwald ripening: American Journal of Science, v. 294, p. 137-172.

Clayton, R.N., O'Neil J.R. and Mayeda T.K., 1972, Oxygen isotope exchange between quartz and water: Journal of Geophysical Research. v. 77, p. 3057-3067.

Darragh, P. J., Gaskin, J., Terrell, B. C. & Sanders, J. V., 1966, Origin of precious opal: Nature. v. 209, p. 13 - 16.

Dennen, W.H. and Blackburn W.H., 1970, Aluminium in quartz as a geothermometer: Contributions to Mineralogy and Petrology, v. 27, p. 332-342.

De Ros, L. F., Morad, S., and Al Aasm, I.S., 1997, Diagenesis of siliciclastic and volcaniclastic sediments in the Cretaceous and Miocene sequences of the NW African margin (DSDP Leg 47A,Site 397), Sedimentary Geology, v. 112, p. 137-156.

Dingley, D.J., 1984, Diffraction from sub-micron areas using electron backscattering in the scanning electron microscope: Scanning Electron Microscopy, v. 2, p. 569-575.

Duarte, L. C., Hartmann L. A., Ronchi L. Hl, Berner Z., Theye T. and Massone H. J., 2011, Stable isotope and mineralogical investigation of the genesis of amethyst geodes in the Los Catalanes gemological district, Uruguay, southernmost Parana volcanic province. Miner Deposita 46, p. 239-255.

Evans, J., Hogg, A. G. C., Hopkins, M. S., and Nadeau, P. H. 1994, Quantification of quartz cements using combined SEM, CL, and image analysis: Journal of Sedimentary Research, v. 64, p. 334-338.

Fisk, H.N. ,1939, Igneous and metamorphic rocks from Pleistocene gravels of central Louisiana. Journal of Sedimentary Petrology, 9, p. 20-27.

Flörke, O.W., Köhler-Herbertz, B., Langer, K., and Tönges, I., 1982, Water in microcrystalline quartz of volcanic origin - agates: Contributions to Mineralogy and Petrology, v. 80, p. 324-333.

Flörke, O.W., Graetsch, H., and Miehe, G., 1983, Crystal structure and microstructure of chalcedony: Fortschritte der Mineralogie, v. 61, no. 1, p. 62–63.

Flörke, O.W., Graetsch, H., Martin, B., Roller, K., and Wirth, R., 1991, Nomenclature of microcrystalline and non-crystalline silica minerals, based on structure and microstructure: Neues Jahrbuch für Mineralogie, Abhandlungen, v. 163, p. 19-42.

Franzke, H.K., 1990, Kinematische Studien an Störungskatklasiten des Harzes und Subherzynen Beckens: Zeitschrift für Geologische Wissenschaften, v. 18, p. 987-996.

French, M. W., Worden, R. H., Mariani, E., Larese, R. E., Mueller, R. R. and Kliewer, C.E., 2012, Microcrystalline quartz generation and the preservation of porosity in sandstones; evidence from the Upper Cretaceous of the Subhercynian Basin, Germany. Journal of Sedimentary Research, v. 82, p. 422-434.

Frondel, C., 1982, Structural hydroxyl in chalcedony (type-B quartz): American Mineralogist, v. 67, p. 1248-1257.

Fynn, G.W., and Powell, W.J.A., 1979, The Cutting and Polishing of Electro-Optic Materials: London, Adams Hilger, 216 p.

Gat J. R. (1996) Oxygen and hydrogen isotopes in the hydrologic cycle. Ann. Rev. Earth and Planetary Sci. 24, 225-262.

Godovikov, A. A., Ripinen, O. I. & Motorin, S. G., 1987, Agates, Moscow, Nedra.

Goldstein, R.H., and Rossi, C., 2002, Recrystallization in quartz overgrowths: Journal of Sedimentary Research, v. 72, p. 432-440.

Götte, T., Pettke, T., Ramswyer, K., Koch-Müller, M., and Mullis, J., 2011, Cathodoluminescence properties and trace element signature of hydrothermal quartz: A fingerprint of growth dynamics: American Mineralogist, v. 96, p. 802-813.

Götze J., 2009, Chemistry, textures and physical properties of quartz – geological interpretation and technical application. Mineralogical Magazine, 73(4), p. 645-671.

Götze J., Plötze M., Tichomirowa M., Fuchs H., and Pilot J., 2001, Aluminum in quartz as an indicator of the temperature of formation of agate. Mineralogical Magazine, 65(3), p. 407-413.

Götze, J., Möckel, R., Kempe, U., Kapitonov, I. & Vennemann, T., 2009, Characteristics and origin of agates in sedimentary rocks from the Dryhead area, Montana, USA. Mineralogical Magazine, 73, p. 673-690.

Götze, J., Nasdala, L., Kleeberg, R. & Wenzel, M., 1998, Occurrence and distribution of "moganite" in agate/chalcedony: a combined micro-Raman, Rietveld, and

cathodoluminescence study. Contributions to Mineralogy and Petrology, 133, p. 96-105.

Götze, J., Tichomirowa, M., Fuchs, H., Pilot, J. & Sharp, Z. D., 2001, Geochemistry of agates: a trace element and stable isotope study. Chemical Geology, 175, p. 523-542.

Graetsch, H., 1994, Structural characteristics of opaline and micro-crystalline silica minerals, in Heaney, P.J., Prewitt, C.T. and Gibbs, G.V., eds., Silica; Physical Behaviour, Geochemistry and Materials Applications: Reviews in Mineralogy, v. 29, p. 209– 232.

Graetsch,H., Flörke, O. W. & Miehe, G., 1985, The nature of water in chalcedony and Opal-C from Brazilian agate geodes: Physical Chemistry of Minerals, v.12, p. 300-306.

Graetsch, H., Florke, O. W. and Miehe, G. 1987, Structural defects in Microcrystalline Silica: Physical Chemistry of Minerals. 14, p. 249-257.

Haddad, S.C., Worden, R.H., Prior, D.J., and Smalley, P.C., 2006, Quartz cement in the Fontainebleau sandstone, Paris basin, France: Crystallography and implications for mechanisms of cement growth: Journal of Sedimentary Research, v. 76, no. 2, p. 244–256.

Haimson, B., and Lee, H., 2004, Borehole breakouts and compaction bands in two high-porosity sandstones: International Journal of Rock Mechanics and Mining Sciences, v. 41, no. 2, p. 287–301, doi:10.1016/j.ijrmms.2003.09.001.

Harwood, J., Aplin, A. C., Fialips, C. I. M, Iliffe, J. E., Kozdon, R., and Valley, J. W., 2009, New constraints on quartz cementation histories with oxygen isotope stratigraphies derived from high precision SIMS: American Association of Petroleum Geologists Annual Convention and Exhibition, Denver, Colorado Program, p. 88-89.

Hattori, I, Umeda, M., Nakagawa, T., and Yamamote, H., 1996, From chalcedonic chert to quartz chert: diagenesis of chert hosted in a Miocene volcanic-sedimentary succession, Central Japan: Journal of Sedimentary Research, Section A: Sedimentary Petrology and Processes, v. 66, p. 163-174.

Heald, M.T., and Renton, J.J., 1966, Experimental study of sandstone cementation: Journal of Sedimentary Petrology, v. 36, p. 977-991.

Heaney, P.J., Veblen, D.R., and Post, J.E., 1994, Structural disparities between chalcedony and macrocrystalline quartz: The American Mineralogist, v. 79, no. 5–6, p. 452–460.

Heaney, P. J. 1993, A proposed mechanism for the growth of chalcedony: Contrib. Mineral. Petrol. v. 115, p. 66-74.

Heaney, P. J. and Davis, A. M., 1995, Observation and origin of self-organized textures in agates: Science, v. 269, p. 1562-1565.

Hendry, J.P., and Trewin, N.H., 1995, Authigenic quartz microfabrics in Cretaceous turbidites—Evidence for silica transfer processes in sandstones: Journal of Sedimentary Research Section a-Sedimentary Petrology and Processes, v. 65, no. 2, p. 380–392.

Herdianita, N. R., Browne, P. R. L., Rodgers, K. A. & Campbell, K. A. 2000, Mineralogical and textural changes accompanying ageing of silica sinter: Mineralium Deposita. V. 35, p. 48 - 62.

Hervig R. L., Williams L. B., Kirkland I. K., and Longstaffe F. J., 1995, Oxygen isotope microanalysis of diagenetic quartz: Possible low temperature occlusion of pores. Geochim. Cosmochim. Acta 59, p. 2537-2543.

Iler, R. K., 1979, The Chemistry of Silica. John Wiley & Sons publishers, New York. 866p.

Inagaki, R., Motomur, Y. & Ogata, S., 2003, Microbial silica deposition in geothermal hot waters. Appl. Microbial. Biotechnol., 60, p. 605-611.

Isaacs, C. M., 1980, Diagenesis in the Monterey Formation examined laterally along the coast near Santa Barbara, California: Stanford University, unpublished Ph.D. thesis, 329 p.

Jahren, J., and Ramm, M., 2000, The porosity-preserving effects of microcrystalline quartz coatings in arenitic sandstones: Examples from the Norwegian continental shelf, in Quartz Cementation in Sandstones, Worden, R.H. and Morad, S.,eds., International Association of Sedimentologists Special Publications, v. 29, p. 271–280.

Jones, J.B., Sanders, J. V., and Segnit, E. R., 1964, Structure of Opal: Nature, p. 204.

Jones, J.B., and Segnit, E.R., 1971, The nature of opal. I. Nomenclature and consistent phases, J. Geol. Soc. Australia, v. 18 (1), p.57.

Kastner M., Keene J.B., and Gieskes J.M., 1977, Diagenesis of siliceous oozes - I. Chemical controls on the rate of opal-A to opal-CT transformation - an experimental study: Geochimica et Cosmochimica Acta, v.41, p. 1041-1059.

Kelly J.L., Fu B., Kita N.T., and Valley J.W., 2007, Optically continuous silcrete quartz cements of the St. Peter Sandstone: High precision oxygen isotope analysis by ion microprobe: Geochimica et Cosmochimica Acta, v. 71, p. 3812-3832.

Kita I., Taguchi S. and Matsubaya O., 1985, Oxygen isotope fractionation between amorphous silica and water at 34-93^{0}C: Nature, v. 314, p. 83-84.

Knauth, L.P. 1973. Oxygen and hydrogen isotope ratios in cherts and related rocks. Unpublished PhD thesis, California Institute of Technology, 90 p.

Knauth L. P. and Epstein S. (1976) Hydrogen and oxygen isotope ratios in nodular and bedded cherts: Geochimica et Cosmochimica Acta, v. 40, p. 1095-1108.

Knauth, P. 1994. Petrogenesis of chert. *In:* Heaney, P. J., Prewitt, C. T. & Gibbs, G. V. eds. Silica. Physical Behaviour, Geochemistry and Materials Applications, p. 233 - 258. Reviews in Mineralogy, v. 29.

Kraishan, G.M., Rezaee, M.R., and Worden, R.H., 2000, Significance of trace element composition of quartz cement as a key to reveal the origin in sandstones: an example from the Cretaceous of the Barrow Sub-basin, Western Australia, in Worden, R.H., and Morad, S., eds., Quartz Cement in Sandstones: International Association of Sedimentologists, Special Publication 29, p. 317-331.

Kronenberg, A. K., 1994, Hydrogen speciation and chemical weakening of quartz. *In:* Heaney, P. J., Prewitt, C. T. & Gibbs, G. V. eds. Silica. Physical Behaviour, Geochemistry and Materials Applications, Reviews in Mineralogy, v. 29, p. 123 - 176.

Lander, R. H., and Walderhaug, O., 1999, Predicting porosity through simulating sandstone compaction and quartz cementation: AAPG Bull. 83, p. 433-449.

Lander, R.H., Larese, R.E., and Bonnell, L.M., 2008, Toward more accurate quartz cement models: The importance of euhedral versus noneuhedral growth rates: The American Association of Petroleum Geologists Bulletin, v. 92, no. 11, p. 1537–1563.

Langer, K. & Flörke, O. W. 1974, Near infrared absorption spectra (4000-9000cm^{-1}) of opals and the role of "water" in these SiO_2 . nH_2O) minerals. Fortschritte der Mineralogie, v. 52, p. 17-51.

Lee, D. R., 2006a, Characterisation of silica minerals in a banded agate: implications for agate genesis and growth mechanisms: in unpublished Master's thesis, University of Liverpool, 18p.

Lee, D. R., 2006b, Characterisation and the diagenetic transformation of non- and microcrystalline silica minerals: in unpublished Master's thesis, University of Liverpool, 20p.

Lehmann K., Berger A., Götte T., Ramseyer K., and Wiedenbeck, M., 2009, Growth related zonations in authigenic and hydrothermal quartz characterized by SIMS-, EPMA-, SEM-CL- and SEM-CC-imaging: Mineralogical Magazine 73(4), p. 633-643.

Lehmann K., Pettke T., and Ramseyer K., 2011, Significance of trace elements in syntaxial quartz cement, Haushi Group sandstones, Sultanate of Oman: Chem. Geol. 280, p. 47-57.

Liebmann, W., 1992, Historischer Bergbau im Harz-Kurzffihrer: Universität Hamburg, Mineralogischen Museum: Schriften Köln, Sven von Loga Verlag, 320 p.

Lima R. D., and De Ros L. F., 2002, The role of depositional setting and diagenesis on the reservoir quality of Devonian sandstones from the Solimoes Basin, Brazilian Amazonia: Marine and Petroleum Geology, v.19, p. 1047-1071.

Lloyd, G.E., 1987, Atomic number and crystallographic contrast images with the SEM: a review of backscattered electron techniques: Mineralogical Magazine, v. 51, p. 3-19.

Lloyd, G. E. & Freeman, B., 1991, SEM electron channelling analysis of dynamic recrystallization in a quartz grain. Journal of Structural Geology, 13, p. 945-953.

McBride, E.F., 1989, Quartz cement in sandstones: A review: Earth-Science Reviews, v. 26, no. C, p. 69–112, doi:10.1016/0012-8252(89)90019-6.

Marchand, A. M. E., Macaulay C. I., Haszeldine R. S., and Fallick A. E., 2002, Pore water evolution in oilfield sandstones: constraints from oxygen isotope microanalyses of quartz cement: Chem. Geol. 191, p. 285-304.

Marfunin, A. S., 1979, spectroscopy, luminescence, and radiation centers in minerals. Translated from the Russian publication by V. V. Schiffer. Berlin: Springer Verlag.

Matsuhisa, Y., Goldmith, J. R., and Clayton, R. N., 1979, Oxygen isotopic fractionation in the system quartz_albite_anorthite_water. Geochim. Cosmochim. Acta. 43, p. 1131-40.

Meheut, M., Lazzeri M., Balan E., and Mauri F., 2007, Equilibrium isotopic fractionation in the kaolinite, quartz, water system: Prediction from first-principles density-functional theory. Geochem. Cosmochim. Acta 71, p. 3170-3181.

Merino, E., Wang, Y. and Deloule, E., 1995, Genesis of agates in flood basalts: Twisting of chalcedony fibers and trace element geochemistry. American Journal of Science. 295, p. 1156-1176.

Miehe, G., Graetsch, H., and Florke, O.W., 1984, Crystal-structure and growth fabric of length-fast chalcedony: Physics and Chemistry of Minerals, v. 10, no. 5, p. 197–199, doi:10.1007/BF00309311.

Mörk, M.B.E., and Moen, K., 2007, Compaction microstructures in quartz grains and quartz cement in deeply buried reservoir sandstones using combined petrography and EBSD analysis: Journal of Structural Geology, v. 29, p. 1843-1854.

Moxon, T. 2002, Agate, a study of ageing. European Journal of Mineralogy., 14, p. 1109-1118.

Moxon, T., Nelson, D. R., and Zhang, M., 2006, Agate recrystallization: evidence from samples found in Archaean and Proterozoic host rocks, Western Australia. Australian Journal of Earth Sciences, v. 53, p. 235-248.

Moxon, T. & Reed, S. J. B. 2006, Agate and chalcedony from igneous and sedimentary hosts aged from 13 to 3480 Ma: a cathodoluminescence study. Mineralogical Magazine, v. 70, p. 485-498.

Moxon, T. & Rios, S., 2004, Moganite and water content as a function of age in agate: an XRD and thermogravimetric study. European Journal of Mineralogy, 16, p. 269-278.

Murata, K.J., Friedman I, and Gleason J.D., 1977, Oxygen isotope relations between diagenetic silica minerals in Monterey Shale, Temblor Range, California: American Journal of Science, v. 277, p. 259-272.

Neumann, B., 2000, Texture development of recrystallized quartz polycrystals unravelled by orientation and misorientation characteristics: Journal of Structural Geology, v. 22, p. 1695-1711.

O'Neil J. R. and Hay R. L. (1973) $^{18}O/^{16}O$ ratios in cherts associated with the saline lake deposits of East Africa: Earth and Planetary Science Letters, v. 19, p.257-266.

Pagel, M., Demars, C., Deloule, E., Blanc, P., and Barbarand, J., 1996, Cathodoluminescence and trace element distribution in authigenic quartz in sandstone: International Symposium of the Society of Core Analysts, Improving Reservoir Management, Proceedings: Montpellier, France, 8-10 September, SCA Conference, n. 9613, 2p.

Pittman, J.S. and Folk, R.L., 1971. Length-slow chalcedony after sulfate evaporate minerals in sedimentary rocks. Nature, 230, p. 64.

Pollington, A.D., Kozdon, R., and Valley, J.W., 2011, Evolution of quartz cementation during burial of the Cambrian Mount Simon Sandstone, Illinois Basin: In Situ microanalysis of $\delta^{18}O$, Geology 39, p. 1119-1122.

Prior, D.J., 1999, Problems in determining the misorientation axes, for small angular misorientations, using electron backscatter diffraction in the SEM: Journal of Microscopy-Oxford, v. 195, p. 217-225.

Prior, D.J., Trimby, P.W., Weber, U.D., and Dingley, D.J., 1996, Orientation contrast imaging of microstructures in rocks using forescatter detectors in the scanning electron microscope: Mineralogical Magazine, v. 60, p. 859-869.

Prior, D.J., Mariani, E., and Wheeler, J., 2009, EBSD in the Earth Sciences: applications, common practice and challenges, *in* Schwatz, A.J., Kumar, M., Adams B.L. and Field, *eds.*, Electron Backscatter Diffraction in Materials Science: 2nd Edition.

Ramm, M., 1992, Porosity-depth trends in reservoir sandstones: theoretical models related to Jurassic sandstones offshore Norway: Marine and Petroleum Geology, v. 9, p. 553-567.

Ramm, M., Forsberg, A.W., and Jahren, J., 1997, Porosity-depth trends in deeply buried Upper Jurassic Reservoirs in the Norwegian Central Graben: an example of porosity preservation beneath the normal economic basement by grain coating microquartz: In: Reservoir quality prediction in sandstones and carbonates (eds. Kupecz, J.A., Gluyas, J. and Bloch, S.) AAPG Memoir, v. 69, p. 177–200.

Rimstidt, J.D., and Barnes, H.L., 1980, The kinetics of silica-water reactions: Geochimica et Cosmochimica Acta, v. 44, no. 11, p. 1683–1699, doi:10.1016/0016-7037(80)90220-3.

Rusk B.G., Lowers, H. A., and Reed, M. H., 2008, Trace elements in hydrothermal quartz: Relationships to cathodoluminescent textures and insights into vein formation. Geology 36, p. 547-550.

Sanders, J. V., 1964, Colour of Precious Opal: Nature, v. 204, p. 1151.

Schmidt, N.H., and Olesen, N.O., 1989, Computer-aided determination of crystal-lattice orientation from electron-channelling patterns in the SEM: Canadian Mineralogist, v. 27, p. 15-22.

Sorby, H.C., 1880, On the structure and origin of non-calcareous stratified rocks: Geological Society of London Quarterly Journal, v. 36, p. 46-92.

Stamatakis, M. G., Kanaris-Soitiriou, R. & Spears, A., 1991, Authigenic silica polymorphs and the geochemistry of Pliocene siliceous swamp sediments of the Aridea volcanic province, Greece: Canadian Mineralogist, v. 29, p. 587 - 598.

Thiry, M., and Marechal, B., 2001, Development of tightly cemented sandstone lenses in uncemented sand: Example of the Fontainebleau Sand (Oligocene) in the Paris Basin. Jour. Sed. Res. 71, p. 473-483.

Troger, K.A., 1995, Die subhercyne oberkreide - Beziehungen zum Variscischen Grundebirge und Stellung innerhalb Europas: Nova Acta Leopodina, N.F., v. 71, p. 217-231.

Vagle, G.B., Hurst, Al, and Dypvik, H., 1994, Origin of quartz cements in some sandstones from the Jurassic of the Inner Moray Firth: Sedimentology, v. 41, p. 363-377.

Venables, J.A., and Harland, C.J., 1973, Electron back-scattering patterns - A new technique for obtaining crystallographic information in the scanning electron microscope: Philosophical Magazine, v. 27, p. 1193-1200.

Voigt, T., von Eynatten, H., and Franzke, H.J., 2004, Late Cretaceous unconformities in the Subhercynian Cretaceous Basin (Germany): Acta Geologica Polonica, v. 54, p. 673-694.

Voigt, T., Wiese, F., von Eynatten, H., Franzke, H.-J., and Gaupp, R., 2006, Facies evolution of syntectonic Upper Cretaceous deposits in the Subhercynian Cretaceous Basin and adjoining areas (Germany): Zeitschrift der Deutschen Gesellschaft für Geowissenschaften, v. 157, no. 2, p. 203–243, doi:10.1127/1860-1804/2006/0157-0203.

von Eynatten, H., Voigt, T., Meier, A., Franzke, H. J., and Gaupp, R., 2008, Provenance of Cretaceous clastics in the Subhercynian Basin: constraints to exhumation of the Harz Mountains and timing of inversion tectonics in Central Europe: International Journal of Earth Sciences, v. 97, p. 1315-1330.

Wahl, C., Miehe, G., and Fuess, H., 2002, TEM characterisation and interpretation of fabric and structural degree of order in microcrystalline SiO_2 phases: Contributions to Mineralogy and Petrology, v. 143, p. 360-365.

Waldmann, S., 2006, Räumliche diageneseanisotropien an kretazischen Quarzareniten am beispiel der "Teufelsmauer" (Oberkreide, Harznordrand) [unpublished Ph.D. thesis]: Georg-August-Universität, Göttingen, 103 p.

Walderhaug, O., 2000, Modelling quartz cementation and porosity loss in Middle Jurassic Brent Group sandstones of the Kvitebjörn field, northern North Sea. AAPG Bull. 84, p. 1325-1339.

Wang, Y. & Merino, E., 1995, Origin of fibrosity and banding in agates from flood basalts. American Journal of Science, 295, p. 49-77.

Warren, E.A., and Pulham, A.J., 2001, Anomalous porosity and permeability preservation in deeply buried tertiary and Mesozoic sandstones in the Cusiana Field, Llanos foothills, Colombia: Journal of Sedimentary Research, v. 71, no. 1, p. 2–14, doi:10.1306/081799710002.

Waugh, B., 1970, Formation of quartz overgrowths in Penrith Sandstone (Lower Permian) of northwest England as revealed by scanning electron microscopy: Sedimentology, v. 14, p. 309-320.

Weibel, R., Friis, H., Kazerouni, A.M., Svendsen, J.B., Stokkendal, J., and Poulsen, M.L.K., 2010, Development of early diagenetic silica and quartz morphologies—Examples from the Siri Canyon, Danish North Sea: Sedimentary Geology, v. 228, no. 3–4, p. 151–170, doi:10.1016/j.sedgeo.2010.04.008.

Wilkinson, A.J., and Hirsch, P.B., 1997, Electron diffraction based techniques in scanning electron microscopy of bulk materials: Micron, v. 28, p. 279-308.

Williams, L.A., and Crerar, D.A., 1985, Silica diagenesis 2: General mechanisms: Journal of Sedimentary Petrology, v. 55, no. 3, p. 312–321.

Williams, L.A., Parks, G.A., and Crerar, D.A., 1985, Silica diagenesis 1: Solubility controls: Journal of Sedimentary Petrology, v. 55, no. 3, p. 301–311.

Williams, L. B., Hervig R. L., and Bjorlykke, K., 1997, New evidence for the origin of quartz cements in hydrocarbon reservoirs revealed by oxygen isotope microanalyses. Geochim. Cosmochim. Acta. 61, p. 2529-2538.

Woodward, T.P., Gueo,A.J. & Frink, J.W., 1941, The sand and gravel deposits of Louisiana. State of Louisiana, Department of Conservation Geological Bulletin, 19, 429p.

Worden, R.H., Mayall, M., and Evans, I.J., 2000, The effect of ductile-lithic sand grains and quartz cement on porosity and permeability in Oligocene and lower Miocene clastics, South China Sea: Prediction of reservoir quality: The American Association of Petroleum Geologists Bulletin, v. 84, no. 3, p. 345–359.

Worden, R.H., and Morad, S., 2000, Quartz cementation in sandstones: A review of the key controversies, in Worden, R.H., and Morad, S., eds., Quartz Cementation in Sandstones: International Association of Sedimentologists Special Publications, v. 29, p. 1–20.

Worden, R.H., French, M.W., and Mariani, E., 2012, Amorphous silica nanofilms result in growth of misoriented microcrystalline quartz cement maintaining porosity in deeply buried sandstones: Geology, v. 40, no. 2, p. 179-182.

Yamagishi, H., Nakashima, S., and Ito, Y., 1997, High temperature infrared spectra of hydrous microcrystalline quartz: Physics and Chemistry of Minerals. 24, p. 66 - 74.

8 Appendix – Analytical Data (See DVD)

All AFM, CL, EDAX, EBSD, Hand Sample Photos, Petrographic, SEM, SIMS, and WDS data for agate, Amethyst, Australian Opal, Fontainebleau, Fulmar (core photos), Heidelberg, Iceland Geyser Sinter, Iceland Pumice, Mexican Opal, Miller, and Opal Butte Opal samples.